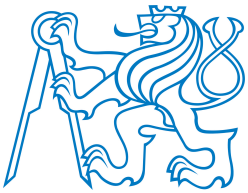

CZECH TECHNICAL UNIVERSITY IN PRAGUE

Faculty of Biomedical Engineering

Department of Natural Sciences

Development of SAW a sensor platform for pathogen detection

Vývoj SAW senzorové platformy pro detekci patogenů

Master thesis

Study Programme: Biomedical and Clinic Technology

Branch of study: Appliances and Methods for Biomedicine

Thesis advisor: Vincent Mortet, PhD.

Bc. Lucie Drbohlavová

Kladno 2016

Abstract

This diploma thesis is focused on the development of diamond based sensor platform for bacteria detection. A nonpathogenic strain of *Escherichia coli* was used as a model organism and bacteriophage T7 was used as a recoginition element of the biosensor.

This work focuses on a particular type of acoustic mass sensors: Love wave type shear horizontal surface acoustic wave sensors (LW-SAW). The LW-SAW sensors have been fabricated on AT-cut and ST-cut quartz crystals. Radio frequency sputtering and photolithography techniques have been used for patterning of interdigitated transducers. SiO_2 guiding layer and nanocrystalline diamond layer have been deposited using chemical vapor deposition techniques. The devices provided a best frequency response for 0.04 and 0.08 SiO_2 normalized thickness. The LW-SAW sensor with 0.08 SiO_2 normalized thickness showed the best sensitivity. Two different schemes of bio-receptors attachment on diamond surface have been studied: 1/ bacteriophages 2/ their fiber tails. First attachment method consisted of T7 bacteriophages attachment on diamond surface via four different terminations: O, H, NH_2 and amino groups activated by glutaraldehyde. Attachment of bacteriophages was confirmed on oxidized and hydrogenated epitaxial diamond layer. Chemical functionalization of diamond surface with hydrophilic biocompatible polymers with antifouling properties was done for fiber tail attachment.

Keywords: biosensors, bacteria detection, bacteriophage T7, CVD diamond, LW-SAW, acoustic sensors, diamond surface functionalization

Czech Technical University in Prague – Faculty of Biomedical Engineering

Department of Natural Sciences Academic Year: 2015/2016

Diploma thesis assignment

Student:	**Bc. Lucie Drbohlavová**
Masters study:	Biomedicínská a klinická technika
Study branch:	Přístroje a metody pro biomedicínu
Title:	Development of saw sensor platform for pathogen detection
Title in Czech:	Vývoj SAW senzorové platformy pro detekci patogenů

Instructions for processing:

The aim of diploma thesis work is development of platform for construction of diamond-based sensor for bacteria detection based on specific recognition properties of bacteriophages or their fibre tail proteins. Pathogen detection has a huge importance in the food industry and it can play significant role in the medical practice. Our study will be directed to detection of a model bacteria *Escherichia coli* using bacteriophage T7 or their fibre tails. This work comprises two main aspects: 1/ the study and the fabrication of the biosensor transducer 2/ the bioreceptor attachment to the diamond surface.

Firstly, different type of bio-sensors/techniques for bacterial detection will be reviewed and compared. In this work we will focus our study on acoustic mass sensors and more particularly on Love wave type shear horizontal surface acoustic wave sensors (SAW). CVD diamond and metals deposition, etching methods and photolithography methods will be developed for fabrication of the bio-sensors. Several characterizations methods will be used for the characterization of materials and SAW devices: Raman spectroscopy, scanning electron microscopy, atomic force microscopy. Different schemes of diamond surface bio functionalization will be studied: 1/ attachment of bacteriophages T7 to the different terminated diamond surface 2/ chemical functionalization of surface of diamond with hydrophilic biocompatible polymers with antifouling properties. Derivatization protocols for attachment of bacteriophage fibre tails via His-tag linkers will be developed.

References:

[1] Mortet V et al., Surface acoustic wave propagation in aluminum nitride-unpolished freestanding diamond structures, Applied Physics Letters, ročník 81, číslo 9, 2002
[2] S. Koizumi, C. Nebel and M, Nesládek, Physics and Applications of CVD Diamond, ed. 1, Wiley, Wiley-VCH, 2008, ISBN 3527408010
[3] P. May, Diamond thin films: a 21st-century material, Philos. Trans. R. Soc., Ser. A, ročník 358, číslo -, 2000

Supervisor of master thesis: Vincent Mortet, Ph.D .

Validity of assignment untill date: 20. 8. 2017

Deadline thesis: 20. 5. 2016 (19. 8. 2016)

.....
Head of Department

.....
Dean

In Kladno 7. 12. 2015

České vysoké učení technické v Praze, Fakulta biomedicínského inženýrství

Katedra přírodovědných oborů | Akademický rok: 2015/2016

Zadání diplomové práce

Student:	**Bc. Lucie Drbohlavová**
Studijní obor:	Přístroje a metody pro biomedicínu
Téma:	**Vývoj SAW senzorové platformy pro detekci patogenů**
Téma anglicky:	Development of SAW sensor platform for pathogen detection

Zásady pro vypracování:

Cílem této diplomové práce je vyvinutí platformy, která bude v navazujících pracích sloužit ke konstrukci biosenzoru na principu diamantové vrstvy pro detekci bakterií. Detekce bakterií bude založena na specifických rozpoznávacích vlastnostech bakteriofágů či pouze jejich bičíkových vláken. Detekce patogenů je důležitá v potravinářském průmyslu a může hrát velkou roli v medicínské praxi. Naše studie bude zaměřena na detekci modelového organismu bakterie Escherichia coli pomocí bakteriofágů T7 nebo jejich bičíkových vláken. Tato práce se skládá ze dvou hlavních částí: 1/ studium a výroba převodníku bioseznoru a 2/ přichycení bioreceptorů k diamantovému povrchu.
Nejdříve bude napsána rešerše různých biosenzorů a technik pro detekci bakterií. Tato práce bude zaměřena na akustické hmotnostní senzory zejména na senzory Loveho typu s horizontální povrchovou akustickou vlnou (SAW). Dále budou nalezeny optimální podmínky depozice CVD diamantu a kovů, metody leptání a fotolitografie pro výrobu platformy biosenzoru. Pro charakterizaci materiálů a SAW senzorů bude použito několik charakterizačních metod: Ramanova spektroskopie, skenovací elektronová mikroskopie a mikroskopie atomárních sil. Bude zkoumáno více způsobů biologické funkcionalizace diamantového povrchu: 1/ přichycení bakteriofágů T7 k různě modifikovanému diamantovému povrchu a 2/ chemická funkcionalizace povrchu diamantu hydrofilními biokompatibilními polymery. Bude vyvinut protokol pro přichycení bičíkových vláken bakteriofága T7 prostřednictvím His-tag linkerů.

Seznam odborné literatury:

[1] Mortet V et al., Surface acoustic wave propagation in aluminum nitride-unpolished freestanding diamond structures, Applied Physics Letters, ročník 81, číslo 9, 2002
[2] S. Koizumi, C. Nebel and M, Nesládek, Physics and Applications of CVD Diamond, ed. 1, Wiley, Wiley-VCH, 2008, ISBN 3527408010
[3] P. May, Diamond thin films: a 21st-century material, Philos. Trans. R. Soc., Ser. A, ročník 358, číslo -, 2000

Vedoucí: Vincent Mortet, Ph.D.

Zadání platné do: 20.08.2017

.....
vedoucí katedry / pracoviště

.....
děkan

V Kladně dne 19.01.2016

Abstrakt

Diplomová práce je zaměřena na vývoj senzorové platformy pro detekci patogenů. Jako modelový organismus byl použit nepatogenní kmen bakterie *Escherichia coli* a jako biologicky citlivý element byl použit bakteriofág T7 kvůli jejich specifickým rozpoznávacím vlastnostem.

Tato práce se zaměřuje na senzory s povrchovou akustickou vlnou, zejména na senzory využívající Loveho vlny (LW-SAW). Pro výrobu LW-SAW senzorů byl použit křemen s AT či ST řezem. Radiofrekvenční naprašování a fotolitografie byly použity pro výrobu elektrod. SiO_2 vrstva a nanokrystalická diamantová vrstva byly deponovány pomocí depozice z plynné fáze. Nejlepší frekvenční odezva byla naměřena u senzorů s normalizovanou tloušťkou SiO_2 rovné 0.04 a 0.08 pro konstantní tloušťku SiO_2 vrstvy 1.3 μm. Nejlepší citlivost LW-SAW senzoru byla prokázána pro SiO_2 normalizovanou tloušťku 0.08. Pro přichycení bioreceptorů k povrchu diamantové vrstvy byly zkoumány dva přístupy. První z nich spočíval v přichycení bakteriofáfů T7 k diamantovému povrchu se čtyřmi různými terminacemi: H, O, NH_2 a NH_2 skupiny aktivované gluteraldehydem. Přichycení bakteriofágů bylo potvrzeno na oxidovaném a hydrogenovaném povrchu epitaxní diamantové vrstvy. Chemická funkcionalizace diamantového povrchu pomocí hydrofilních biokompatibilních polymerů byla provedna pro následné přichycení bičíkových proteinů bakteriofágů T7.

Klíčová slova: biosenzor, detekce bakterií, bakteriofág T7, CVD diamant, LW-SAW, akustické senzory, funkcionalizace povrchu diamantu

Acknowledgements

It is a great pleasure to thank my supervisor Vincent Mortet for all of his patience and advice. I would like to thank also all of colleagues from the research group Materials for Nanosystems and Biointerfaces (MNB), they were there always for me with advice or help. Then I would like to thank people from group of Mr. Pátek from Microbiological Institute CAS, v.v.i. and group of Mr. Cígler from Institute of Organic Chemistry and Biochemistry CAS, v.v.i. Without their help and collaboration it would not be possible to realize this work.

I highly thank my family for all their kind words and support during whole studies. I would like to thank my roommates and friends, for all their crazy ideas that make student life unforgettable. Many thanks belong also to my friend Johnny Walker, that went through all hard times with me.

And last but not least thank belongs to this opportunity...

"Would it save you a lot of time if I just gave up and went mad now?"

˘ Douglas Adams, The Hitchhiker's Guide to the Galaxy

Declaration

Hereby I declare, that this thesis entitled "Development of a SAW sensor platform for pathogen detection" is my original work and that I have not received any outside assistance. All sources used in this work are listed in the end and are cited within the text itself. I agree that this work can be treated according to the law No. 121/2000 Coll. of 7 April 2000 on Copyright, Rights Related to Copyright and on the Amendment of Certain Laws (Copyright Act).

.....	.....
Prague (date)	author's signature

List of Figures

1.1 Prokaryotic cell . . . 15
1.2 Lytic cycle of bacteriophages . . . 16
1.3 Bacteriophage T7 . . . 17
1.4 Principle of different types of ELISA method . . . 18
1.5 Principle of biosensor with a molecular recognition layer . . . 19
1.6 Schematic pictures of the types of acoustic sensors . . . 24
1.7 Schematic of Thickness shear mode resonator and AT-cut of crystal . . . 25
1.8 Schematic diagram of interdigitated transducers and cross section of piezoelectric substrate with deposited IDTs on top of it . . . 27
1.9 Schematic representation of Rayleigh wave's propagation and particles displacement in the material . . . 28
1.10 Schematic representation of two modes of Lamb waves . . . 28
1.11 Dispersion of velocity of symmetric and anti-symmetric Lamb waves . . . 28
1.12 Schematic representation of Love wave's propagation and particles displacement in the material . . . 29
1.13 Possible hybridization of atomic orbital of carbon atoms . . . 31

3.1 CVD system AX5010 from Seki Diamond System . . . 36
3.2 Illustration of the role of CH_3 as a growth species of diamond . . . 37
3.3 Home made magnetron sputtering system . . . 38
3.4 VacuTech 1540 apparatus used for dry etching . . . 39
3.5 Carl Zeiss optical microscope . . . 40
3.6 Used SEM microscope Tescan FERA3 . . . 41
3.7 Icon Dimension, Brüker AFM microscope and schematic diagram of an atomic force microscope . . . 42

3.8 Principle of Raman scattering 43
3.9 Raman spectra of CVD nanocrystalline diamond layer 44
3.10 Schematic diagram of the XPS process and formation of XPS spectra 46
3.11 Contact angle, hydrophilic and hydrophobic surfaces 47
3.12 Relationship between transducer periodicity and excited waves 48
3.13 Transducer's frequency response 49
3.14 Used apparatus for frequency measurement 50
3.15 Scheme of inoculating of bacteria culture onto the soft agar's surface 51
3.16 Typical bacterial growth curve 51

4.1 Schematic of LW-SAW sensor 53
4.2 Phase velocity dispersion and electromechanical coupling coefficient curves for AT-cut quartz as a function of different SiO_2 normalized thicknesses for different diamond normalized thicknesses 54
4.3 Phase velocity dispersion and electromechanical coupling coefficient curves for ST-cut quartz as a function of different SiO_2 normalized thicknesses for different diamond normalized thicknesses 54
4.4 Sensitivity as a function of SiO_2 normalized thickness 55
4.5 Procedure for determination of RIE rate of different materials 58
4.6 Calibration curves for etching of different materials 58
4.7 Raman spectra and AFM picture of NCD layer deposited using AX5010 apparatus . . 59
4.8 Raman spectra nad AFM picture of 200 nm thick diamond layer 60
4.9 Raman spectra nad AFM picture of NCD layer deposited on (100) single crystal 61
4.10 Two approaches of fabrication of IDTs 62
4.11 Picture of fabricated IDTs using lift-off technique 62
4.12 Process of fabrication of LW-SAW sensor - deposition of guiding and NCD layer 63
4.13 Raman spectra and AFM picture of NCD layer 64
4.14 Picture of fabricated LW-SAW sensor 64
4.15 S_{21} parameter for different IDTs spatial period on AT-cut quartz 66
4.16 S_{21} parameter for SAW devices fabricated from different metal on ST-cut quartz 67
4.17 AFM pictures of first nine layers of NCD deposited on SAW sensor 68
4.18 S_{21} parameter for SAW sensor with deposited different numbers of NCD layer 68

4.19 Insertion loss as a function of different number of NCD layers for normalized SiO_2 thickness 0.04 69
4.20 Phase velocity and relative frequency shift as a function of number of NCD layers . . . 69
4.21 S_{21} parameter for diamond coated and uncoated LW-SAW sensors with deposited different numbers of LOR layers 71
4.22 Phase velocity and relative frequency shift as a function of thickness of LOR layers . . 71
4.23 Raman spectra of annealed SCD layer 73
4.24 Results of XPS analysis of the diamond surfaces treated with 4-(2-azidoethyl)alanine . 74
4.25 Results of the XPS analysis of the diamond surface after reduction of azide groups . . . 75
4.26 Droplet of water on different functionalized NCD layers 76
4.27 Results of plaque assay method 79
4.28 SEM micrographs of functionalized NCD layers 81
4.29 TEM image of bacteriophages solutions after negative staining 82
4.30 SEM image of silicon substrate with attached bacteriophages 83
4.31 SEM image of SCD substrate with epitaxial diamond layer with attached bacteriophages 84
4.32 Scheme of attachment of bacteriophage's fiber tails to the diamond surface 85
4.33 Reaction equation for grown of silica layer 86
4.34 PM-IRRAS spectra of silica coated NCD layer and pure NCD layer 86
4.35 PM-IRRAS spectra of silica coated NCD layer with or without use of PVP 87
4.36 Reaction equation for polymer layer coating 88
4.37 PM-IRRAS spectra of polymer coated NCD layer 89

List of Tables

1.1 Sensor characteristic for bacterial detection 20

1.2 The types of hybrid orbital sets and their orientation in space 30

3.1 Composition and etching rates of etchants for different metals 39

3.2 Parameters for selected piezoelectric materials 49

4.1 Conditions used for deposition of different metal layers 56

4.2 Used conditions for deposition of photoresist layer 56

4.3 Optimal conditions for fabrication of IDTs on different substrates 57

4.4 Conditions used for RIE of diamond and silicon 57

4.5 Calculated etching rates for different materials 58

4.6 Deposition conditions of NCD layer using AX5010 apparatus 59

4.7 Deposition conditions of NCD layer using MW-LA-PECVD system 60

4.8 Conditions used for deposition of epitaxial layer onto (100) single crystal substrate using AX5010 apparatus 61

4.9 Conditions used for deposition of amorphous SiO_2 guiding layer 63

4.10 Conditions used for deposition of NCD layer 63

4.11 Calculated resonant frequency of SAW sensor for different spatial periods of IDTs . . . 65

4.12 Measured resonant frequency for different IDTs period 65

4.13 Conditions used for deposition of NCD layer on SAW sensors 67

4.14 Conditions used for H-termination of NCD layer 72

4.15 Measured contact angles for different functionalized NCD layer 76

List of Abbreviations

Acronyms

AFM	Atomic force microscopy
APM	Acoustic plate mode
BAW	Bulk acoustic wave
cfu	Colony forming unit
CVD	Chemical vapor deposition
DNA	Deoxyribonucleic acid
dsDNA	Double-stranded deoxyribonucleic acid
ELISA	Enzyme-linked immunosorbent assay
FBAR	Thin-film acoustic resonator
FPW	Flexular plate wave
HPHT	High pressure high temperature
IDT	Interdigital transducer
IR	Infrared
LB	Luria-Bertani
LOR	Lift-off resist
LW-SAW	Love wave surface acoustic wave
MW-LA-PECVD	Microwave linear antenna plasma enhanced chemical vapor deposition
NCD	Nanocrystalline diamond
PCD	Polycrystalline diamond
PCR	Polymerase chain reaction
PECVD	Plasma enhanced chemical vapor deposition

pfu	Plaque forming unit
PM-IRRAS	Polarization-modulation infrared reflection absorption spectroscopy
PVD	Physical vapor deposition
QCM	Quartz crystal microbalance
RF	Radiofrequency
RIE	Reactive ion etching
RNA	Ribonucleic acid
SAW	Surface acoustic wave
SEM	Scanning electron microscopy
SH-SAW	Shear-horizontal surface acoustic waves
SPR	Surface plasmon resonance
TEM	Transmission electron microscopy
tRNA	Rransfer ribonucleic acid
TSM	Thickness shear mode
UNCD	Ultra-nanocrystalline diamond
UV	Ultra violet
XPS	X-ray photoelectron spectroscopy

Chemicals

AIBN	Azobis(isobutyronitrile)
AzMA	3-(azidopropyl)methacrylamide
DMSO	Dimethyl sulfoxide
HF	Hydrofuloric acid
HPMA	N-(2-hydroxypropyl)methacrylamide
IPA	Isopropyl alcohol
PVP	Polyvinylpyrrolidone
TEOS	Tetraethyl orthosilicate

Contents

Introduction **13**

1 Background **14**

1.1 Bacteria 14

1.1.1 *Escherichia coli* 15

1.2 Bacteriophages 16

1.2.1 Bacteriophage T7 17

1.3 Detection of bacteria 18

1.3.1 Conventional methods 18

1.3.2 Biosensor-based detection methods 19

1.4 Acoustic wave devices 24

1.4.1 Thickness shear mode resonators 25

1.4.2 Surface acoustic wave devices 26

1.5 Diamond 30

1.5.1 Diamond synthesis 32

1.5.2 Surface functionalization 32

2 Aims of the study **34**

3 Materials & methods **36**

3.1 Fabrication methods 36

3.1.1 Thin film deposition methods 36

3.1.2 Microprocessing methods 38

3.2 Characterization methods 40

3.2.1 Optical microscopy 40

3.2.2 Transmission electron microscopy (TEM) 40

3.2.3 Scanning electron microscopy (SEM) . . . 41
3.2.4 Atomic force microscopy (AFM) . . . 42
3.2.5 Raman spectroscopy . . . 43
3.2.6 Polarization Modulation Infrared Reflection Absorption Spectroscopy (PM-IRRAS) . . . 45
3.2.7 X-ray photoelectron spectroscopy (XPS) . . . 45
3.2.8 Contact angle measurement . . . 46
3.2.9 LW-SAW characterization . . . 47
3.3 Microbiological methods . . . 50
3.3.1 The plaque assay method . . . 50
3.3.2 Bacterial cell culture . . . 50
3.3.3 Centrifugation . . . 52

4 Results & discussion **53**
4.1 Fabrication and characterization of SAW sensor . . . 53
4.1.1 Theoretical study of LW-SAW sensor . . . 53
4.1.2 Methods for fabrication of LW-SAW sensor . . . 55
4.1.3 Fabrication of LW-SAW sensor . . . 61
4.1.4 Characterization of LW-SAW sensor . . . 65
4.2 Attachment of bioreceptors to diamond surface . . . 72
4.2.1 Diamond surface functionalization for bacteriophage attachment . . . 72
4.2.2 Attachment of bacteriophages to the diamond surface . . . 77
4.2.3 Attachment of bacteriophage's fiber tails to the diamond surface . . . 85

5 Conclusions **90**

Bibliography **93**

Appendix A **99**
List of publication published during the traineeship . . . 99
Participation to international conferences . . . 99

Introduction

Infections by pathogenic bacteria related to food and water contamination causes a serious threat to public health [1]. According to WHO, it is estimated that 3.6% of the total global burden are diarrheal diseases. Diarrhea is responsible for about 1.5 million deaths per year. It is estimated that 58% of these burdens are attributed to unsafe water supply [2]. Dissemination of harmful bacteria in food and water supply can be a result of accidents or pollution even in developed countries [3]. For example, the water supply was contaminated in Prague in May 2015 and more than 4 thousand people were sick. Contamination of water by Legionella was also recorded in Prague in January 2016. Another threat to public health is antibiotic resistance. Resistance to the most widely used antibiotic for cure of infections caused by *E. coli* or *Stahpylococcus aureus* is known. These are the reasons why it is necessary to develop fast and real-time bacteria detection method for many applications, such as the food industry or water supply quality monitoring. Biosensors are good candidates to meet these requirements.

In this work we investigated the development of biosensor using shear-horizontal surface acoustic wave (SH-SAW) sensors integrating a CVD diamond layer for bioreceptors attachment. SH-SAW sensors, especially Love wave SH-SAW sensors, are reported to have high sensitivity among acoustic sensors [4]. A long stability of attached bioreceptors is very important to ensure real-time monitoring. Diamond with its properties such as good mechanical stability, chemical inertness or possibility of surface functionalization can be advantageously used. A prolonged stability of attached biomolecules was also reported. Good specificity of bioreceptors is also demanded for proper function of biosensor. Bacteriophages are viruses which are very specific to their host bacteria strains. Their attachment to the diamond surface has been studied.

1 Background

1.1 Bacteria

Bacteria are prokaryotic single-celled organisms. The structure of prokaryotic cell is shown in figure 1.1. Generally, bacteria has the following structural characteristics [5] :

- The nucleus of procaryotic cells is called the nucleoid. The nucleoid is not separated from the cytoplasm by a membrane and consists of a single molecule of double-stranded deoxyribonucleic acid (dsDNA) which is circular. This dsDNA is called chromosomal DNA and contains the information absolutely necessary for the life of the bacteria.
- Besides the nucleoid, the bacterial cell contains small circular molecules of DNA called plasmids. Plasmids are not necessary for life, but they contain important information, for example resistance to antibiotics.
- The surface of the bacterial cell is formed by the cell wall. The main component of the cell wall is peptidoglycan (murein).
- Bacterial cells contain neither mitochondria nor plastids.
- Ribosoms are found only in cytoplasm.
- They multiply asexually by budding or binary divison.
- They are ubiquitous and many of them are pathogenic.

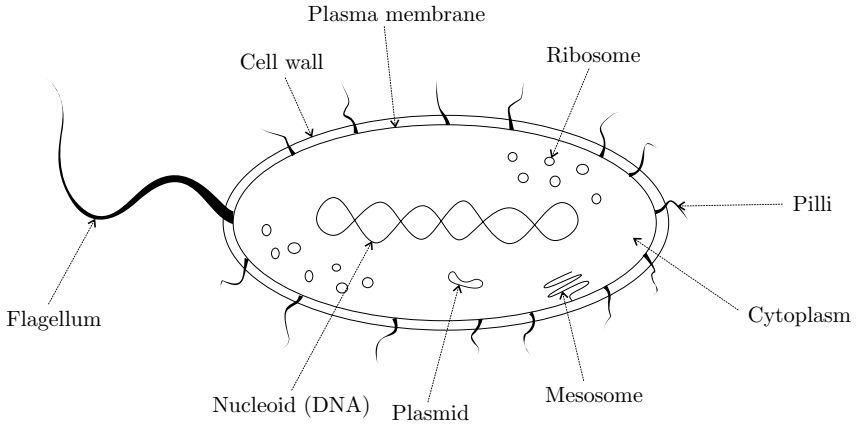

Figure 1.1: Schematic picture of prokaryotic cell

1.1.1 *Escherichia coli*

Bacterium *Escherichia coli* belongs to the large family of gram-negative bacteria called Enterobacteriaceae. Members of the Enterobacteriaceae family are rod-shaped cells, their length is typically 1-5 μm and they are cosmopolitan. Many species are pathogenic and cause human diarrheal disease, for example *Salmonella*, *Shigella dyseteriae* or well-known *Escherichia coli* [5].

Most of *E. coli* strains are non-pathogenic and they are an ordinary commensals of human colon. Some *E. coli* strains are pleuripotent pathogen causing a wide variety of illnesses. Diseases caused by *E. coli* include diarrhea, the hemolytic-uremic syndrom and dysentery. Outcomes includes sepsis followed by renal failure that can end with death. These strains are also a major factor for nosocomial infections [6]. One of the pathogenic strain is O157:H7 *E. coli* which causes hemorrhagic colitis and hemolytic uremic syndrome. Primary sources of O157:H7 *E. coli* are unpasteurized milk, raw beef, vegetables, fruit and contaminated water [3].

1.2 Bacteriophages

Viruses are nucleoprotein particles characterized by the ability to infect their host cell and reproduce within them. Bacteriophages cannot be classify very easily because of their diversity. The main classification criterion is based on their morphology. Their capsid is composed of two main protein parts: head (icosahedral symmetry) containing their nucleic acid and tail with helical symmetry. Bacteriophage's tail is not used to activate its movement. After bonding to specific receptors of host bacterial cell, bacteriophage inserts its nucleic acid via its tail into the bacterial cell. Their nucleic acid can be DNA or RNA and either single-stranded and/or double-stranded [5].

Bacteriophage's biological activity is limited to reproduction. They use bacteria's free aminoacids, nucleotids and another molecules and enzymes. Replication of bacteriophage's nucleic acid depends on the enzymes of the host cell. Synthesis of bacteriophage's protein is carried out on the ribosomes of the host cell and viruses are using cell's transfer ribonucleic acid (tRNA). The reproductive cycle ends with destruction of the host cell and the whole process of infection is called the lytic cycle. This cycle takes place in seven steps and is shown in figure 1.2 [5]. In contrary to lytic cycle, lysis of bacteria does not occur during the lysogenic cycle. Bacteriophages just insert their DNA into host cell and this DNA is inserted into chromosomes of the host bacterium until some stress starts its production [7].

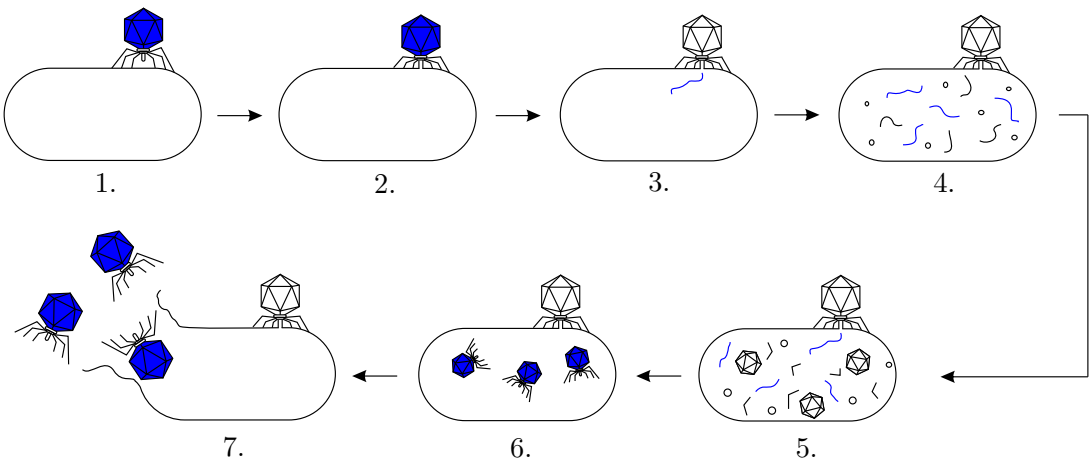

Figure 1.2: Lytic cycle of bacteriophages: 1/ bonding of virion to the host cell, 2/ penetration into the host cell, 3/ release of nucleic acid from capsid, 4/ replication of bacteriophage's nucleic acid, 5/ synthesis of bacteriophage's proteins, 6/ maturation of virions and 7/ release virions from host cell.

1.2.1 Bacteriophage T7

In this work we used Bacteriophage T7 as a model organism. It is a virulent phage growing on the host strain *E. coli* B. Its virion is made up of a linear dsDNA with length of 12 μm. DNA is enclosed in an icosahedral head with a diameter approximately 60 nm. A short tail with length of 20 nm and diameter of about 10 nm is attached to the head. Attached to the tail are fiber tails used to bind bacteriophage to the targeted bacterium. The tail is composed of at least a three proteins, one of them constitutes the tail fiber, and six proteins are found in the head [8].

T7 genom is divided into three groups: 1/ an early region expressed from the onset until about 8 minutes after infection and these class I proteins prepare the intracellular environment for phage multiplication, 2/ class II proteins are expressed about 6 to 15 minutes after infection and are responsible for phage DNA synthesis and 3/ class III proteins are expressed from about 8 minutes after infection until lysis. Class III genes code for coating proteins and are involved in maturation of progeny particles (all of the times refer to the conditions at 30 °C). Phages particles maturation starts about 9 minutes after infection at 37 °C (18 min at 30 °C). The final step of T7 growth is bacteria cell lysis and this occurs about 30 min after infection [8].

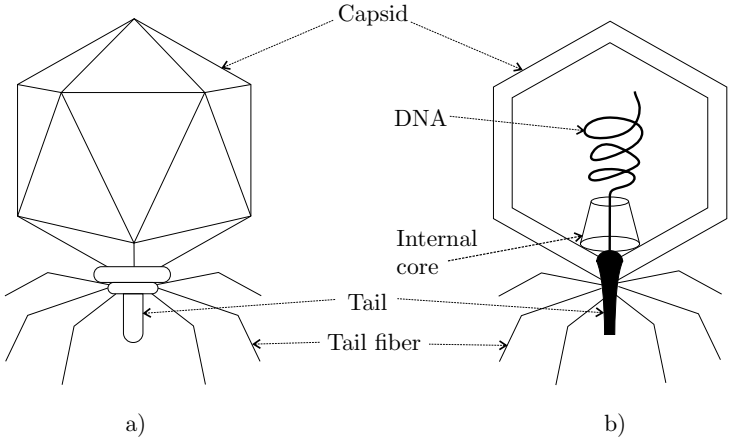

Figure 1.3: Schematic picture of bacteriophage T7, a) model of bacteriophage T7, b) schematic cross-section of bacteriophage T7

1.3 Detection of bacteria

Food born bacterial contamination as well as bioterrorism threats requires development of new effective detection methods of pathogenic microorganisms. These methods must be fast, highly sensitive and highly specific [9]. In the following section, conventional detection methods and biosensor-based techniques for bacteria detection are described.

1.3.1 Conventional methods

Plate counting and culturing methods are conventional microbiological identification approaches. These methods are based on the ability to investigate organisms grown in various culture mediums [9]. The enzyme-linked immunosorbent assay (ELISA) is another widely accepted conventional detection method. ELISA is based on the antibody – antigen recognition. In direct assay ELISA the sample is added to antibody, which is specific to the targeted bacteria. The secondary labeled antibody is added after incubation and several washing steps. Detection is performed by enzyme – substrate (e.g. colorimetric) reaction or by fluorescence detection in the case of conjugation the secondary antibody to a fluorophore [10].

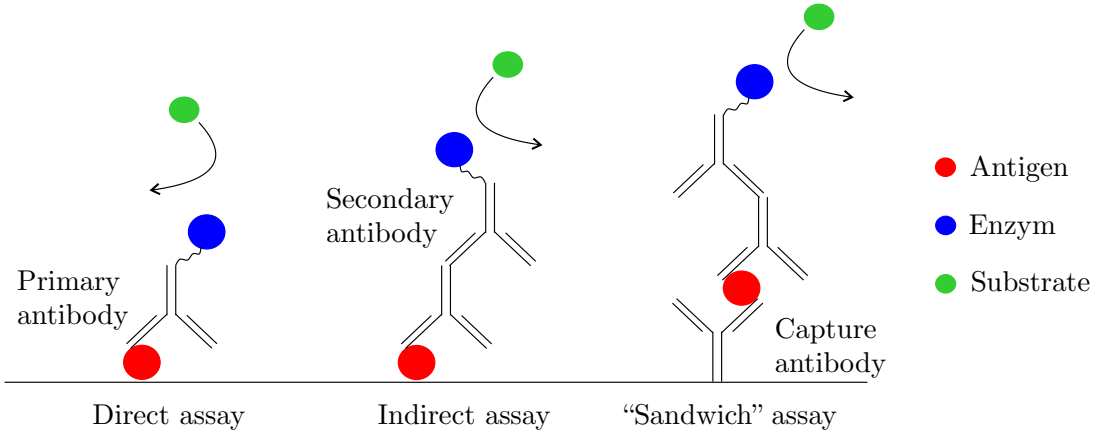

Figure 1.4: Principle of different types of ELISA method

Polymerase chain reaction (PCR) is another method for detection of pathogens. DNA is isolated from the sample, cut by restriction endonuclease and amplified. Electrophoresis is used for evaluation of the size of DNA fragments [11]. Plate counting, ELISA and PCR usually require enrichment, isolation, morphological investigation and biochemical or serological testing for positive identification of pathogens. This is the reason why

these techniques are time-consuming and must be carried out in specific laboratories [12]. Mass and infrared (IR) spectrometry have also been used for detection of bacteria. Both methods are based on the measurement of chemical components of bacteria cells. IR spectrometry usually showed similar results at the molecular level as mass spectrometers while the mass spectrometers are expensive, not portable and measurements must be done in vacuum. [9].

Conventional methods take several hours and the identification of bacteria needs further serological and biologiacal investigation. These tests are time-consuming (plating and culturing), expensive (mass spectrometry, DNA microarrays), give total bacterial load instead of the number of viable cells (ELISA) and they need specific laboratory equipment [13, 14]. This is why it is necessary to develop a new rapid bacteria detection systems - biosensors.

1.3.2 Biosensor-based detection methods

A biosensor is a device which converts chemical or biological signal into a signal which can be measured by different means. The output is usually an electrical signal: either voltage or current. Biosensors are composed of three main parts: 1/ biological probes which are in contact with studied analyte, 2/ a transducer that converts biological recognition into a measurable signal and 3/ an electronic read-out system that provides information to users [13, 15].

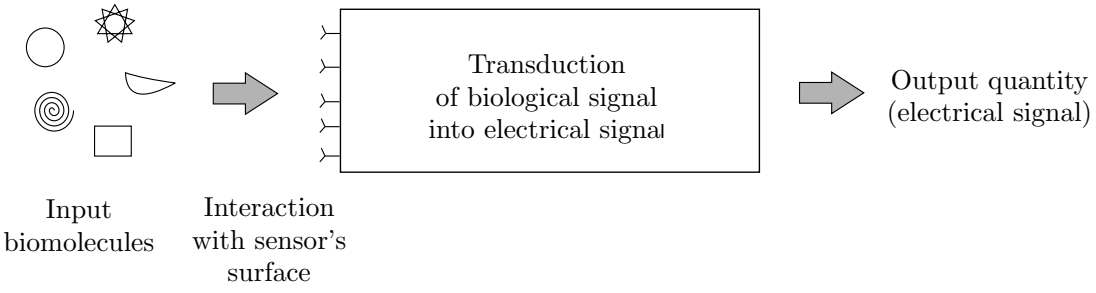

Figure 1.5: Principle of biosensor with a molecular recognition layer that has highly selective properties.

Biosensors have three important characteristics [15]: 1/ sensitivity is the magnitude of the output signal produced in response to a concentration of the studied analyte, 2/ selectivity is the ability to distinguish between different biomolecules and 3/ resolution is the measure of the minimal change in the input quantity that biosensor is able to detect.

Biological/chemical probes used for the analyte recognition varies in nature: they can be enzymes, antibodies, nucleic acids, aptamers, etc [9]. Biosensors for bacterial detection should meet certain requirements which are outlined in table 1.1. The first biosensor described by Clark and Lyons in 1962 was an electrochemical sensor and it was used for detection of glucose in blood. Later, discovery of two technologies helped the development of new biosensors. The first is the new discovery of evanescent wave phenomenon. This phenomenom occurs when light is reflected at the optical interface with a change in refractive index. There is a leak of energy from the point of reflection into the surrounding medium and this is used for surface plasmon sensors. The second major development was done in the field of acoustic wave sensors after discovery of piezoelectricity. [14].

Table 1.1: Sensor characteristic for bacterial detection [16]

Requested characteristics of the biosensor	
Low detection limit	Ability to detect single bacteria in reasonably small sample volume
Assay time	5 - 10 min for a single test
Assay protocol	No reagent addition needed
Measurement	Direct
Format	Highly automated format
Operator	Minimum skill required to use the assay
Viable cell count	Should discriminate between live and dead cells
Size	Compact, hand-held, portable, design for field use
Species selectivity	Ability to distinguish individual bacterial species in the presence of other microorganisms or cells

Biorecognition elements

The most used biorecognition elements are antibodies, nucleic acid, and aptamers. Antibodies can be used for pathogen detection or for detection of their components such as enzymes or spores. Depending on the production process, anti-bodies are divided into two groups – polyclonal and monoclonal. Monoclonal anti-bodies are more specific, but they are more expensive to produce. Immobilization of antibodies onto the sensing surface is performed by chemical conjugation or cross-linking through interaction with functional groups such as amines and carboxylates. The biorecognition using nucleic acid rely on single-stranded DNA or RNA binding to the complementary sequence of the nucleic acid of the targeted organism. Aptamers are engineered nucleic acids. They can be chemically synthesized *in vitro* and they are more resistant than antibodies to freezing and drying

cycles [9].

Attachment of bacteriophages for biorecognition element

Several studies were performed in the field of attachment of bacteriophages. Different substrates and attachment methods of bacteriophages have been studied. Histidine, cysteine, dextrose or sucrose were used for immobilization of bacteriophages on gold substrate. Amino groups of histidine or cystein were also activated by gluteradehyde and substrates were immersed into a solution of bacteriophages (with titre 10^{12} plaque forming unit per milliliter (pfu/ml) for 20 hours at a temperature range from 25 °C to 60 °C. Cysteamine modified gluteraldehyde activated surface with bacteriophages immobilized at 40 °C provided the highest surface density of phages 18 ± 0.15 phages/μm^2 [13]. Silicon substrates were also used for immobilization of P22 bacteriophage's tail spike proteins. Two forms of these proteins were used: one with C-terminal cystein and N-terminal poly-histidine (His_6) and second one with N-terminal cystein [17]. These genetically engineered tailspike proteins were used also for immobilization onto gold surface using thiol-chemistry [18]. Another possible method consisted of attachment of phage using biotin-streptavidin interaction. Biotin-streptavidin interaction is one of the strongest non covalent interaction in nature. In this method bacteriophages are genetically modified such that the capsid head of the bacteriophage contains biotin protein. This approach was used for the attachment of bacteriophages T4 to streptavidin-functionalized gold surfaces [19, 20].

Transducer elements

a) Optical biosensors

In optical biosensors, attachment of targeted bacteria to the sensor's receptors causes a change of light absorption/emission or refractive index of the transducer. Several approaches are used for bacterial detection, e.g. surface plasmon resonance (SPR) or functionalized optical fibers. SPR is a technique in which the incident beam is directed onto a gold or silver surface at the resonance angle. The beam induces oscillation of the free electrons at the metal surface which generates an evanescent field. Attachment of bacteria to this surface causes a change in the surface plasmon resonance frequency [9]. Numerous studies have been carried out to develop surface plasmon resonance biosensors using different recognition elements.

The first biosensor based on this technique was made for detection of *E. coli* O157:H7 using specific antibodies - protein A or protein G. Its detection limit was 10^7 colony forming unit per mililiter (cfu/ml) [21]. Later, different antibodies were attached to the gold surfaces or gold nanoparticles for detection of bacteria as *E. coli*, methicillin-resistant *S. aureus*, *L. acidophilus* or *S. typhimurium* and the detection limit ranged from 10^3 cfu/ml to 10^4 cfu/ml [22–24]. Functionalized optical fibers are another type of optical sensors. The principle of detection bacteria by optical fibers is absorption/emission of light caused by attachment of bacteria onto the functionalized fiber's surface [25, 26]. These fibers were used for detection of methicillin-resistant or methicillin-sensitive *Staphylococcus aureus* using monoclonal antibodies [25] or *E. coli* by bacteriophage T4 as bioreceptor with detection limited to 10^4 – 10^9 cfu/ml [26].

b) Electrochemical sensors

Electrochemical sensors are generally more sensitive, simpler and less expensive than optical sensors. There are three main electrochemical detection methods – amperometry, potentiomentry and impedimetry. Amperometric sensors operate at a fixed voltage and measure the current which is directly proportional to the concentration of analyte. Potentiometric sensors measure the changes in a potential caused by the interaction of the analyte molecules with the probe-modified surface. Impedimetric sensors measure changes in an impedance caused by bacteria attachment/growth on sensors surface [9]. The usability of these methods for bacteria detection using different bioreceptors has been studied.

Dual aptamer-based sandwich method was used for detection of *Staphylococcus aureus* in study of Abbaspour *et al.* Biotynilated primary aptamer was immobilized on magnetic beads coated by streptavidin. A secondary aptamer was attached to the silver nanoparticles. In the presence of targeted bacteria an Apt/*S. aureus*/apt-AgNP sandwich complex was created. The electrochemical signal of AgNPs was detected by anodic stripping voltammetry. This sensor showed the low detection limit of 1.0 cfu/ml [27]. *E. coli* O157:H7 was detected by impedimetric measurement using gold electrode modified by Polyaniline (PANI) film with attached antibody. Concentration of 10^2 cfu/ml was successfully detected on the Au/PANI/Glu/antibody sensor [28].

c) Acoustic sensors

Acoustic sensors are based on the variation of resonance frequency upon attachment of targeted element to bioreceptors on their surface by mass loading. The most commonly used acoustic mass sensor is quartz crystal microbalance (QCM) [9]. Acoustic sensors are good candidates for bacteria detection and several studies were carried out to develop biosensors using different biorecognition elements.

QCM with immobilized polyclonal antibodies was used for detection of *L. acidophilus* and *B. bifidum*. The sensor was made from AT-cut piezoelectric quartz with gold layer. The microbial cells were detected directly by the measuring of the frequency change observed after binding of the bacteria. The bacteria could be detected in the range of 10^4 – 10^7 cfu/ml within 60 minutes [29]. QCM were also used in combination with a magnetic bead purification system for detection of *Salmonella enterica* cells in the food samples. Specific detection of *Salmonella* cells was done using aptamers attached to the magnetic bead and detection limit has been reported as 100 cfu/ml from model food sample (milk) [30]. A SH-SAW biosensor for point of care testing were developed by Yatsuda *et al.* The sensor chip is a quartz-based 250 MHz SH-SAW delay line. Antibodies attached to the gold surface of the chip were used as pathogens receptors. Direct assay and sandwich assay were tested. Larger phase shifts were obtained in the sandwich assay [31]. Surface acoustic wave (SAW) sensors were used for determination of *E. coli* in water sources. Signal was enhanced by detecting the gaseous CO_2 generated by *E. coli*. Metabolization of carbohydrates and some amino acids by the *E. coli* bacteria cells produces CO_2. When the CO_2 contacts the sensor electrodes, the sensor's frequency shifts [32].

1.4 Acoustic wave devices

Principle of acoustic mass sensors is briefly described in the chapter 1.3, subchapter c) Acoustic mass sensors. In this chapter, we will review different configurations used for construction of acoustic sensors. Main SAW configurations are as follows and are represented in figure 1.6 [33]:

- The Thickness Shear Mode (TSM) resonator,
- The Surface Acoustic Wave (SAW) device,
- The Flexural Plate Wave (FPW) or Lamb device,
- The Acoustic Plate Mode (APM) device.

.

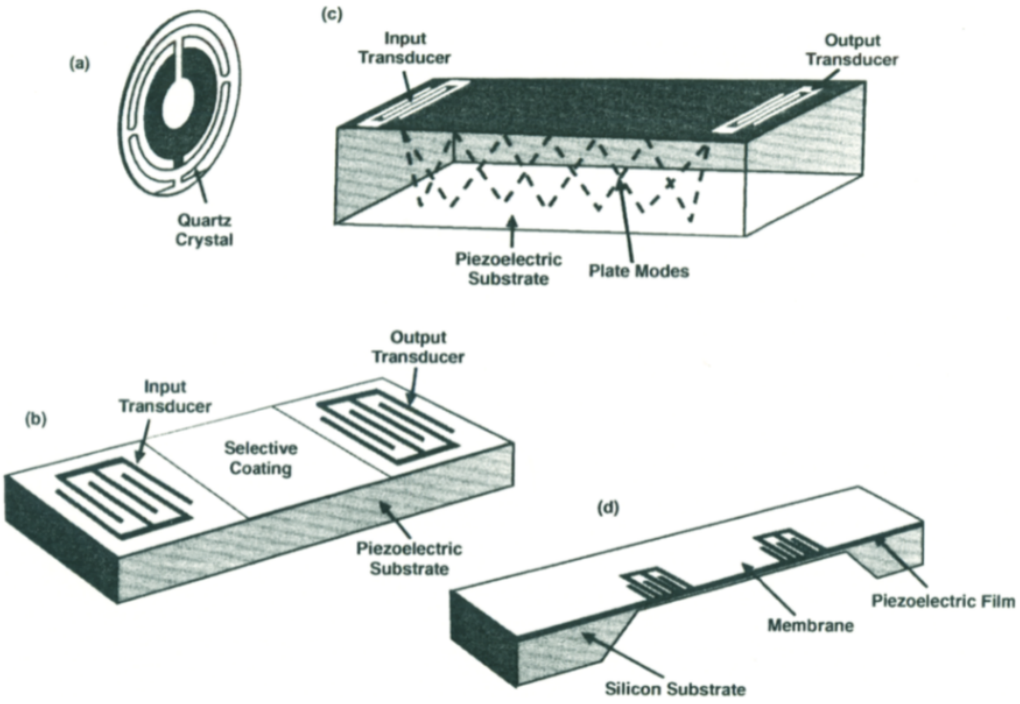

Figure 1.6: Schematic pictures of the types of acoustic sensors, a) Thickness Shear Mode (TSM) resonator, b) Surface Acoustic Wave (SAW) sensor, c) Acoustic Plate Mode (APM) device and d) Flexural Plate Wave (FPW) device (reproduced from [15])

1.4.1 Thickness shear mode resonators

TSM resonators, most often called QCM, belong to the family of bulk acoustic wave (BAW) sensors. Typically, TSM resonators consists of one thin plate of AT-cut quartz crystal (figure 1.7A) with circular metal electrodes on both sides, as shown in figure 1.7B. Applied electric field across the resonators electrodes results in a generation and propagation of acoustic waves in the device due to mechanical and piezoelectric properties of the quartz [15].

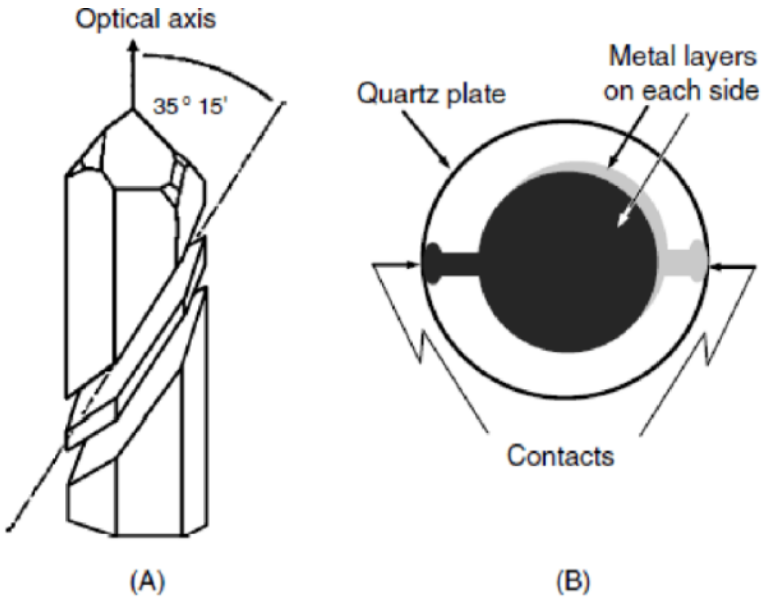

Figure 1.7: A) AT-cut of crystal, B) Schematic of TSM resonator (reproduced from [34])

TSM resonators were first used for measurement of metal deposition rates. The discovery that TSM resonators can operate in contact with liquids, makes them good candidate for biosensors [15, 33]. For biosensor applications, quartz's surface is coated by sensitive thin film. Variations in properties of this thin film (thickness, density) affect sensor's resonant frequency [15]. Advantages of TSM resonators sensors are simplicity of manufacturing, good temperature stability and ability to operate in harsh environments. Unfortunately, these sensors have the lowest mass sensitivity. They typically operate at frequency from 5 MHz to 30 MHz. Operating at higher frequencies can increase their sensitivity, but it requires fabrication very thin and fragile plates [33]. Another option to increase operating frequency is to use thin-film bulk acoustic resonators (FBARs). These devices are made from metal electrodes deposited on both sides of very thin piezoelectric film deposited by PVD or CVD method. When the acoustic waves travel in the direction

of the film thickness, wave is reflected at the interface of the piezoelectric film and the electrodes. When the thickness of the thin film is equal to the half of wave's wavelength, an acoustic standing wave is formed. The resonant frequency f is given by equation as for QCM:

$$f = \frac{v_a}{2d} \tag{1.1}$$

where v_a is an acoustic wave velocity and d is thickness of the piezoelectric film. In solid materials typical velocity of acoustic waves is about 5 000 m/s [35]. Assuming the thickness of piezoelectric film is 100 nm, the resonant frequency of the resulting device is 25 GHz.

1.4.2 Surface acoustic wave devices

The piezoelectric effect description by Pierre and Paul-Jacques Curie and surface acoustic waves propagation studies by John William Scrutt in late 19$^{\text{th}}$ century are at the origin of development of SAW devices [4].

In SAW devices, surface acoustic waves are generated by metal electrodes called interdigital transducers (IDTs) deposited on the surface of the piezoelectric crystal, as shown in figure 1.8a, and propagated within the surface [15]. When the radio frequency signal is applied to the IDTs, the electric field is produced within the piezoelectric material, as shown in figure 1.8b. The spatial periodicity λ_T of the transducers determines the operational frequency f_0 of the sensor, according to following relation:

$$f_0 = \frac{v}{\lambda_T} \tag{1.2}$$

where v is the phase velocity of the acoustic waves [36].

The waves travel across the surface, which can be functionalized by biomolecules with specific recognition properties and be modified by bio-chemical events at the surface. These waves are converted back by second IDTs into an electrical signal to be measured. Change in frequency is associated with the corresponding variation of mass biomolecules [4]. Mass sensitivity (S_m) is defined as the incremental frequency change that occurs in response to an incremental change in mass per unit area on the sensor's surface [37]:

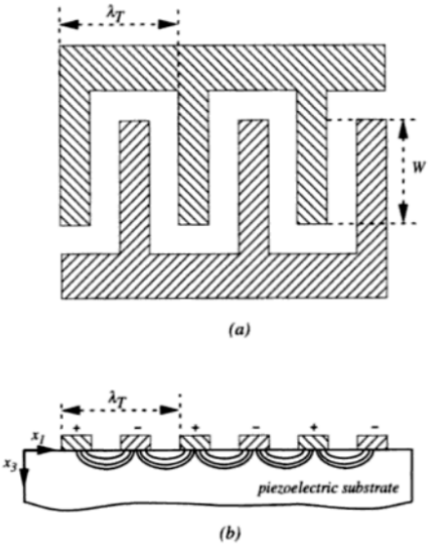

Figure 1.8: a) Schematic diagram of interdigitated transducers and b) cross section of piezoelectric substrate with deposited IDTs on top of it (reproduced from [36])

$$S_m = \lim_{\Delta m \to 0} \frac{\Delta f / f_0}{\Delta m}, \tag{1.3}$$

where Δm is the uniformly distributed mass per unit area of the sensor's surface, f_0 is the unperturbed frequency of the device and Δf is the change in the operational frequency caused by mass loading of the sensor [37].

The most frequently used SAW sensors are: 1/ Rayleigh-SAW sensor, 2/ Lamb-wave sensors and 3/ Love-wave sensors. In Rayleigh-SAW sensor the material displacement occurs in the x-axis and z-axis. X-axis is direction of acoustic waves propagation as is shown in figure 1.9. In contact with liquid part of SAW energy is dissipated in the liquid. This is the reason, why Rayleigh-SAW sensors are not used in liquids.
FPW or Lamb devices are composed of thin membrane deposited on the piezoelectric substrate. Lamb waves, also called plate waves, exist in thin plate-like medium. They are guided by the free upper and lower surfaces. They can occur in two mode type: 1/ symmetric and 2/ anti-symmetric (see figure 1.11), where symmetric waves have radial in-plain displacement of particles and anti-symmetric waves have out-of-plane displacement (see figure 1.11) [39]. In FPW devices, first anti-symetric wave mode has a low propagation velocity, hence waves propagation velocity is slower than in the fluid in contact with the sensor's surface. Disadvantage of FPW sensor is thin and fragile membrane to achieve a

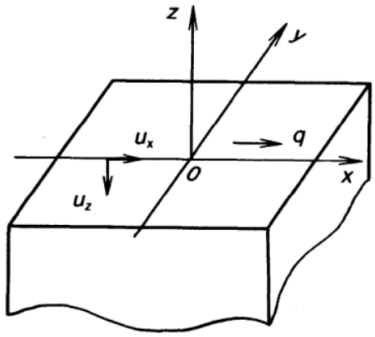

Figure 1.9: Schematic representation of Rayleigh wave's propagation and particles displacement in the material, u_x and u_z shows displacement of particles and q shows propagation of wave (reproduced from [38])

high mass sensitivities as well as their difficult fabrication [4].

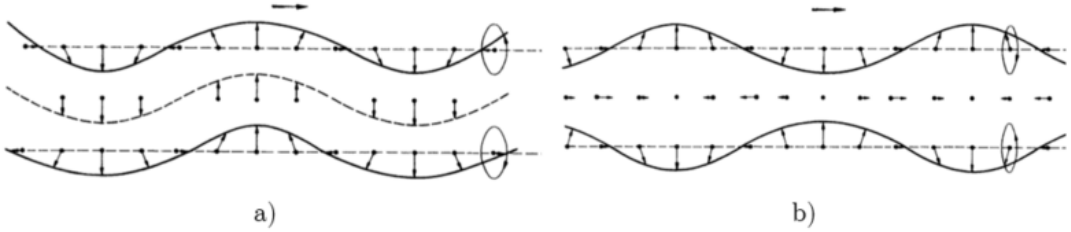

Figure 1.10: Schematic representation of two modes of Lamb waves, a) anti-symmetric mode and b) symmetric mode, (reproduced from [39])

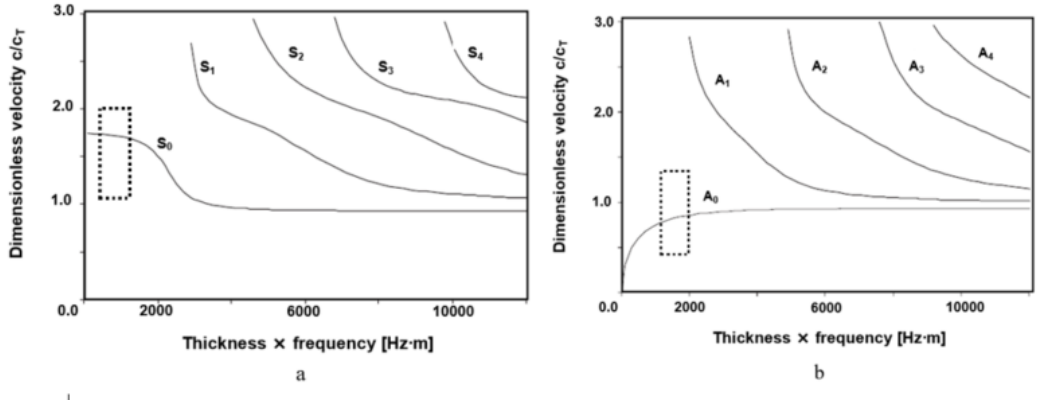

Figure 1.11: Dispersion of velocity of a) symmetric and b) anti-symmetric Lamb waves as a function of normalized thickness (reproduced from [40])

Love wave surface acoustic wave sensors (LW-SAW)

Love waves were firstly described by Mr. Love in 1911 as waves with pure shear horizontal motion. The displacement of particles in matter is then horizontal, parallel to the

free surface and perpendicular to the direction of propagation, as shown at figure 1.12 [41].

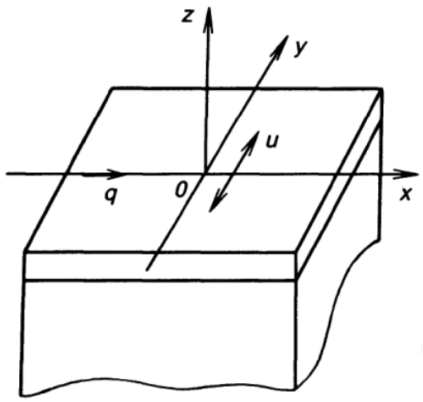

Figure 1.12: Schematic representation of Love wave's propagation and particles displacement in the material, u shows displacement of particles and q shows direction of propagation of wave (reproduced from [38])

For production of SH-SAW Love waves, the material of guiding layer must have lower acoustic velocity than the piezoelectric substrate. The acoustic energy is then concentrated in the guiding layer which leads to the increase of sensor's sensitivity and the thickness of the substrate does not influence the detection ability of the LW-SAW sensor [4]. When the thickness of the guiding layer is less than one-tenth of the acoustic wavelength, first-order perturbation theory can be used. The change of the operational frequency is then given by [37]:

$$\Delta f = -\frac{V}{4} f_0 \rho d \, [1 - (\frac{V}{V_{S2}})^2] \, |\hat{v}|^2_{z=0}, \tag{1.4}$$

where V is the acoustic phase velocity in the media, f_0 is the operational frequency, ρd represents the mass loading per unit area, the term $1 - (\frac{V}{V_{S2}})^2$ represents a reduction in mass sensitivity with the increase of the thickness of the layer and $|\hat{v}|^2_{z=0}$ is the particle velocity at the surface [37].

Typically, LW-SAW sensors operate on frequencies between 120 and 200 MHz in liquids. The penetration depth is dependent on the frequency – with increasing frequency, the penetration depth decreases. The sensitivity of the LW-SAW sensor increases by the square of frequency but it is affected also by choice of material and the design of guiding layer. LW-SAW sensors have the highest sensitivity among the acoustic sensors [4].

1.5 Diamond

Diamond is one form of carbon, which is the first element of the column IV in the periodic table with the atomic number six. Its electron configuration in the ground state is $1s^2,\ 2s^2,\ 2p^2$. The $1s^2$ state contains 2 strongly bound electrons, called core electrons. Remaining four electrons in the states $2s^2$ and $2p^2$ are called valence electrons. These electrons are involved in forming of chemical bonds. In the crystalline phase the electrons give rise to $1s,\ 2p_x,\ 2p_y$ and $2p_z$ orbitals that are important to form covalent bonds [42]. In the comparison with the energy gain in forming the chemical bond, the difference in the energy between the upper *2p* energy level and the lower *2s* energy level is relatively small (4 eV). This is reason why the electronic wavefunctions of these four electrons can mix with each other and electrons can change the occupation of *2s* and three *2p* atomic orbitals. This mixing of *2s* and *2p* orbitals is defined by sp^n hybridization. During the hybridization, the direction of chemical bonds is changed and the total energy of molecule is lower. Carbon processes three hybridizations: sp, sp^2 and sp^3 and can exists in many different forms, called allotropes [42, 43].

Table 1.2: The types of hybrid orbital sets and their orientation in space (reproduced from [44])

Hybrid orbitals	**Atomic orbitals used**	**Number of hybrid orbitals**	**Electron-pair geometry**
sp	$s + p$	2	Linear
sp^2	$s + p + p$	3	Trigonal-planar
sp^3	$s + p + p + p$	4	Tetrahedral

One of the well-known carbon allotropes is graphite, that is composed from sp^2 hybridized carbon [46]. In this type of hybridization, three identical in-plane orbitals with angles 120 ° are formed together with a fourth unhybridized p orbital perpendicular to the plane formed by the three other orbitals [45]. Carbon atoms can form a double bond. This bond is formed by combination of σ bond with π bond and contains two pairs of electrons [47]. Carbon atoms in graphite are bonded trigonally with another three carbon atoms in planar hexagonal rings [46]. The minimum distance of atoms in the hexagonal lattice is 1.42 Å. Layers of carbon hexagons are weakly bonded via Van der Waals force in the equilibrium distance of 3.4 Å [43]. Under the standard conditions, graphite is the

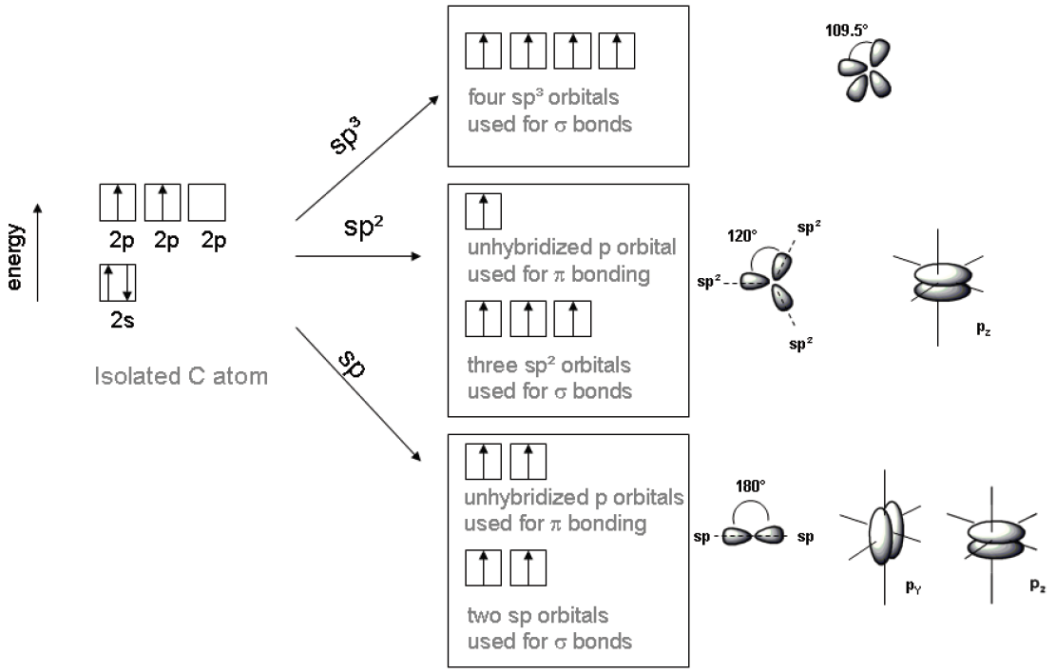

Figure 1.13: Possible hybridization of atomic orbital of carbon atoms (reproduced from [45])

stable form of carbon. In contrary to diamond, graphite is an electrical conductor with a resistivity of $3 - 60{\cdot}10^{-5}\ \Omega \cdot \mathrm{m}$ thanks to delocalization of π bond electrons.

Another well-known carbon allotrope is diamond that is formed by sp^3 hybridized carbon atoms. Four molecular orbitals with the same shape and energy are formed and each of them is occupied by one electron. Orbitals are arranged in a tetrahedral structure with an angle of 109.5 ° [45]. These orbitals have two lobes as p orbital, but they are of unequal size. It means that for each orbital is higher electron density on one side of the nucleus. This make possible to form stronger and much more stable bonds than unhybridized orbital. A sp^3 hybridized carbon can bonds with four σ (single) bonds [47]. Diamond lattice is formed from 8 atoms arranged in a cube. Each carbon atom is bonded to four atoms in a tetrahedral structure with an inter-atomic distance of 1.42 Å. Diamond is the hardest known natural mineral [48]. A sp hybridization is not important for this work and will not be discussed here.

Diamond is a very promising material in the field of biosensor technology due to its favorable properties such as chemical inertness and stability, superior hardness, biocom-

patibility, high electrical resistivity. Furthermore the recently developed surface chemistry allows different types of surface functionalization such as attachment of biomolecules or chemical modifications [49, 50]. In the case of biomolecules, their superior stability is a key point for practical use. Silicon dioxide (SiO_2) and gold are the most used materials for construction of biosensors, but direct interaction of proteins with their surfaces can cause protein's denaturation. Stability of proteins can be prolonged by co-immobilization of polyethylene glycol (PEG) molecules or lipid bilayers on Au or SiO_2 surface. Extended stability of proteins at physiological conditions was recently shown on diamond surface [51].

1.5.1 Diamond synthesis

Diamond can be obtained from nature by mining, but there are also synthesized artificially by High Pressure High Temperature (HPHT) method and Chemical Vapor Deposition (CVD). HPHT method is used for synthesis of bulk crystalline diamonds as well as diamond nanoparticles. Thin diamond films are formed from the gaseous phase via a chemical reactions by CVD method. This method is discussed in figure 3.1.1 [48, 52].

1.5.2 Surface functionalization

As it was mentioned, diamond is chemically inert. Nevertheless, several methods were developed to introduce various reactive groups on its surface. Diamond films with different film terminations can be used for attachment of different organic compounds as small molecules like allyl alcohol or complex structures as enzymes or DNA. Typically, the as-grown surface of CVD diamond layer is hydrogen terminated. Hydrogenated surface is very stable. H-terminated diamond is normally not conducting, but it shows p-type surface conductivity in air and hydrophobic wetting characteristics. The hydrophobicity is an issue for attachment of many hydrophilic biomolecules [45, 49, 53]. Oxidized diamond surface can be obtained by using oxygen plasma, chemical wet treatment or ozone treatment. This surface can carry different ketone related groups or so-called "bridge" configuration. In the ketone conformation, the oxygen is double-bonded to surface carbon atom (C=O). In the "bridge" formation, the oxygen atom is single-bonded to two surface carbon atoms (C-O-C). Additional oxygen containing species, such as hydroxyl (-OH) or carboxyl (-COOH), can be introduced on the diamond surface by chemical wet treatment.

On contrary to H-terminated surface, oxidized diamond surface is hydrophilic and is not electrically conducting [45, 49, 54].

Except these two basic terminations, further surface terminations of diamond were studied, such as introduction of halogen groups (fluorine, chlorine) or amino groups onto its surface [45, 54]. In this work we used diamond films terminated by amino groups. Several methods have been developed to NH_2 terminated diamond surface. For instance, Cl-terminated diamond is obtained by ultra violet (UV) illumination (245 nm/24 h) by an Hg-arc lamp of H-terminated pollycrystalline diamond (PCD) in Cl_2. Cl-terminated surface is UV illuminated (245 nm/24 h) under ammonia (NH_3). Another method to functionalize diamond surface with amino groups is ammonia plasma treatment. In the study of J. Miksovsky *et al.* gas mixture of 5% ammonia in nitrogen at working pressure 1.8 Pa and radiofrequency (RF) power 150 W was used during 5 minutes [55]. Direct ammination of diamond surface has also been reported. PCD was irradiated by UV light in ammonia gas flow [56].

2 | Aims of the study

This work aims to develop a diamond-based SAW sensor for bacteria detection. The sensor consists of a SH-SAW Love wave sensor coated with NCD layer on which specific bacteria bioreceptors are attached. To achieve this objective, following goals are studied:

Fabrication and characterization of LW-SAW sensor

1. **Development of microfabrication processes and LW-SAW fabrication methods**.
    - Photolithography
    - Etching
    - RF sputtering
    - CVD methods
2. **Characterization of fabricated LW-SAW sensors**
    - Study of effect of IDTs fabricated from different metals - Cr, Al.
    - Investigation of dependence of NCD layer thickness on the frequency response.
    - Measure the sensitivity of the fabricated LW-SAW sensor.

Attachment of bioreceptors to the diamond surface

1. **Bacteriophages T7 attachment study**
    - Microbiological methods: cultivation of bacteria, multiplication and purification of bacteriophages.
    - Diamond surface treatment: hydrogenation, oxidation and amination.

- T7 bacteriophage attachment studies.

2. **Bacteriophage's fiber tails attachment study**

   - Coating of NCD layer with silica layer.
   - Growth of copolymer layer on the silica coating.
   - Introduction of ligand to the surface of copolymer layer by click reaction.
   - Attachment of bacteriophage's fiber tails via His-tag linkers.

3 | Materials & methods

3.1 Fabrication methods

3.1.1 Thin film deposition methods

Diamond film preparation

Figure 3.1: CVD system AX5010

All of the NCD films used in this work were prepared using microwave plasma enhanced chemical vapor (PECVD) deposition system AX5010 from Seki Diamond System, Japan and microwave linear antenna plasma enhanced chemical vapor deposition system (MW-LA-PECVD) from Leybold Optics Dresden, Germany. Before deposition of diamond layer, samples were 1/ cleaned by sonication in Acetone, Isopropyl Alcohol (IPA) and distilled water for 10 minutes each and 2/ seeded with diamond nanoparticles by spin coating using nano-diamond dispersion in water (NanoAmando®B) from NanoCarbon Research Institute Ltd. Diamond layer can be deposited on different substrates that withstand deposition conditions, such as glass, silicon or quartz. To obtain semiconducting diamond, boron and phosphorous impurities can be added during deposition process.

The microwave (usually 2.45 GHz) generates a plasma with high energy electrons and a high degree of ionization [48]. CVD diamond deposition requires three main ingredients: 1/ a substrate pretreatment, 2/ a carbon-containing precursors and 3/ an atomic hydro-

gen. The pretreatment aims to create a large surface density of diamond seeds on the substrate's surface. The precursor mixture contains a carbon precursor (usually methane) mixed in hydrogen. The gas mixture is activated, either thermally (hot filament), or electrically (microwave plasma, DC-discharge) [45]. The role of the hydrogen is crucial for diamond growth as it stabilizes diamond surface's sp^3 dangling bonds during growth [57]. The most important "growth species" promoting the diamond growth are CH_3 radicals that are formed by reaction of atomic hydrogen with methane:

$$CH_4 + H^* \leftrightarrow CH_3^* + H_2 \tag{3.1}$$

This chemical reaction is more favorable from the energy point of view from left to right [45]. Process of diamond growth is illustrated on the figure 3.2. At first, hydrogen radical from plasma reacts with hydrogen at the surface and form H_2. Then reaction of dangling bond with CH_3 or H occurs. Probability of reaction with H is much more higher than reaction with CH_3 species. When the dangling bond reacts with CH_3 radical, CH_3 is formed on the surface. When this reaction happened with both free dangling bonds, hydrogen radicals can react with the CH_3 on the surface and remove one hydrogen from CH_3 and CH_2 is formed. This radical reacts with CH_3 on the surface.

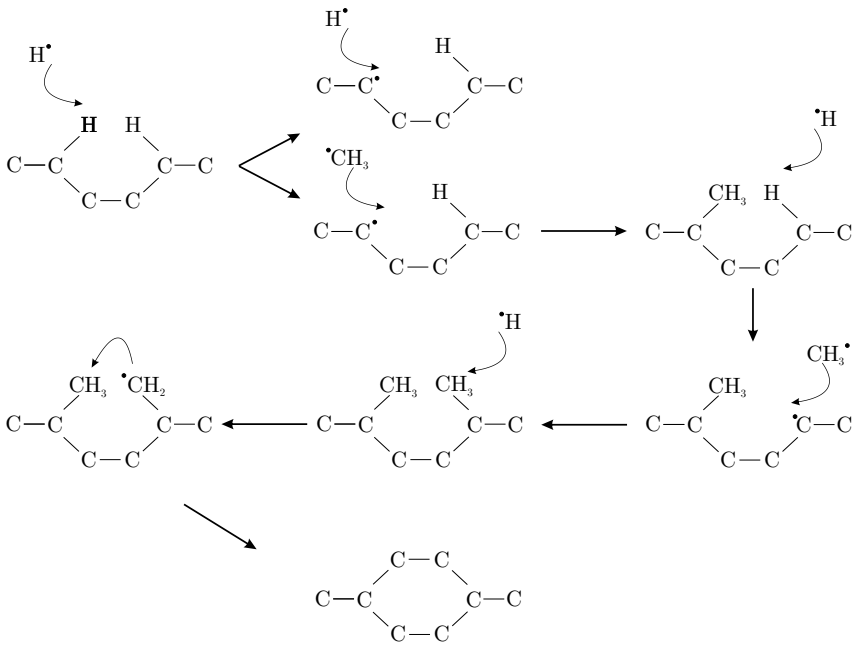

Figure 3.2: Illustration of the role of CH_3 as a growth species of diamond (redraw from [45])

Sputtering method

Figure 3.3: Home made magnetron sputtering system

All metal layers used in this work were deposited by sputtering method. Sputtering deposition is low temperature and low pressure physical vapor deposition (PVD) technique. Various sputtering methods have been developed to increase deposition rate and to deposit non conductive materials - magnetron sputtering, DC sputtering, triode sputtering, reactive sputtering or RF sputtering. An electric discharge is created between two electrodes in a low pressure gas and positive ions (usually argon) presented in plasma are accelerated towards the negatively bias target made of the material to be deposited. Sputtered particles due to ion bombardment on the cathode condense on substrate's surface [58]. Aluminum and titanium layers were deposited at Institute of Physics CAS, v.v.i. using an home made magnetron sputtering system. Chromium layers were deposited at J. Heyrovsky Institute of Physical Chemistry CAS, v.v.i. using Quorum Technologies Q300TD system by DC sputtering.

3.1.2 Microprocessing methods

Photolithography

Photolithography was used for the fabrication and patterning of IDTs. Desired patterns are transferred on the thin layer of photo sensitive material deposited on substrate's surface using light ray [59]. Typically, a mask aligner is used for exposition of photoresist. The mask is in direct contact with the sample and whole surface is exposed at once. In this work, we used a maskless direct-writing laser photolithography machine Micro Writer ML from Durham Magneto Optics Ltd [60]. Masks were designed using CleWin 5 software from PhoeniX Software company. Two types of photoresist were tested – Positive photoresist ma-P 1210 and Negative photoresist ma-N 1410 (from Micro resist technology). After exposure, samples were developed in ma-D 331 (positive photoresist) or ma-D 533/S developers (negative photoresist) obtained from Micro resist technology. From exposed

areas, positive photoresist is removed whereas negative photoresist stays and is removed from unexposed areas.

Etching

Figure 3.4: VacuTech 1540 apparatus used for dry etching

Two types of etching techniques were used – wet etching and dry etching, i.e. reactive ion etching. Dry etching refers to etching method using ion bombardment (usually from plasma) of reactive gas (O_2, N_2, CF_4, CCl_4, Cl_2) or none reactive gases (Ar, Kr, ...) accelerated with high energy. Dry etching methods are usually anisotropic [61]. Reactive ion etching was tested on silicon and diamond substrates using VacuTech 1540 series plasma system at Institute of Phycics CAS, v.v.i.

Wet etching, a liquid chemical etching, is a simple and cheap method. Table 3.1 shows few examples of etchant's composition for different metals with their etching rates. Most of the etchants contains acids, especially hydrofluoric acid (HF) that is extremely dangerous, so worker should wear specific protections (chemically resistant glasses, lab coat and gloves). Wet chemical etchant can be isotropic like metal etchant or anisotropic like potassium hydroxide (KOH) for Si etching.

Table 3.1: Composition and etching rates of etchants for different metals

Metal	**Etchant composition**	**Etching rate**
Al	$H_3PO_4 : HNO_3$ $CH_3COOH : H_2O$	1μm/min at 20 °C
Cr	$(NH_4)_2[Ce(NO_3)]_6 : HClO_4 : H_2O$	60 nm/min at room temperature
Au	$KI : I_2 : H_2O$ (4 g : 1 g : 40 ml)	1 μm/min

Wet etching was tested on aluminum, chromium and gold layers. Samples were immersed into appropriate mixture and time was unfolded according to etching rate and thickness

of metal layer. Several washing steps followed after the etching. Samples were sonicated in distilled water for removing of etchant residues, in acetone for removing photoresist layer and distilled water for 5 minutes each at 50 °C.

3.2 Characterization methods

3.2.1 Optical microscopy

Figure 3.5: Carl Zeiss optical microscope

Optical microscopy uses visible light and its resolution is limited by diffraction of light and is given by equation:

$$d = \frac{\lambda}{2 \cdot NA}, \tag{3.2}$$

where λ is wavelength of light and NA is numerical aperture of microscope. In practice the lowest resolution limit of standard optical microscope is above 200 nm [62]. In this work, Carl Zeiss optical microscope was used to check microstructures fabricated by photolithography at Institute of Physics CAS, v.v.i.

3.2.2 Transmission electron microscopy (TEM)

In TEM, electrons go through a thin sample and are scattered. Their kinetic energy and angular distribution is changed. In the mass thickness contrast imaging, electrons are scattered in the wide range of angles, but only electrons scattered through an angle smaller than $\sim 10^{-2}$ mrad can contribute in the forming of image. Scattering of the electrons is stronger in the sample's region that are thicker or with higher density. More electrons are scattered through an angle grater than 10^{-2} mrad causing that these areas appear darker in the image. This contrast is exhibited by all specimens - amorphous and crystalline. Staining with heavy metals can be used for observation of biological samples. Areas with incorporated stain becomes darker in the resulting image [62]. Transmission

electron microscope Phillip CM100 was used for observation of bacteriophages at the Microbiological institute CAS, v.v.i. TEM image allows to recognize presence of nucleic acid inside bacteriophage's head.

TEM samples with bacteriophages were prepared on 3 mm diameter copper grid (400 mesh and more) with very thin carbon film. These disks were first activated using a glow discharge. Then 5 - 10 μl of bacteriophages suspension was dropped on activated grid for bacteriophages absorption. The suspension was removed by a strip of filter paper after 1 min and immediately after that the grid was washed with a 1% suspension of ammonium molybdate in distilled water for 30 seconds. Rinse solution was removed by filter paper and 2% of uranyl acetate in distilled water was added for 30 seconds. Then the uranyl acetate was removed and grids were left to dry in the Petri dish on filter paper.

3.2.3 Scanning electron microscopy (SEM)

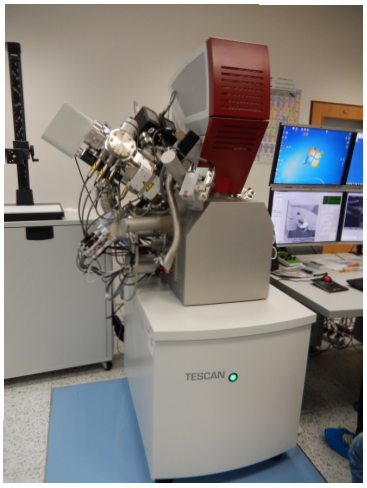

Figure 3.6: Used SEM microscope Tescan FERA3

SEM has been used for observation of surfaces and microstructures of diamond thin films before and after chemical functionalization and observation of bacteriophages. Different types of observation modes exist depending on the type of detected electrons – secondary electron imaging and backscattered electron imaging. Secondary electrons are released from valence orbital during the interaction with high-energy primary electron and their kinetic energy is below 50 eV. Backscattered electrons are primary electrons that undergo large deflections and leave the surface without a significant kinetic energy loss [62]. Before imaging, samples are glued onto aluminum stubs (holders) using a SPI Conductive Carbon Paint or carbon tape NEM tape from Nisshim Em.Co.LTD. Three scanning electron microscopes were used in this work: Tescan FERA3 at Institute of Physic CAS, v.v.i., Nova^{TM} NanoSEM 450 at Institute of Organic chemistry and biochemistry CAS, v.v.i. and Nova^{TM} NanoSEM 450 at Microbiological institute CAS, v.v.i.

3.2.4 Atomic force microscopy (AFM)

Surface morphology and surface roughness of diamond layers were measured by AFM. In this technique a sharp tip, about 2 μm long and approximately 20 nm in diameter at its apex is located on the free end of the cantilever and scans over the sample's surface. Forces between the tip and the sample's surface cause bending or deflection of the cantilever. The position of cantilever is detected optically using a laser beam, that is reflected from back side of cantilever onto a position-sensitive detector and map of surface topography is generated [62]. This mode is not suitable to measure soft synthetic materials or biomaterials. Tapping mode can be used for this purposes. The cantilever vibrates at its fundamental flexural resonance frequency. The amplitude of the vertical oscillation must be large enough to overcome adhesion forces between tip and surface. When the tip goes close to the surface, the Z scanner is displacing the cantilever to keep constant amplitude of oscillations in surface elevations. This Z scanner displacement is measured and image of surface morphology can be constructed. Another mode, that can be used to determine the surface hardness or adhesive forces, is Peak Force mode. The force is controlled by using maximal exerted force of the tip on the sample in each pixel of image. From an analysis of obtained force-displacement curve can be determined sample deformation, stiffness or adhesive forces [63]. In this work we used Icon Dimension, Brüker at Institute of Physics CAS, v.v.i. All measurements were done at room temperature.

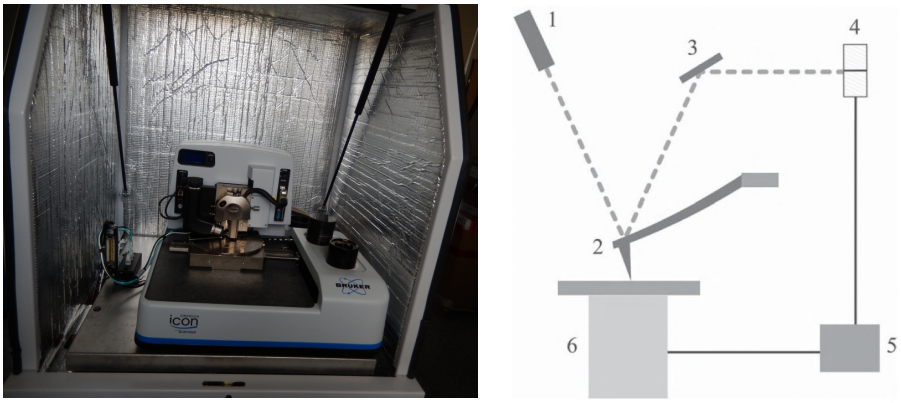

Figure 3.7: a) Used AFM microscope Icon Dimension, Brüker b) Schematic diagram of an AFM: 1. laser diode, 2. cantilever and tip, 3. mirror, 4. position-sensitive photodetector, 5. electronics and 6. piezoelectric scanner with sample, reproduced from [64]

3.2.5 Raman spectroscopy

The quality of diamond layer was investigated using Raman spectroscopy. This optical spectroscopy method is based on inelastic Raman scattering of light with mater. Incident light with energy $h\nu_0$ exchange energy with mater that leads to the emission of light with energy of $h\nu_0 \pm h\nu_s$. When the material is in their vibrational ground state, there are emitted quanta with lower energy – Stokes shift ($h\nu_R = h\nu_0 - h\nu_s$). When the molecule is in their vibrational excited state, emitted quanta has higher energy – Anti-Stokes shift ($h\nu_R = h\nu_0 + h\nu_s$), as is shown in figure 3.8 [65].

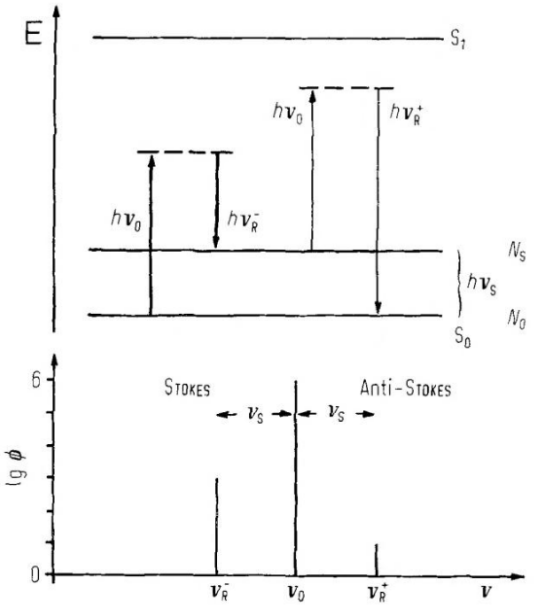

Figure 3.8: Principle of Raman scattering: The photon with energy $h\nu_0$ hits the molecule, molecules in the vibrational ground state may lead to vibrational excited state, the photon with energy $h\nu_R^- = h\nu_0 - h\nu_s$ is emitted. Some molecules are in excited state, the process which produces photon with energy $h\nu_R^+ = h\nu_0 + h\nu_s$ is also possible. In the Raman spectrum two peaks with different frequency than excited radiation ν_0 can be observed. Raman line with lower frequency ν_R^- (the Stokes line) and Raman line with larger frequency ν_R^+ (the Anti-Stokes line) (Reproduced from [65])

Raman signal depends on crystalline structure, elements and chemical bonds of studied materials. Raman spectroscopy is widely used in diamond technology as a quick test to determine the quality of diamond i.e. non diamond carbon concentration (i.e. sp^2 carbon), as well as others impurities as boron (peak at 500 cm^{-1}), nitrogen, silicon,... via their photoluminescence. Diamond has a well-known Raman peak at 1332 cm^{-1}. In CVD

diamond, one can also observe peaks at 1600 cm^{-1} (so called G band) and 1345 cm^{-1} (so called D band) attributed to sp^2 carbon forms as well as peaks at 1100 – 1150 cm^{-1} and 1430 – 1470 cm^{-1} attributed to transpolyacetylene [66]. Raman spectroscopy were also used for confirmation of sp^2 formation after annealing process. From Raman spectra can be calculated $\frac{sp3}{sp2}$ ratio using fitting of attributed peaks by Lorentzian function in OriginLab software and area under the curve for each peak is obtained. For 488 nm excitation laser wavelength is $\frac{sp3}{sp2}$ ratio then given by equation:

$$\frac{sp^3}{sp^2} = \frac{0.75 \cdot S_{sp^3}}{0.75 \cdot S_{sp^3} + S_{sp^2}} \tag{3.3}$$

where S_{sp^3} is area under the sp^3 peak and S_{sp^2} is area under the sp^2 peaks.

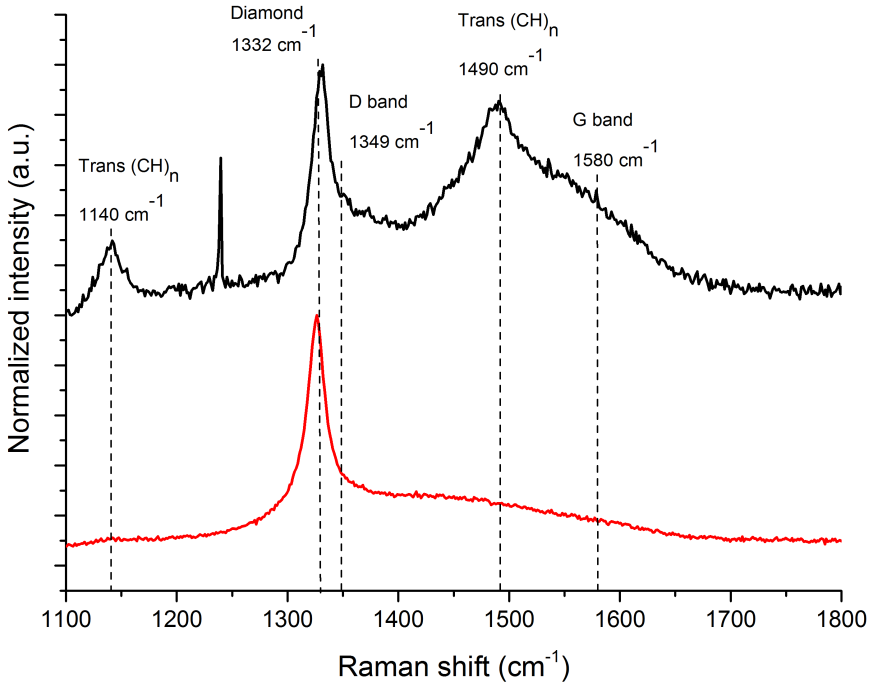

Figure 3.9: Raman spectra of CVD nanocrystalline diamond layer. Red line - NCD layer without impurities, clear diamond peak at 1332 cm^{-1}. Black line - NCD layer with a significant fraction of non diamond carbon, diamond peak at 1332 cm^{-1}, peaks attributed to sp^2 forms of diamond D and G band are observed as well as peaks attributed to transpolyacetylene. Peak around 1250 cm^{-1} is probably related to cosmic rays

Raman spectroscopy does not need samples preparation. Measurements are performed in the dark room at room temperature. All samples were measured using a Renishaw InVia Raman microscope with a 488 nm excitation laser (at power 25 mW). Measured data were

processed in OriginLab software and Raman spectra were normalized to diamond peak.

3.2.6 Polarization Modulation Infrared Reflection Absorption Spectroscopy (PM-IRRAS)

PM-IRRAS was used to check attachment of polymer and protein layers on the diamond surface. This method is based on the selective absorption of s- and p-polarized light at the sample (usually a metal) interface, i.e. sample surface and surrounding gas phase. The metal layer does not absorb s-polarized (polarization perpendicular to the plane of incidence) light, therefore all measured signal is pertained to gas phase. In contrast, p-polarized (polarization parallel to the plane of incidence) light excites both gas phase and investigated surface. Subtraction of both spectra gives specific vibrations of molecules adsorbed on the metal surface [67]. This method does not need samples preparation. To study the diamond surface functionalization using PM-IRRAS, diamond layers were deposited on top of titanium layer acting as a mirror. Measurement were done using Nicolet 6700 with PEM module at Institute of organic chemistry and biochemistry CAS, v.v.i. Data were processed in OMNIC software and OriginLab software.

3.2.7 X-ray photoelectron spectroscopy (XPS)

The main principle of X-ray photoelectron spectroscopy (XPS) is photoemission. As the name implies, the electrons are ejected from a core level by an X-ray photon with energy $h\nu$. The kinetic energy of ejected electron is measured by spectrometer. The kinetic energy of the electron is related to the energy of the X-ray photon and it is not an intrinsic properties of studied material. The electron binding energy is given by [68]:

$$E_B = h\nu - E_K - W \tag{3.4}$$

where $h\nu$ is energy of incident X-ray photon, E_K is kinetic energy of ejected electron and W is spectrometer work function. All of these three energies are known or measurable so binding energy of ejected electron can be calculated. Electron binding energy identifies specifically its parent element as well as atomic energy level. Process of photoemission is shown on figure 3.10a), where the electron is ejected from K shell of atomic orbital (a 1s photoelectron). Figure 3.10b) shows that electrons that are excited and escape with-

out energy loss give rise to characteristic peaks at the spectrum. Electrons that undergo inelastic scattering and lose their energy contribute to the formation of background of spectrum [68].

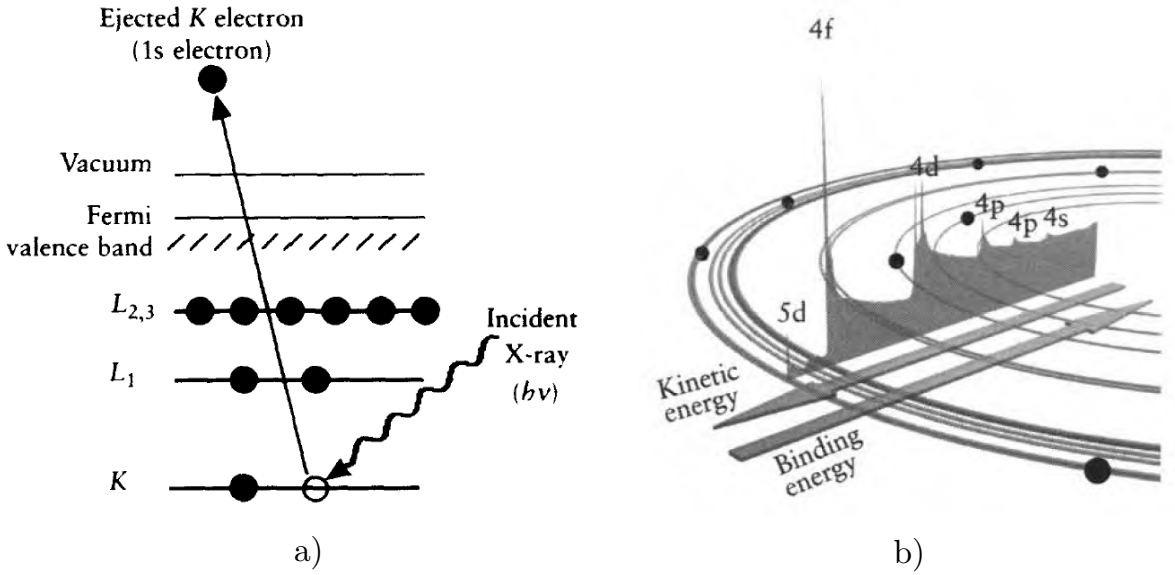

Figure 3.10: a) Schematic diagram of XPS process with ejection of electron from K shell, b) Schematic of electronic structure to illustrate how each electronic orbital contributes in formation of photoelectron lines, reproduced from [68]

In this work XPS analysis was used for confirmation of presence specific functional groups attached to the diamond surface after its functionalization. ESCA PROBE P (Omicron Nanotechnology Ltd.) with aluminum anode (energy 1486.7 eV) was used. Measurements were performed at very low pressure 10^{-8} Pa in CAE mode. Sputtering of surface was done using argon ions with energy 5 keV for 5 minutes. Data were processed in CASA XPS software and they were corrected to 1s orbital of carbon.

3.2.8 Contact angle measurement

Contact angle measurement was used to determine wettability of diamond surfaces after surface treatment. Wettability is ability of liquid to maintain contact with a solid surface. This property is determined by microscopic molecular interactions of liquid, solid surface and air, such as short-ranged chemical interactions and long-ranged van de Walls forces. Wetting can be described by Young's equation [69]:

$$\gamma^{lv} \cdot \cos\theta = \gamma^{sv} - \gamma^{sl} \tag{3.5}$$

where γ^{lv}, γ^{sv} and γ^{sl} are liquid-vapor, solid-vapor and solid-liquid interfacial tension and θ is the local contact angle between liquid and the solid surface. When the contact angle is grater than 90 °, surface is hydrophobic. If the contact angle is smaller, surface is called hydrophilic [69].

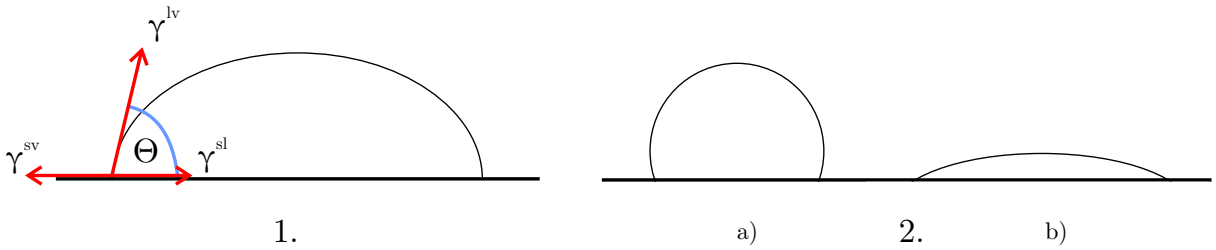

Figure 3.11: 1. Contact angle between liquid and solid surface is affected by interfacial tensions γ^{lv}, γ^{sv} and γ^{sl}, 2. Two surfaces with different wettability: a) hydrophobic surface and b) hydrophilic surface

On each sample was dropped at least three drops of distilled water with a volume of approximately 1-2 μl by a Hamilton syringe and the contact angle was measured immediately after the stabilization of drops. Droplet's shape was approximated by a software using Young-Laplace equation to calculate contact angle. Mean value and standard deviation was calculated for each sample. Measurement were done at Joint Department of Biomedical Engineering CTU and Charles University in Prague.

3.2.9 LW-SAW characterization

Surface acoustic waves are excited and detected by lithographically fabricated IDTs on the surface of piezoelectric crystal. Transducers work most efficiently when their periodicity d matches to SAW wavelength λ. This occurs, when they are excited at the synchronous frequency f_0 given by equation 1.2. When array of fingers (IDTs) is excited with alternating voltages $V_n = (-1)^n V_0$, the wave potential for a rightward propagating wave ϕ^+ is given by equation [15]:

$$\phi^+(0) = \mu_s V_0 \sum_{n=0}^{N_f-1} (-1)^n e^{-jn(kd)/2} \tag{3.6}$$

when N_f is the total number of fingers, μ_s is a substrate-dependent constant. When $\frac{kd}{2} = m\pi$, and k = $\frac{2\pi}{\lambda}$, then $m = \frac{d}{\lambda}$. This equation give relationship between SAW

wavelength λ and IDT periodicity d. When m is a odd number, the IDTs are excited by odd harmonics and constructive addition occurs, as is shown in figure 3.12 [15].

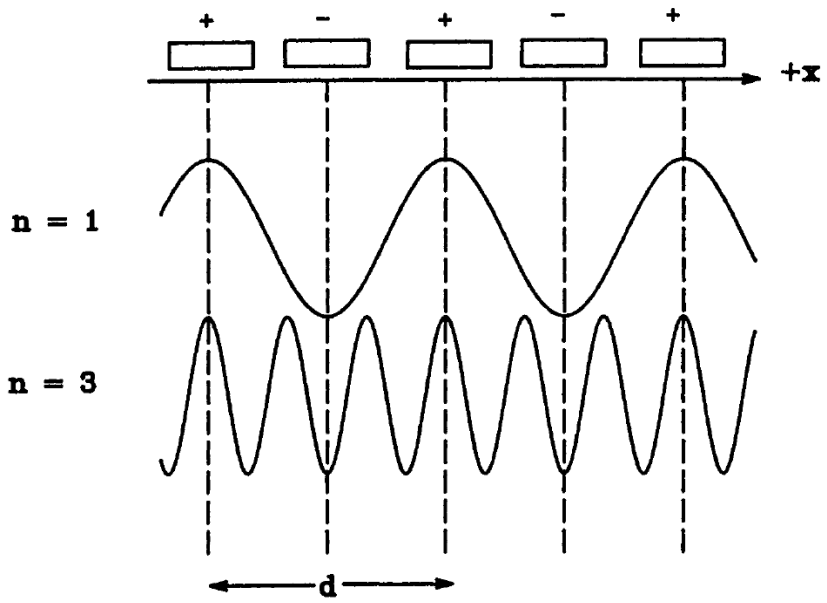

Figure 3.12: Relationship between transducer periodicity and excited waves (reproduced from [15])

The frequency response of IDTs is given by equation [15]:

$$\phi^{+}(f) = \left| \frac{sin(X)}{X} \right| \tag{3.7}$$

in which

$$X = \frac{N_p \pi (f - f_0)}{f_0} \tag{3.8}$$

where f_0 is the transducer's frequency and N_p is the number of IDT period: $N_p = \frac{N_f}{2}$. It is obvious, that when X = π then $\phi^{+} = 0$ and it results in complete cancellation of wave propagation. The transducer bandwidth B is given by [15]:

$$B = \frac{2}{N_p} \tag{3.9}$$

where N_p is number of IDTs fingers. Typical response of IDTs is shown in figure 3.13. There are two main material parameters used in SAW sensor design - the electromechanical coupling coefficient K^2 and SAW velocity. K^2 is the measure how efficiently given piezoelectric material converts electrical signal into mechanical energy associated with acoustic waves. Values for some typical piezoelectric materials are given in table 3.2.

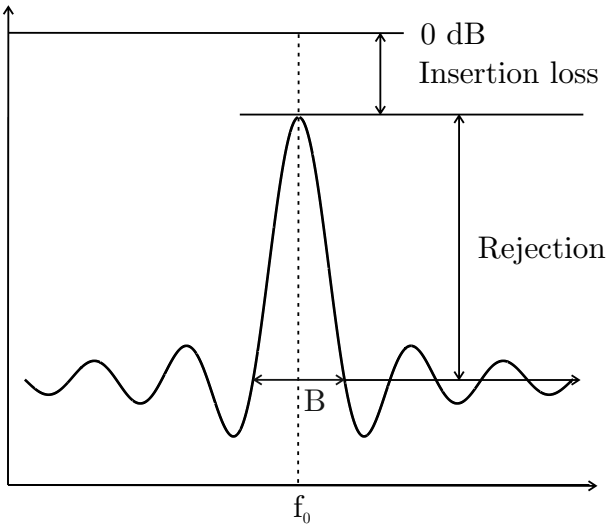

Figure 3.13: Transducer's frequency response

Table 3.2: Parameters for selected piezoelectric materials, (reproduced from [70])

Material	**Crystal cut**	**SAW axis**	**Velocity (m/s)**	K^2 **(%)**
Quartz	ST	X	3158	0.11
$LiNbO_3$	Y	Z	3488	4.5
$LiTaO^3$	Y	Z	3230	0.72

In this work, frequency measurement was performed using E8364B PNA Series Network Analyzer and 9000 Analytical Probe Station from SUMMIT Cascade Microtech with Infinity Probes. Calibration has to be done before the measurement. Both S_{21} transmission and S_{22} reflection parameters were measured in magnitude and phase of fabricated SAW sensors. Magnitude of S_{21} parameter is related to the frequency response of the sensor. In the figure 3.14a) can be seen attached probe to the IDTs electrodes with Network Analyzer and in figure 3.14b) is shown probe station with microscope.

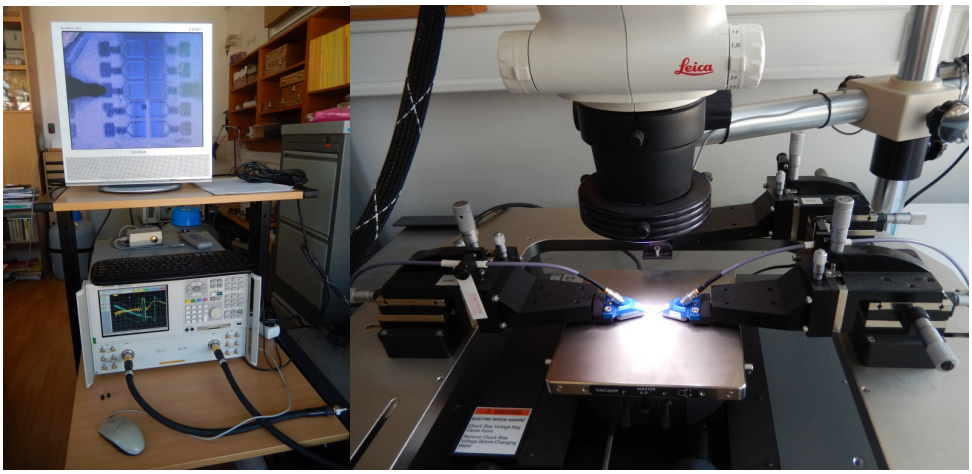

a) b)

Figure 3.14: a) E8364B PNA Series Network Analyzer and b) 9000 Analytical Probe Station

3.3 Microbiological methods

All of the microbiological work was done at Microbiological institute CAS, v.v.i. and all of used materials were obtained from this institute.

3.3.1 The plaque assay method

For the determination of phage concentration or the verification of the bacterial lysis we used the plaque assay method. The result is expressed as pfu/ml. One plaque correspond to the one infective particle. The principle of this method is based on the ability of single phage particle to lyse one host bacteria growing on Petri dish (with growth media). Realizing progeny lyse surrounding bacteria and the visible clear area called "plaque" is formed [71].

3.3.2 Bacterial cell culture

There are a plenty of bacteria species in our world with various optimal cultivation conditions. The composition of culture medium is variable and is largely determined by the nutritional requirements of the organism to be cultured [72].

Bacteria can be cultured using solid or liquid medium. In liquid medium an aliquot of the organism to be grown is inoculated into flask and left on an orbital shaker to ensure that

culture is kept in suspension. Solid medium are prepared by solidifying of selected liquid medium with 1 – 2 % of an seaweed agar extract. Diluted bacterial culture is spread onto a soft agar's surface using a sterile inoculating loop [72].

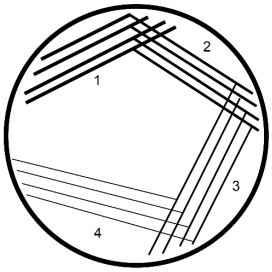

Figure 3.15: Scheme of inoculating of bacteria culture onto the soft agar's surface

Bacterial growth curve

In laboratory, bacteria growth follow a geometric progression: $2^0, 2^1, 2^2, 2^3, ..., 2^n$, where n is the number of generations. This exponential growth does not correspond to the normal bacterial growth in the nature as it does not includes bacteria life cycle. In laboratory conditions four phases of the bacteria growth cycle are recognized [73].

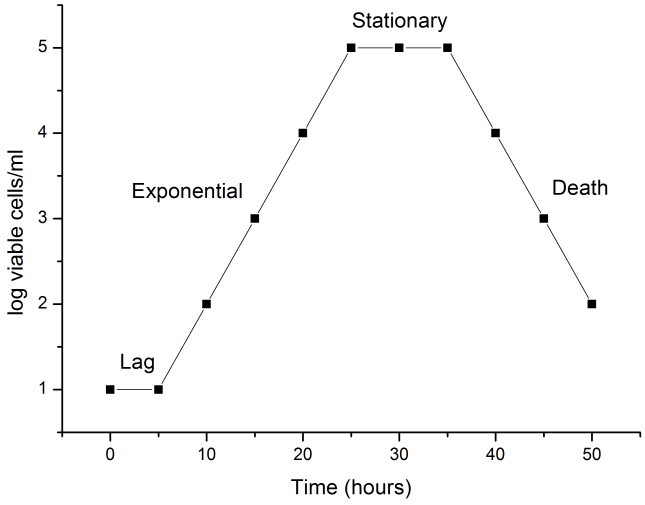

Figure 3.16: Typical bacterial growth curve includes four phases: lag, exponential, stationary and death phase

- **Lag phase**

  Lag phase occurs immediately after inoculation of bacterial cells into the fresh liquid

medium. The cells are not dividing, but their volume or mass is increasing due to synthesis of enzymes, proteins, RNA and their metabolic activity is increasing as well. The length of this phase depend on different factors as for example the size of the inoculum, time necessary for recovery from physical damage of shock, time required for synthesis of necessary coenzymes and new enzymes essential to metabolize the substrates in the culture medium [73].

- **Exponential (Log) phase**

  In this phase the cells are dividing and are growing by geometric progression. The rate of dividing of the cells is dependent on the composition of the growth medium and the conditions of incubation [73].

- **Stationary phase**

  Exponential phase cannot be continued forever in a close system such as test tube or flask. The end of the growth is determined by one of three factors: 1) depletion of nutrients 2) exhaustion of space and 3) accumulation of the inhibitors of metabolism. This phase is not necessarily the period of quiescence. Bacteria can produce secondary metabolites (metabolites produced after the active phase of the growth), such as antibiotics [73].

- **Death phase**

  If incubation continues after stationary phase, death phase follows. The number of viable cells is decreasing geometrically. It is reverse of the growth in the exponential phase [73].

3.3.3 Centrifugation

Centrifugation is a separation technique that is based on the behavior of the molecules in an applied centrifugal field. In a solution with the large particles left to rest, the particles will tend to sediment due to gravity. Main objective of the centrifugation is to exert a larger force than is gravitational field of Earth to increase sedimentation rate. The particles with different size, shape, density or molecular weight have different sedimentation rate that makes possible their separation by centrifugation. The tube with the solution containing particles for separation is located in the rotor of centrifuges [74].

4 | Results & discussion

4.1 Fabrication and characterization of SAW sensor

Figure 4.1 shows the schematic of the biosensor studied in this work: a Love wave - shear horizontal surface acoustic waves sensor. The sensor consists of crystalline quartz. Two types of quartz crystal cuts have been used - AT and ST cut. On the quartz are deposited a pair of metallic interdigitated electrodes covered by a thin layer (1 - 2 μm) of amorphous SiO_2. This sensor is then coated by a thin NCD layer for surface functionalization.

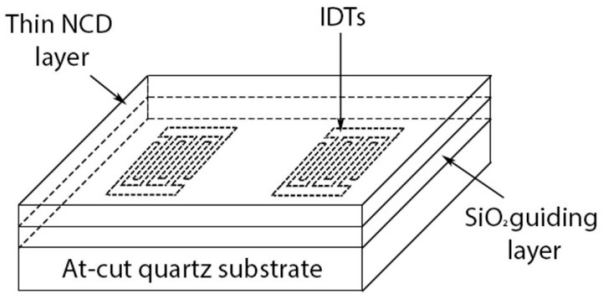

Figure 4.1: Schematic of LW-SAW sensor on quartz substrates with IDTs, SiO_2 guiding layer and thin NCD layer deposited on top. (Reproduced from [60])

4.1.1 Theoretical study of LW-SAW sensor

The theoretical study of LW-SAW sensors was carried out in collaboration with A. Talbi and A. Soltani at Joint International Laboratory LIA LEMAC/LICS-IEMN UMR CNRS 8520 in France. Theoretical calculations were carried out for a 1.3 μm thick SiO_2 guiding layer and for variable NCD layer thicknesses (0 - 100 nm). Legendre and Laguerre polynomial approach of wave propagation in layered magneto-electro-elastic structures was used for determination of the phase velocity and electromechanical coupling coefficient

(K^2) of these structures [75].

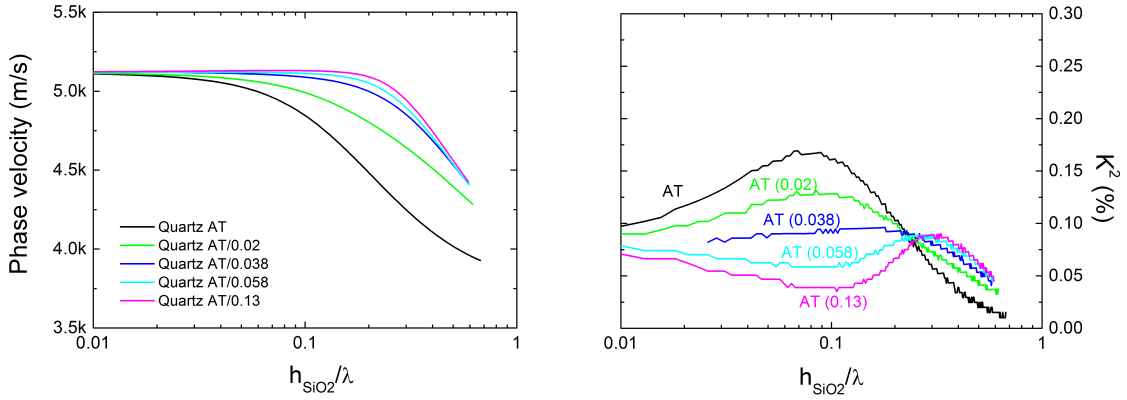

Figure 4.2: Phase velocity dispersion and electromechanical coupling coefficient curves for AT-cut quartz as a function of different SiO_2 normalized thicknesses for different diamond normalized thicknesses

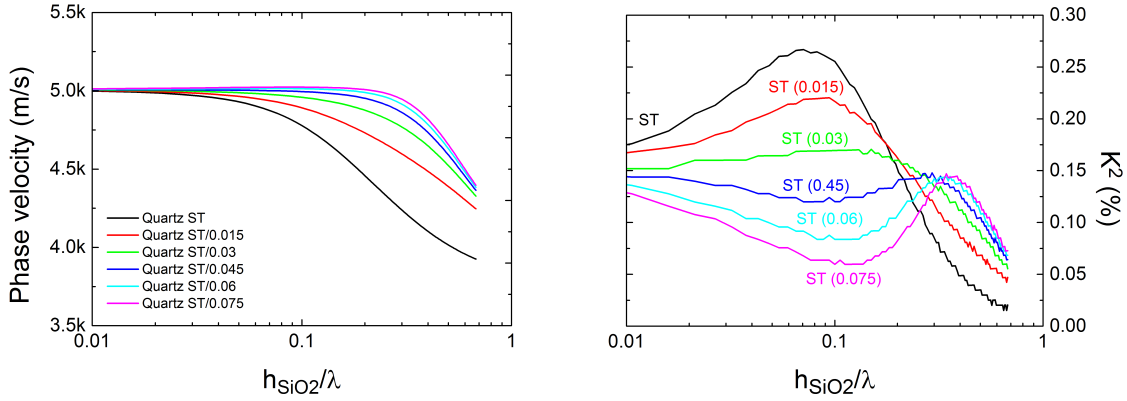

Figure 4.3: Phase velocity dispersion and electromechanical coupling coefficient curves for ST-cut quartz as a function of different SiO_2 normalized thicknesses for different diamond normalized thicknesses

Figure 4.2 and figure 4.3 show dispersion of phase velocity and the electromechanical coupling coefficient as a function of normalized SiO_2 thickness for various normalized diamond thickness. One can see, that electromechanical coupling coefficient is lower for AT-cut quartz crystal. LW-SAW without NCD coating shows a maximum K^2 coefficient for both cuts of crystal for a normalized SiO_2 thickness about $h_{SiO_2}/\lambda = 0.08$. It can be also observed, that for a given SiO_2 thickness, the addition of the diamond layer steadily decreases the K^2 coefficient. The strongest dispersion of K^2 coefficient is observed for $0.03 < h_{SiO_2}/\lambda < 0.3$. It can be also observed, that with increasing thickness of the diamond layer, phase velocity is increased as well. This is caused by increased surface rigidity. The slope or derivative of the phase velocity dispersion curves give information

on the sensitivity of the sensor. It can be seen that for $0.01 < h_{SiO_2}/\lambda < 0.09$ curves are almost linear which indicates a loss of sensitivity. Figure 4.4 shows, that with the addition of diamond layers, sensitivity of sensor decrease in region of SiO_2 normalized thickness to 0.1. It can be also observed, that for diamond normalized thickness from 0.045 there is a increase of the sensitivity in the region $0.1 < h_{SiO_2}/\lambda < 0.3$. Then the sensitivity decreases again.

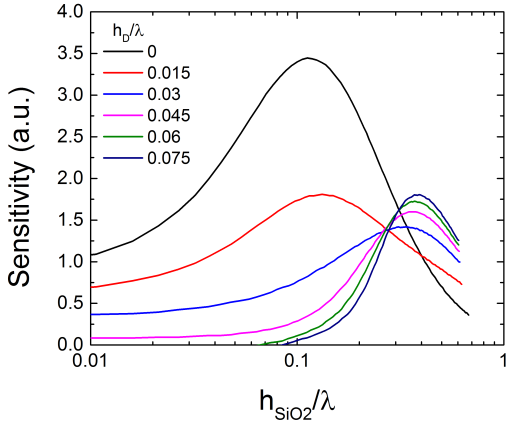

Figure 4.4: Sensitivity as a function of SiO_2 normalized thickness

According to these theoretical results, for fabrication of LW-SAW sensor it is necessary to minimize the NCD layer thickness and set h_{SiO_2}/λ to obtain a high electromechanical coupling coefficient and good sensibility of sensor. There are a few limitations in fabrication of LW-SAW sensors. It is not possible to deposit a closed diamond layer thinner than 50 nm due to initial nucleation density and the van der Drift growth mode. Another limitation is the spatial resolution of the microfabrication process (1 μm). In this work we used IDTs with spatial periods of 8, 12, 16 and 32 μm.

4.1.2 Methods for fabrication of LW-SAW sensor

Patterning of electrodes

IDT electrodes were patterned by a combination of photolithography and wet etching of metals. Metals were first deposited by sputtering technique and then patterned by wet etching using a photoresist mask prepared using photolithography technique.

1. Metal deposition by sputtering techniques

Metal layers were deposited by RF or DC sputtering as is written in chapter **??**. Aluminum and chromium were tested for IDTs fabrication. Deposition conditions of each metal are written in table 4.1.

Table 4.1: Conditions used for deposition of different metal layers

Metal	**Pressure (Pa)**	**Gas**	**RF power (W)**	**RF frequency (MHz)**	**Deposition rate (nm/min)**
Al	2	Ar (16 sccm)	200	13.6	25
Cr	2	Ar	-	-	10

2. Photoresist mask patterning

The patterning of photoresist mask requires several steps: 1/ deposition of photoresist, 2/ exposure of photoresist, 3/ development of photoresist and 4/ hard baking. Firstly, all of the samples were cleaned by sonication in Acetone and IPA for 15 minutes each followed by 10 minutes in distilled water. Two types of photoresist have been tested. Deposition conditions for each photoresist are reported in table 4.2. Deposition of photoresist was done in three steps: 1/ prebaking of the substrate, 2/ deposition of photoresist by spin coating and 3/ baking.

Table 4.2: Used conditions for deposition of photoresist layer

Photoresist	**Prebake**		**Spin coating**		**Baking**	
	Time (s)	Temperature (°C)	Time (s)	Speed (rpm)	Time (s)	Temperature ($°C$)
ma-P 1210	60	100	30	3000	60	100
ma-N 1410	90	100	30	3000	90	100

Photoresist layers were exposed using Micro Writer ML apparatus. Several parameters of the MicroWriter must be adjusted to optimize the photoresist exposure: quality of exposure (fast, normal, high), dose and focus correction, exposure mode (x or y raster) and used laser (5 μm, 1 μm or 0.6 μm). The wavelength of lasers is 405 nm. Influence of all of these parameters were investigated using different substrates and photoresist types. Developed optimal conditions are written in table 4.3. Hard baking of photoresist layer at

120 °C on a hot plate for 2 minutes was done to increase the resistance of the photoresist during metal deposition or etching.

Table 4.3: Optimal conditions for fabrication of IDTs on different substrates

Substrate	**Photoresist type**	**Laser's diameter (μm)**	**Quality of exposure**	**Exposure dose (mJ/cm^2)**	**Exposure mode**	**Developing time (s)**
SiO_2	ma-P 1210	0.6	Fast	71	Y raster	20
Si	ma-P 1210	0.6	Fast	105	Y raster	20
Al	ma-N 1410	0.6	Normal	370	Y raster	30
Cr	ma-N 1410	0.6	Normal	351	Y raster	30
Au	ma-N 1410	0.6	Normal	370	Y raster	30

Reactive ion etching - RIE

In this work we studied RIE of diamond for potential fabrication of diamond microcantilever sensor. We studied not only etching rate of diamond but also aluminum and silicon. Determination of etching rate of aluminum is important as aluminum is used as hard mask for diamond etching. Simple Al patterns were fabricated by photolithography and wet etching technique to determine the etching rate of diamond and Al. RIE conditions are reported in table 4.4.

Table 4.4: RIE conditions for diamond and silicon

Pressure	**RF power**	**Gases (sccm)**		
(Pa)	**(W)**	**O_2**	**CF_4**	**Ar**
26.6	400	40	2	10

Diamond and Si samples with Al mask were etched for different time durations (30, 60 and 90 min). To determine etching rates, the samples with Al mask were measured before RIE etching, after RIE etching and after Al mask removal by wet etching (see figure 4.5) using a profilometer KLA Tencor P-6.

Figure 4.6 shows etched thickness of Al, Si and diamond as function of etching time. Calculated etching rates are reported in table 4.5. One can notice the low etching rate of

Figure 4.5: Procedure for determination of RIE rate of different materials, 1. Diamond or Si substrate with Al mask, 2. Etched substrate with etched Al mask, 3. Etched substrate after removal of Al mask

Al in comparison to diamond and Si, which confirms its usability as a hard mask for RIE of diamond.

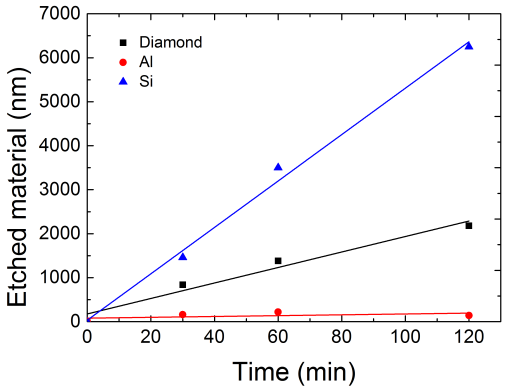

Figure 4.6: Calibration curves for etching of diamond, aluminum and silicon substrate

Table 4.5: Calculated etching rates for different materials

	Diamond	**Aluminum**	**Silicon**
Etching rate (nm/min)	23	3.4	53

Diamond deposition

1. Deposition of NCD layers

Before diamond deposition, samples were sonicated in IPA for 15 min and in distilled water for 10 min. After the cleaning procedure, samples were seeded by spin coating with nanodiamond dispersion. Deposition conditions for diamond layers deposited in AX5010 are reported in table 4.6. Diamond layers were deposited on Si and glass substrates. We noticed a variation in deposition rate with the type of substrate. The deposition rate on Si substrates is about 50 nm/h whereas it is about 100 nm/h on SiO_2. This difference might be attributed to different substrate temperature. Figure 4.7 shows AFM image of 100 nm thick NCD layer deposited on silicon substrate. The layer is smooth and homogeneous

without any pinholes. Raman spectra shows clear diamond peak at 1332 cm^{-1}. Peaks at 1140 and 1490 cm^{-1} are related to transpolyacetylene and disappears after annealing at high temperature.

Table 4.6: Deposition conditions of NCD layer using AX5010 apparatus

Power	**Pressure**	**Temperature**	**Gases (sccm)**			
(W)	**(kPa)**	**(°C)**	**H_2**	**CH_4**	**O_2**	**TMB**
1050	5	700	398	2	0.2	0

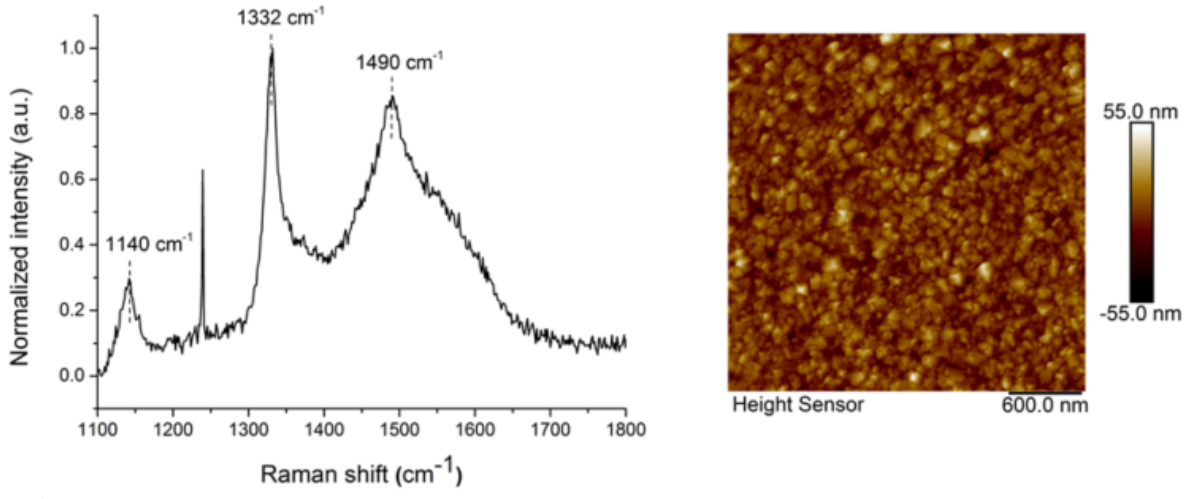

Figure 4.7: Raman spectra (left) of NCD layer deposited using AX5010 apparatus shows diamond peak at 1332 cm^{-1}. Peaks at 1140 cm^{-1} and 1490 cm^{-1} are related to transpolyacetylene. AFM picture (right) demonstrate homogeneous layer without pinholes.

In this work, NCD diamond thin films were also prepared using MW-LA-PECVD system. One main advantage of this system is deposition at low temperature (< 500 °C), which is necessary to preserve piezoelectric properties of quartz crystal. An example of deposition conditions for NCD layer used for attachment of bacteriophage's fiber tails are given in table 4.7. AFM picture in figure 4.8 shows homogeneous and smooth 200 nm thick NCD diamond layer deposited on titanium layer. Raman spectra of this NCD layer shows a clear diamond peak at 1332 cm^{-1}.

Table 4.7: Deposition conditions of NCD layer using MW-LA-PECVD system

Power	**Pressure**	**Temperature**	**Gases (%)**			
(kW)	**(Pa)**	**(°C)**	**H_2**	**CH_4**	**CO_2**	**TMB**
2x2.75	32	< 500	92	5	3	0

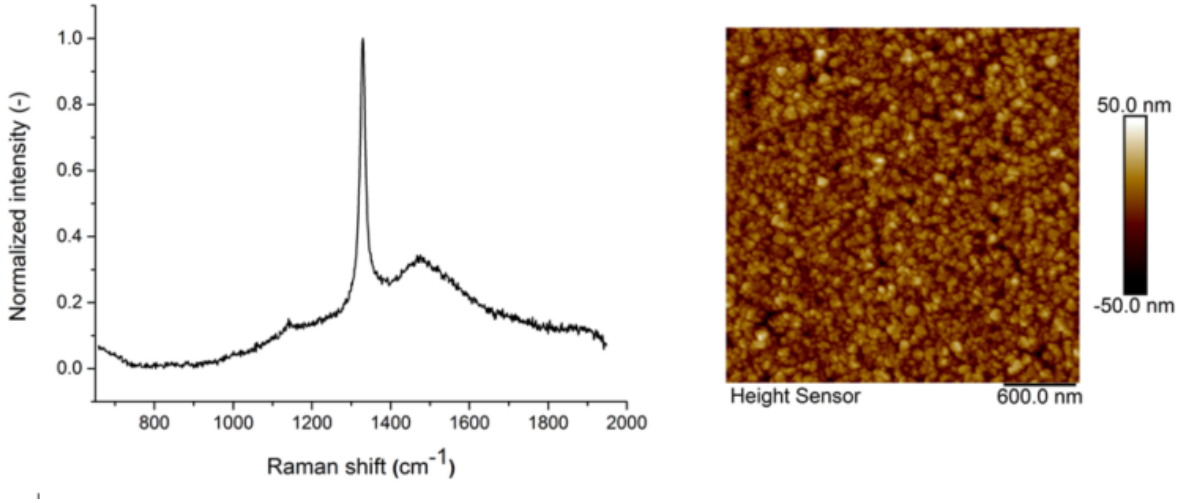

Figure 4.8: Raman spectra (left) of 200 nm thick diamond layer, clear diamond peak at 1332 cm^{-1}, peaks at 1150 cm^{-1} and 1470 cm^{-1} are related to transpolyacetylene. AFM picture (right) of NCD layer

2. Deposition of boron doped epitaxial diamond layer on (100) substrate

Deposition of epitaxial boron doped diamond layers was carried out to obtain flat conductive surfaces for observation of bacteriophage's attachment by SEM. This depositions were carried out in the AX5010 system. Preparation of high quality epitaxial layers requires careful preparation and several deposition steps. Diamond substrates from Sumitomo Electric Hartmetall GmbH have been first carefully repolished to remove damage of previous rough polishing and to produce a smooth surface. Polished samples were then carefully chemically cleaned. Single crystal substrates were immersed into mixture of H_2SO_4 with KNO_3 at 180 °C for 10 min and several additional washing steps followed. Single crystal were sonicated in hot distilled water, acetone and IPA for 10 min each. After loading the sample into the deposition system, the sample was 1/ exposed to pure H_2 plasma at 100 mbar, 500 W for 5 min, 2/ etched in 99% of H_2 and 1% of O_2 plasma at 100 mbar, 500 W for 10 min, 3/ cleaned by pure hydrogen plasma a second time and 4/ growth of the epitaxial layer was carried out using following conditions:

Table 4.8: Conditions used for deposition of epitaxial layer onto (100) single crystal substrate using AX5010 apparatus

Power	**Pressure**	**Time**	**Gases (sccm)**			
(W)	**(kPa)**	**(Min)**	**H_2**	**CH_4**	**O_2**	**TMB**
550	5	30	970	10	0	20

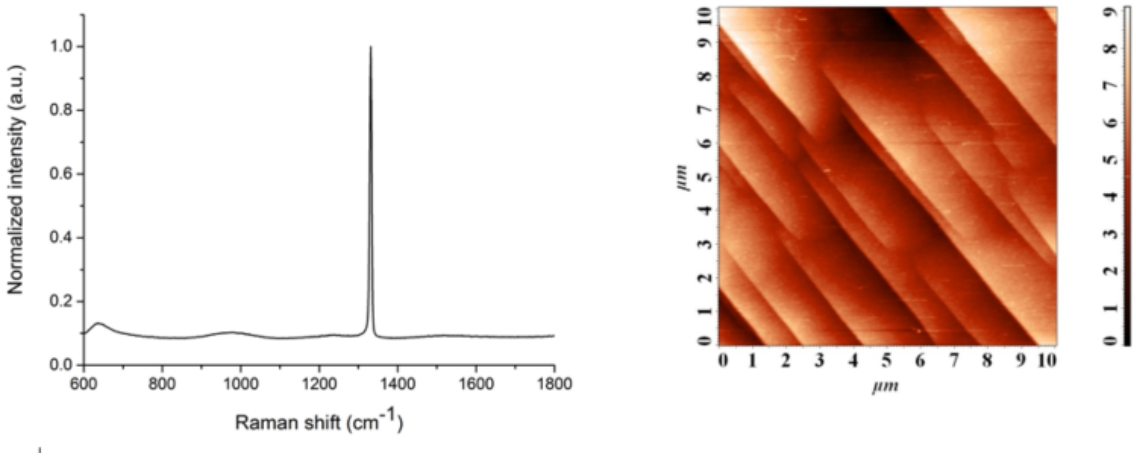

Figure 4.9: Raman spectra (left) of NCD layer deposited on (100) single crystal, clear diamond peak at 1332 cm^{-1} AFM picture (right) shows a smooth surface with terraces

4.1.3 Fabrication of LW-SAW sensor

Fabrication of IDTs

For fabrication of LW-SAW sensors, firstly IDTs electrodes were patterned on top of ST or AT-cut crystal. IDTs can be fabricated by using different four schemes depending on the type of photoresist (negative, positive) and type of mask (negative, positive): 1/ photolithography using positive photoresist and positive mask followed by metal deposition and lift-off technique, 2/ metal deposition followed by photolithography using positive photoresist and negative mask followed by etching, 3/ metal deposition followed by photolithography using negative photoresist and positive mask and etching techniques and 4/ photolithography using negative photoresist and negative mask followed by metal deposition and lift-off techniques. Approaches 1/ and 3/ are shown in figure 4.10.

Aluminum or chromium IDTs were fabricated by photolithography using positive photoresist, RF sputtering and lift-off techniques, developed conditions for each technique

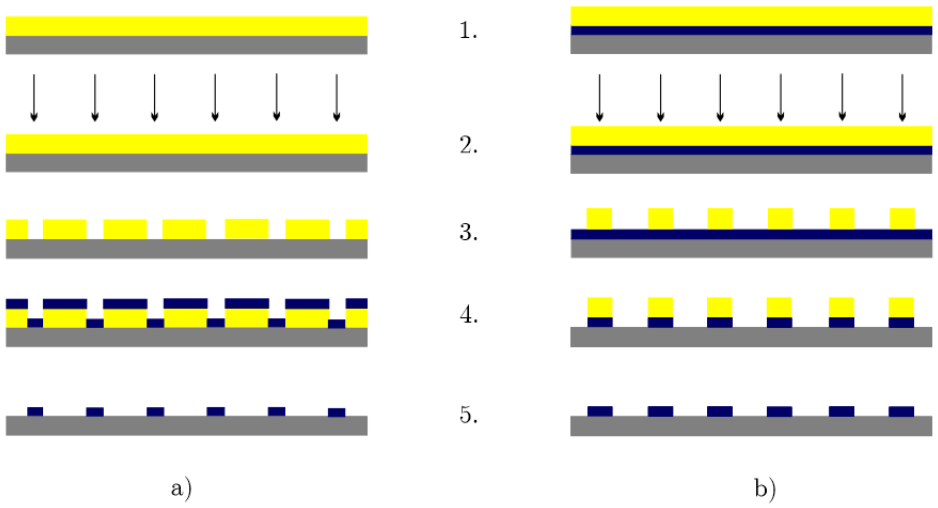

Figure 4.10: Two approaches of fabrication of IDTs: a) Process of fabrication using positive photoresist and lift off technique (1. Deposition of photoresist, 2. Exposure of photoresist, 3. Development of photoresist, 4. Deposition of metal layer and 5. Lift off technique) and b) Process of fabrication using negative photoresist and etching techniques (1. Deposition of metal layer and photoresist on top of it, 2. Exposure of photoresist, 3. Development of photoresist, 4. Etching of metal layer and 5. Removing of photoresist layer)

are reported in table 4.1.2. At first, photolithography technique was done, used conditions for SiO_2 substrate are written in table 4.3. After patterning of the photoresist electrode's mask, deposition of metal layer by RF or DC sputtering followed. Then samples were immersed into acetone. In this lift-off process, photoresist with a metal layer on top of it is removed leaving the metal layer deposited directly on the substrate. This approach is shown on figure 4.10a). Fabricated IDT is shown in figure 4.11.

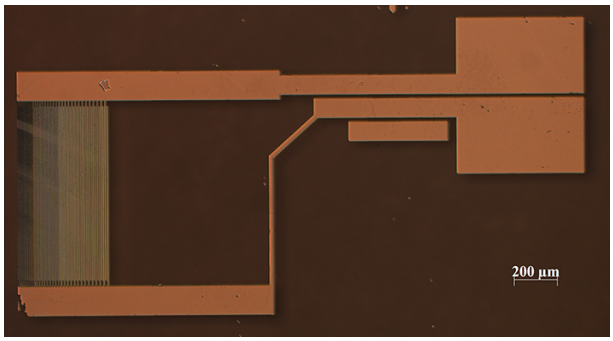

Figure 4.11: Picture of fabricated IDTs using lift-off technique

Deposition of NCD and SiO_2 guiding layer

The deposition of SiO_2 guiding layer and NCD layer followed after the fabrication of IDTs, as shown in figure 4.12. The amorphous silicon dioxide guiding layer was deposited by PECVD System Plasma Lab 80 plus at IEMN. Deposition was held at low temperature to preserve piezoelectric properties of quartz crystal. During the deposition, metal pads of IDTs were mechanically protected. Deposition conditions are reported in table 4.9.

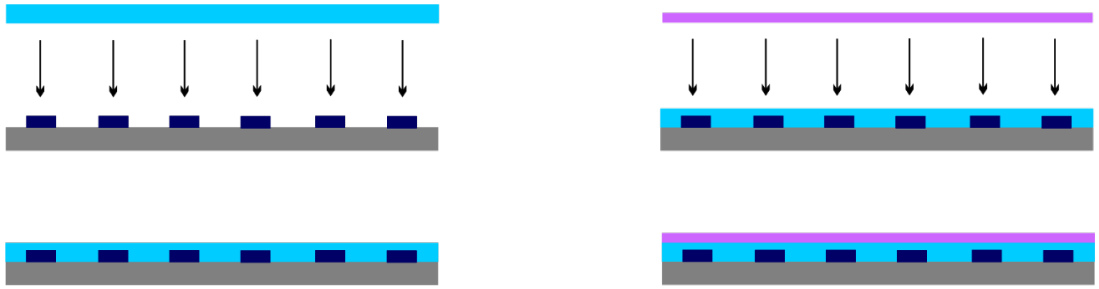

a) b)

Figure 4.12: Process of fabrication of LW-SAW sensor, a) deposition of SiO_2 guiding layer and b) deposition of thin NCD layer on top of it.

Table 4.9: Conditions used for deposition of amorphous SiO_2 guiding layer

Pressure	**Temperature**	**Microwave**	**Gases (sccm)**		**Thickness of**
(Pa)	**(°C)**	**power (W)**	**SiH_4**	**N_2O**	**layer (μm)**
130	300	20	150	700	1.3

A thin NCD layer is then deposited at low temperature using MW-LA-PECVD. IDTs pads were also mechanically protected from diamond seeding using clean room tape. Used conditions are reported in table 4.9. After the deposition, NCD layers were characterized by Raman spectroscopy and AFM. Raman spectra of diamond layers showed clear diamond peak at 1332 cm^{-1} and surface of the 80 nm thick diamond layer is smooth and without any pinholes, as shown in figure 4.13.

Table 4.10: Conditions used for deposition of NCD layer using MW-LA-PECVD

Power	**Pressure**	**Temperature**	**Gases (%)**				**Deposition**
(kW)	**(Pa)**	**(°C)**	**H_2**	**CH_4**	**CO_2**	**TMB**	**rate (nm/h)**
2 x 2.75	32	450 - 500	93.2	4.2	2.5	0.1	30

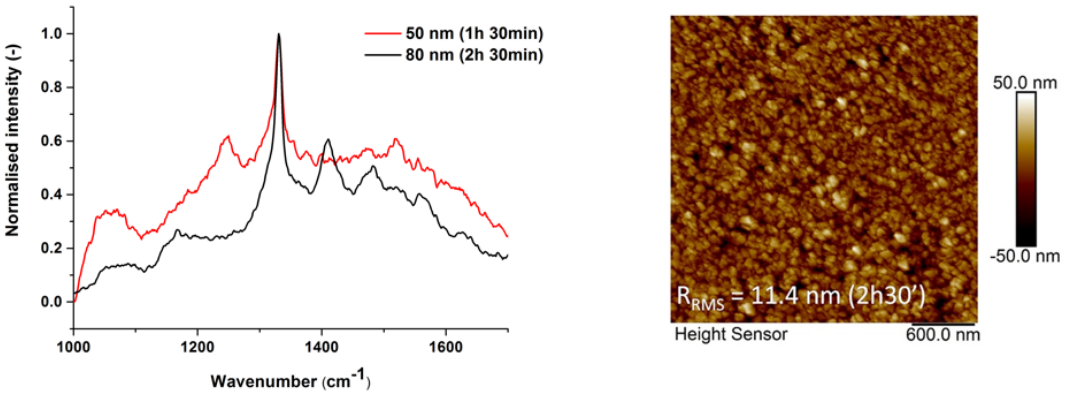

Figure 4.13: Raman spectra (left) of NCD layer deposited on SiO_2 guiding layer and AFM picture (right) of 80 nm NCD layer

Final LW-SAW sensors were fabricated at IEMN. 225 nm thick aluminum IDTs were deposited on AT-cut or ST-cut quartz crystals. IDTs consist of 28 pairs of electrodes with different spatial periods - 8, 12, 16 and 32 μm and acoustic aperture 800 μm. LW-SAW type of sensor was obtained by deposition of 1.3 μm thick SiO_2 guiding layer followed by deposition of 80 nm NCD layer at AT-cut the both using PECVD at low temperature. Fabricated sensor is shown in figure 4.14.

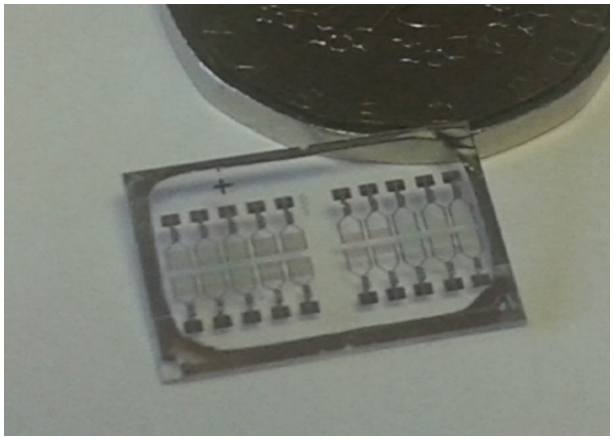

Figure 4.14: Picture of fabricated LW-SAW sensor

4.1.4 Characterization of LW-SAW sensor

Characterization of fabricated LW-SAW sensors was done before and after diamond layer coating. At first, different devices with different IDTs spatial periods and different metals used for their fabrication were studied. On the devices, with the best working IDTs, the dependence of thickness of diamond layer was investigated. Another study was done using diluted Lift-off resist (LOR), normally used for photolithography technique, to investigate sensibility of the sensor. Obtained results were compared with theoretical ones.

IDTs with different spatial period study

For SAW devices with different spatial periods of IDTs, resonant frequency of the sensor can be calculated according to the equation 1.2. Calculated resonant frequency for used spatial periods are written in table 4.11, used phase velocity of SAW waves was 5100 m/s , which is based on theoretical studies of AT-cut sensor. Table 4.12 shows measured resonant frequency of fabricated sensor and calculated phase velocity.

Table 4.11: Calculated resonant frequency of SAW sensor for different spatial periods of IDTs

Spatial period λ (μm)	**Resonant frequency f_0 (MHz)**
8	637.5
12	425
16	318.75
32	159.38

Table 4.12: Measured resonant frequency for different IDTs period and calculated phase velocity

Spatial period λ (μm)	**Resonant frequency f_0 (MHz)**	**Phase velocity (m/s)**
8	610	4800
12	411	4932
16	277	4432
32	152.7	4886.4

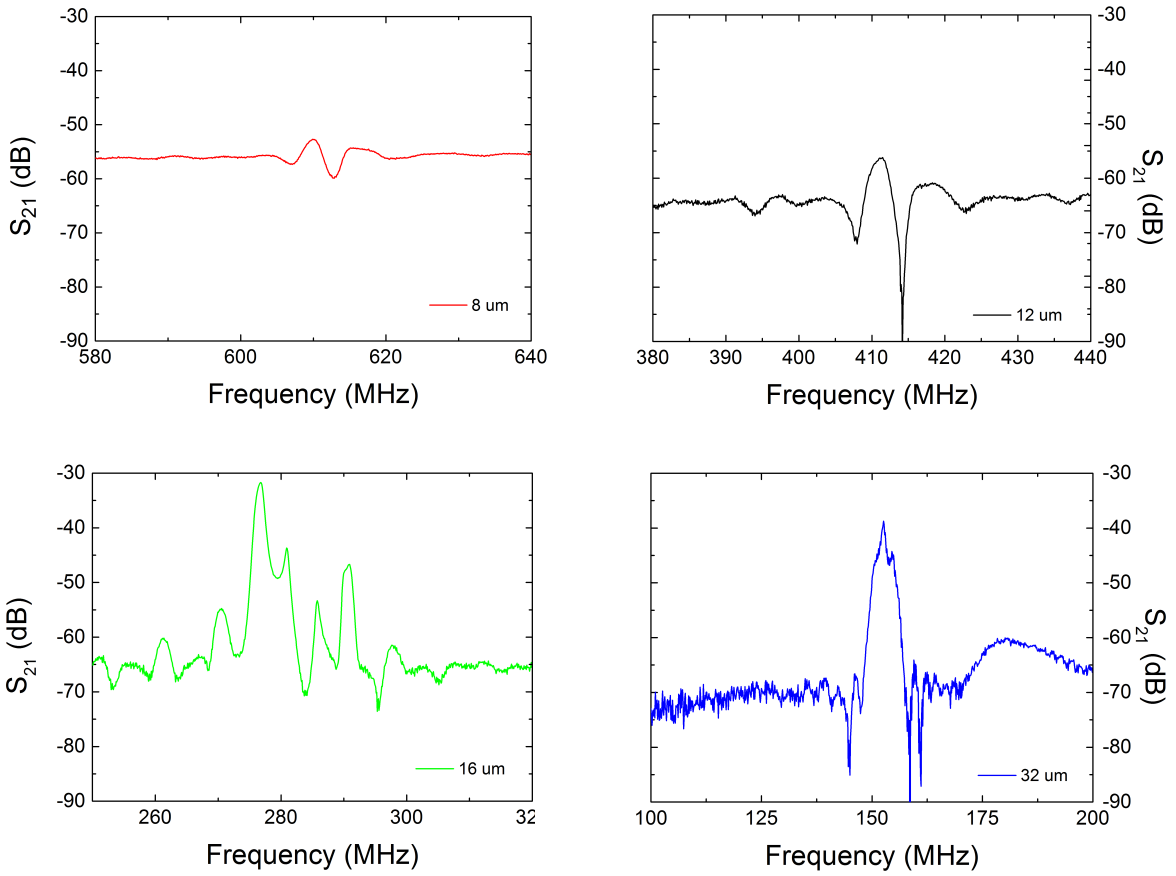

Figure 4.15: S_{21} parameter for different IDTs spatial period on AT-cut quartz: 8 μm (red line), 12 μm (black line), 16 μm (green line), 32 μm (blue line)

From figure 4.15 it can be seen, that the best frequency response is obtained for devices with $\lambda = 32$ μm. Devices with spatial periods 16 and 32 μm have lower insertion loss than the other devices. According to these results IDTs with spatial periods 16 and 32 μm were chosen for further work.

IDTs different metal study

Response of SAW device fabricated from two different metal - aluminum and chromium - was investigated for different spatial period.

From figure 4.16 can be seen, that SAW devices with aluminum IDTs has lower insertion loss (-31.9 dB or -37.3 dB for 16 μm or 32 μm respectively) than for SAW devices fabricated with chromium IDTs (-50 dB). According to this result, we decided to use aluminum electrodes for SAW devices fabrication.

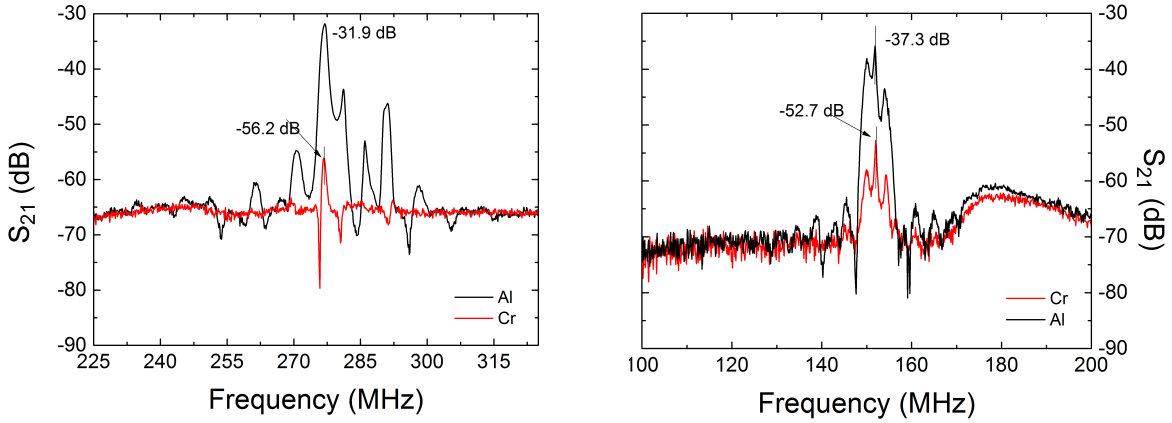

Figure 4.16: S_{21} parameter for SAW devices fabricated from different metal on ST-cut quartz

Diamond thickness dependence study

For the diamond thickness dependence study, we used ST-cut quartz crystal with IDTs fabricated from aluminum with spatial periods 16 μm and 32 μm and a 1.3 μm thick SiO_2 guiding layer. Normalized SiO_2 thickness is then 0.04 or 0.08 respectively. Diamond layers were deposited using MW-LA-PECVD system from Leybold Optics Dresden. The diamond layer had to be deposited at low temperature (< 500 °C) to preserve the piezoelectric properties of the quartz substrate. Conditions used for deposition of diamond layers are written in table 4.13. The SAW device with deposition of 12 NCD layers was studied.

Table 4.13: Conditions used for deposition of NCD layer on SAW sensors

Layers	**Pressure**	**Temperature**	**Gases (%)**				**Duration**
(-)	**(Pa)**	**(°C)**	**H_2**	**CH_4**	**CO_2**	**TMB (ppm)**	**(min)**
1-6	25	470	93.27	4.21	2.52	15060	90
7-12	25	460	93.4	4.06	2.54	15384	90

All of the deposited diamond layers were investigated using AFM measurement to confirm homogeneity of diamond layer. After the deposition of each diamond layer the frequency measurement was done as well.

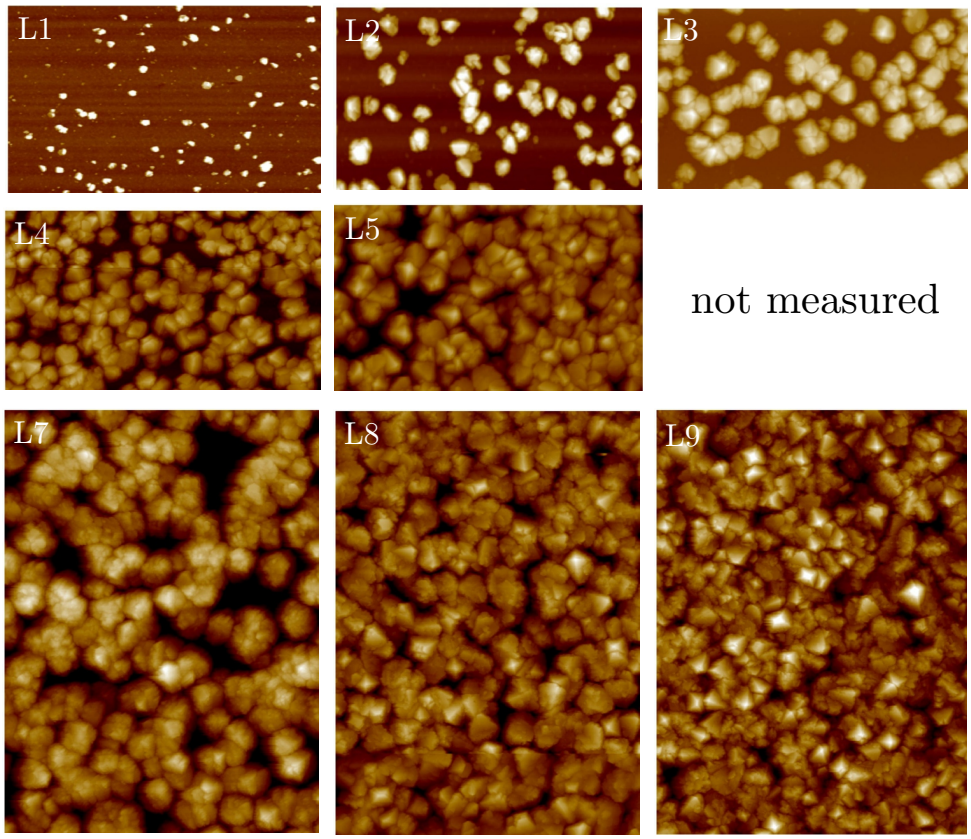

Figure 4.17: AFM pictures of first nine layers of NCD deposited on SAW sensor

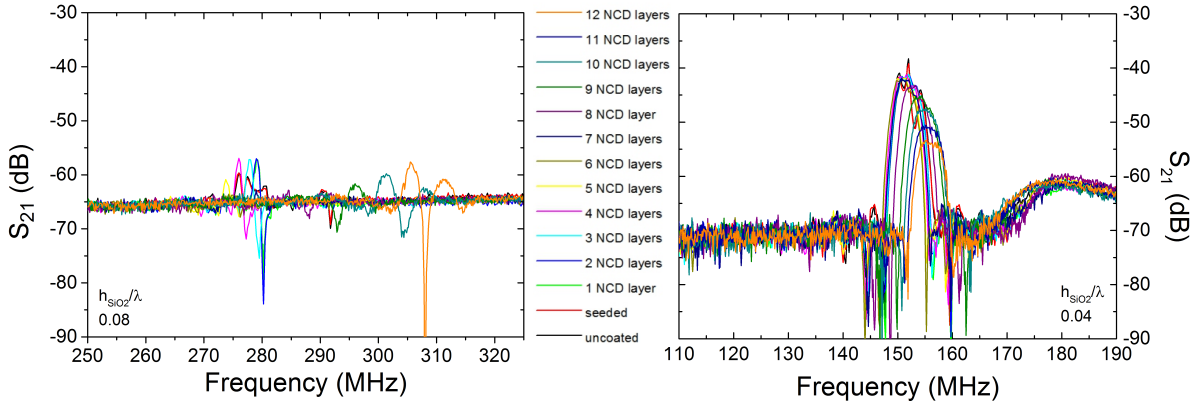

Figure 4.18: S_{21} parameter for SAW sensor with deposited different numbers of NCD layer

In the figure 4.17 one can see , that after the deposition of three layers, there were just a few diamond crystals on the sensor. It can be observed, that layers 8 and 9 show a closed surface of diamond layer. Figure 4.18 shows frequency response of SAW device deposited with 1 to 12 NCD layers. Insertion loss of IDTs with 16 μm spatial period is around -55 dB. On the other side, insertion loss of IDTs with 32 μm on uncoated SAW sensor is around -40 dB. The insertion loss is increasing with an increasing number of NCD layers.

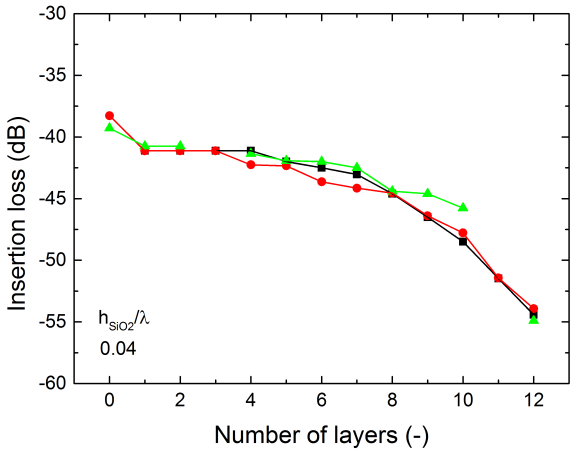

Figure 4.19: Insertion loss as a function of different number of NCD layers for normalized SiO_2 thickness 0.04

From figure 4.18 can also be observed the shift of the resonant frequency with addition of each diamond layer. Relative frequency shift f_{rel} (%) was calculated according to following equation:

$$f_{rel} = \left(\frac{f - f_0}{f_0} \right) \cdot 100 \tag{4.1}$$

where f (Hz) is resonant frequency of sensor with diamond layer and f_0 (Hz) is resonant frequency of uncoated device. From resonant frequency was also calculated SAW phase velocity according to equation 1.2 and results are shown in figure 4.20.

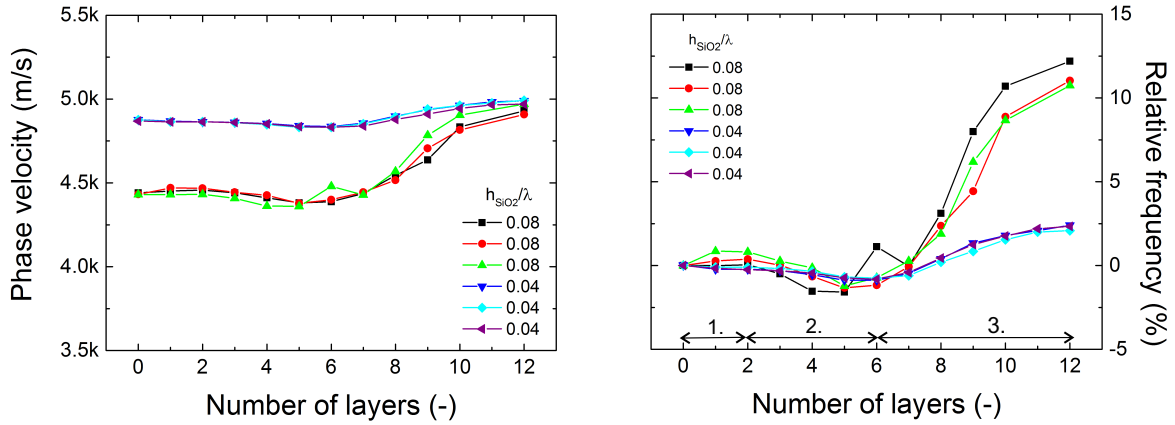

Figure 4.20: Phase velocity and relative frequency shift as a function of number of NCD layers

According to theoretical results, phase velocity of SAW should increase with deposition of diamond layer. In figure 4.20 it is shown, that the phase velocity is rather constant

until deposition of the seventh NCD layer, then the phase velocity increases for both SiO_2 normalized thicknesses. This result is consistent with theoretical calculations. The phase velocity calculated from the measured data is lower than the phase velocity obtained by simulations. It can be caused by using parameters for simulation that are different from real ones. From equation 1.2 is also obvious, that with increasing phase velocity, relative frequency has to increase as well. In the figure 4.20 one can see three specific parts. In the first part the resonant frequency is increasing. This can be caused by the annealing effect of the quartz during the deposition. This annealing might change a slightly the properties of the quartz crystal. In the second part the resonant frequency is decreasing. This is attributed to mass loading of the sensor, but the deposited diamond layer is not closed. In the third part the resonant frequency is increasing again. This is due to the increase of surface rigidity, with the formation of a uniform closed diamond layer.

LW-SAW sensor sensitivity study

To study sensitivity of fabricated SAW sensors on ST-cut quartz crystal with aluminum IDTs with spatial periods 16 and 32 μm and 1.3 μm thick SiO_2 guiding layers were used to compare sensitivity of uncoated LW-SAW sensor and sensor with 12 deposited diamond layers.

Six consecutive layers of LOR polymer were deposited on each LW-SAW sensor. After each deposition frequency measurement was done. In parallel a set of six silicon samples with the same number of LOR layers was also prepared and their thickness was measured by SEM. Measured parameter S_{21} for all six LOR layers for different SiO_2 normalized thicknesses is shown in figure 4.21.
Figure 4.21 shows S_{21} parameter for different normalized thicknesses of SiO_2 layer and for uncoated and diamond coated devices. A shift in the resonant frequency between coated and uncoated devices can be observed as well as an increase in insertion loss for the diamond coated LW-SAW sensor. One can also see the higher shift of resonant frequency for normalized thickness 0.08 than for 0.04. It refers to the higher sensitivity of sensor with normalized thickness 0.08 and this result is consistent with theoretical studies. Phase velocity was calculated from measured resonant frequency.

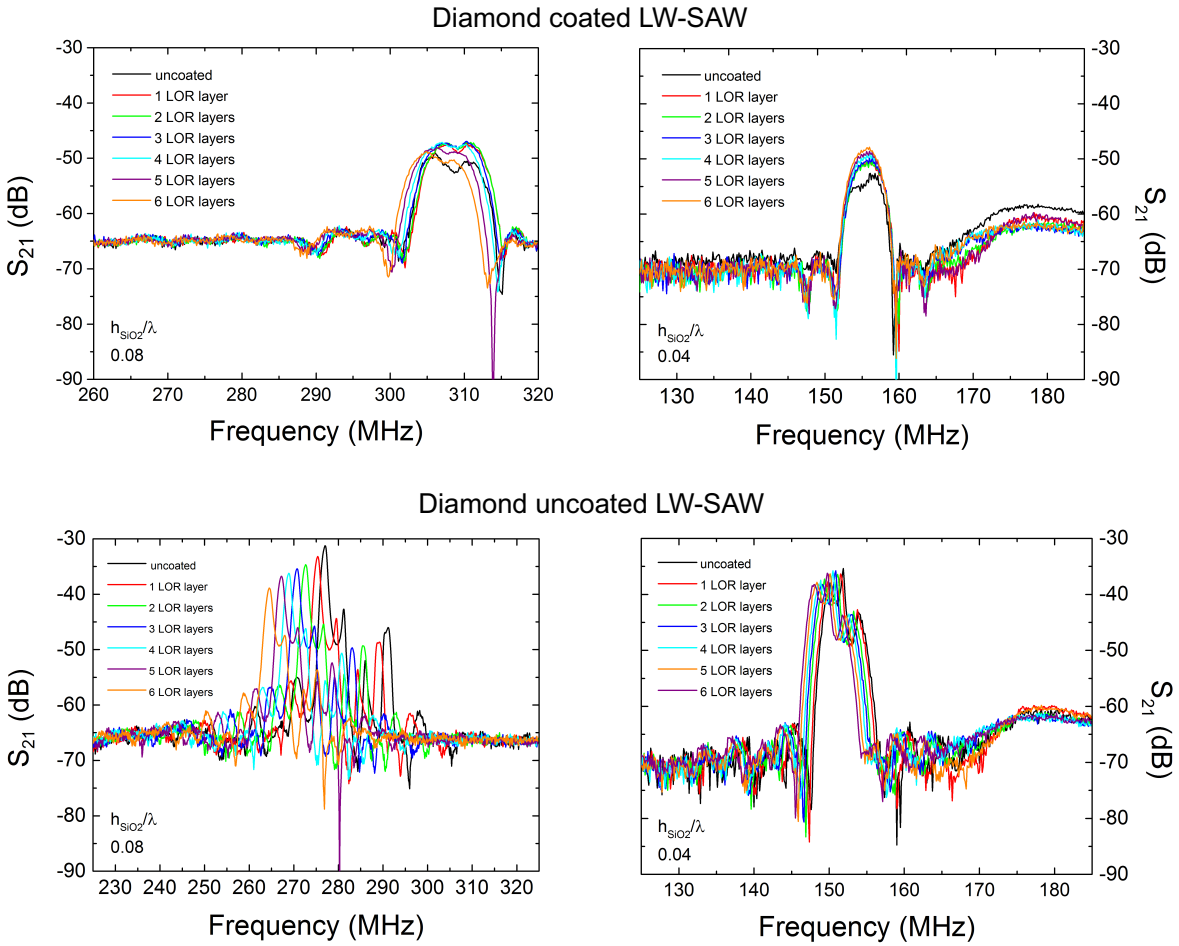

Figure 4.21: S_{21} parameter for diamond coated and uncoated LW-SAW sensors with deposited different numbers of LOR layers

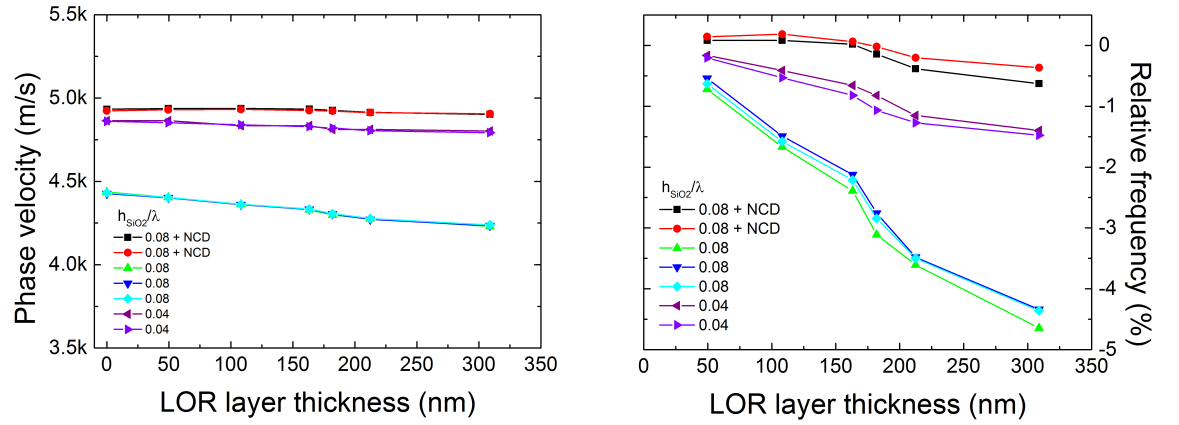

Figure 4.22: Phase velocity and relative frequency shift as a function of thickness of LOR layers

From the figure 4.22 it can be seen, that the phase velocity of acoustic waves is almost constant for the diamond coated sensor with SiO_2 normalized thickness 0.04 and diamond uncoated sensor with SiO_2 normalized thickness of 0.08. This results leads to the conclu-

sion, that for better sensitivity of diamond coated sensor, the SiO_2 normalized thickness has to be changed. There are two possibilities: 1/ fabrication of SAW with different IDTs spatial periods and 2/ with different thickness of SiO_2 guiding layer. Aim is to obtain SiO_2 normalized thickness about 0.2 - 0.3 by combination of proposed possibilities.

4.2 Attachment of bioreceptors to diamond surface

In parallel to the development and fabrication of LW-SAW sensor we studied biofunctionalization of diamond surface. Two approaches were studied - attachment of bacteriophages T7 and attachment of bacteriophage's fiber tails to the diamond surface. For attachment of bacteriophages, different surface functionalization of diamond surface and development of microbiological methods had to be carried out.

4.2.1 Diamond surface functionalization for bacteriophage attachment

In this work, we studied three types of diamond surface termination for attachment of bacteriophage. The different surfaces were characterized by contact angle measurement.

H-terminated diamond surface

As-grown diamond layers are terminated with hydrogen atoms. Hydrogenated surface is known to be hydrophobic. Hydrogen plasma was used to obtain H-terminated diamond using AX5010 PECVD system and conditions are written in table 4.14.

Table 4.14: Conditions used for H-termination of NCD layer

Power (W)	**Pressure** (kPa)	**Gas** (sccm)	**Time** (min)
1150	5	H_2	10

O-terminated diamond surface

Four different processes for preparation of oxygen terminated surface were studied: 1/ pure oxygen plasma treatment at power 1000 W, pressure 500 Pa for 5 min using AX5010 PECVD system, 2/ O_3 treatment under UV light 3/ oxidation in hot H_2SO_4 (180°C) with

KNO_3 for 10 min, 4/ oxidation in hot H_2SO_4 (100°C) with H_2O_2 for 30 min. After wet chemical treatment, samples were rinsed and sonicated into distilled water, acetone and IPA for 5 min each. Finally, samples were dried using compressed air. Diamond oxidized surface is known to be hydrophilic hence contact angle of oxidized surfaces must be very low. Contact angle of surfaces terminated by wet chemical treatment was measured using contact angle measurement apparatus at Institute of Physics CAS, v.v.i.

NH_2 termination

Chemical treatment was used to obtain amino groups onto diamond surface. Diamond layer was first annealed to form sp^2 hybridization of the carbon on top of diamond layer. Then the surface was terminated by azide groups, that are reduced to form amino groups. The success of this process was evaluated using XPS analysis. Contact angle of aminated diamond layer was also measured.

Annealing

Annealing of the NCD layers were done at 900 °C at argon flow for one hour. Raman spectra were measured for confirmation of forming of sp^2 hybridization and are shown in figure 4.23.

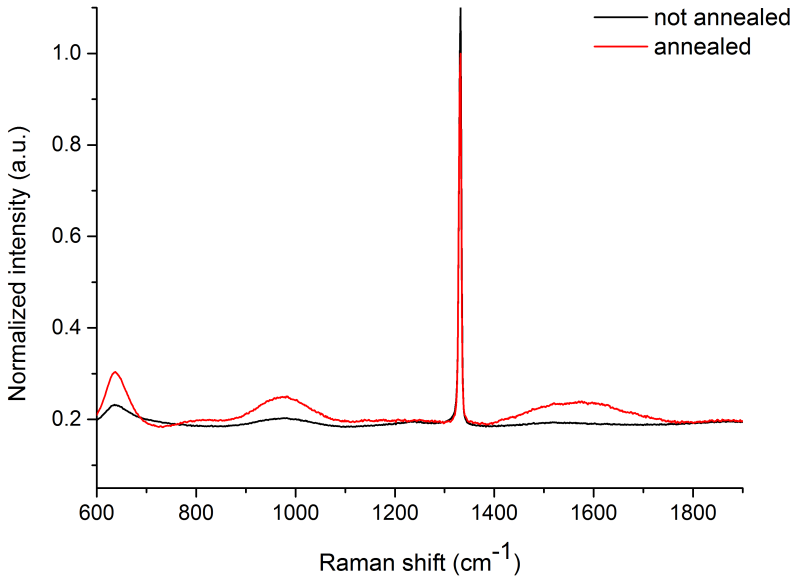

Figure 4.23: Raman spectra of annealed SCD layer, band at 1600 cm^{-1} refers to the forming of sp^2 hybridization of carbon during the annealing process

Termination of diamond surface with azide groups

A diamond layer was placed in the conical vial with distilled water (1.5 ml). 4-(2-azidoethyl)alanine hydrochloride (10 μg) and isopentyl nitrite (20 μl) were added to distilled water. The reaction mixture with immersed sample was stirred overnight at 80 °C. Reaction mixture was sucked up and followed by several washing steps. The sample was washed three times in acetone (2 ml) and methanol (MeOH, 2 ml) and once in distilled water (2 ml), dichloromethane (2 ml), acetone (2 ml), MeOH (2 ml) and distilled water (2 ml) for 10 minutes each. Surface of the diamond layer was then characterized by XPS method. Figure 4.24 shows results of the XPS analysis of the diamond surface after treatment with 4-(2-azidoethyl)alanine. Peak around 407.63 eV confirms the presence azide groups, second peak at 399.75 eV refers the presence of C-N bonds on the diamond surface.

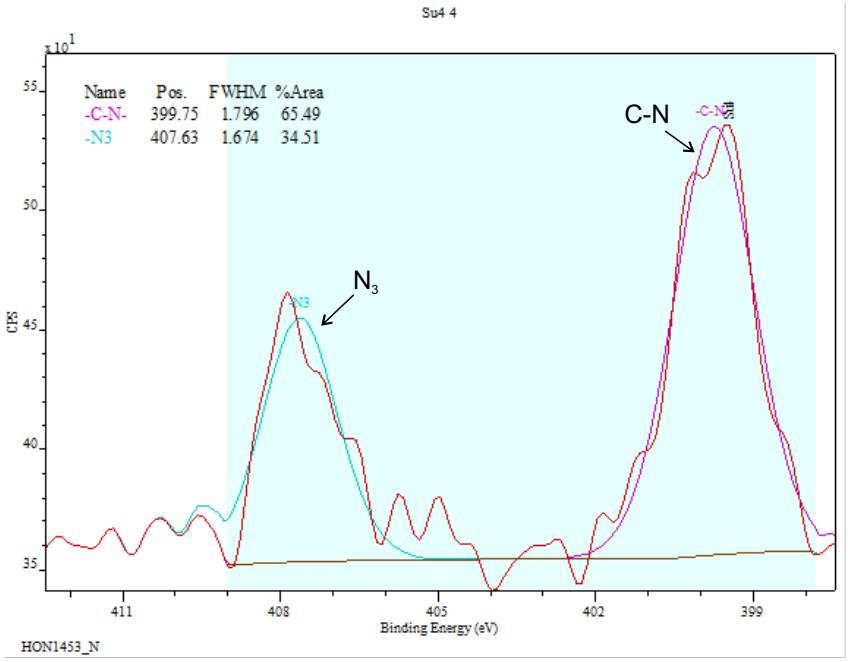

Figure 4.24: Peak at 407.63 eV confirm the presence of azide groups onto diamond surface after 4-(2-azidoethyl)alanine treatment

Reduction of azide groups to amino groups

Diamond layer terminated by azide groups was then reduced to obtain amino groups. The diamond sample was placed in the conical vial and distilled water (1 ml) in which tetrahydrofuran (1 ml) and triphenylphosphine (20 μg, 0.073 mmol) was added. The mixture with sample was stirred overnight at 50 °C. Reaction mixture was then sucked up and then the sample was washed three times with acetone (2 ml) and MeOH (2 ml) and once with distilled water (2 ml), dichloromethane (2 ml) and acetone (2 ml) for 10 minutes each. 4-(2-azidoethyl)alanine was reduced onto 4-(2-aminoethyl)alanine. The following XPS analysis confirmed the reduction of azide: peak corresponding to azide groups disappeared and remains only the C-N peak, see figure 4.25.

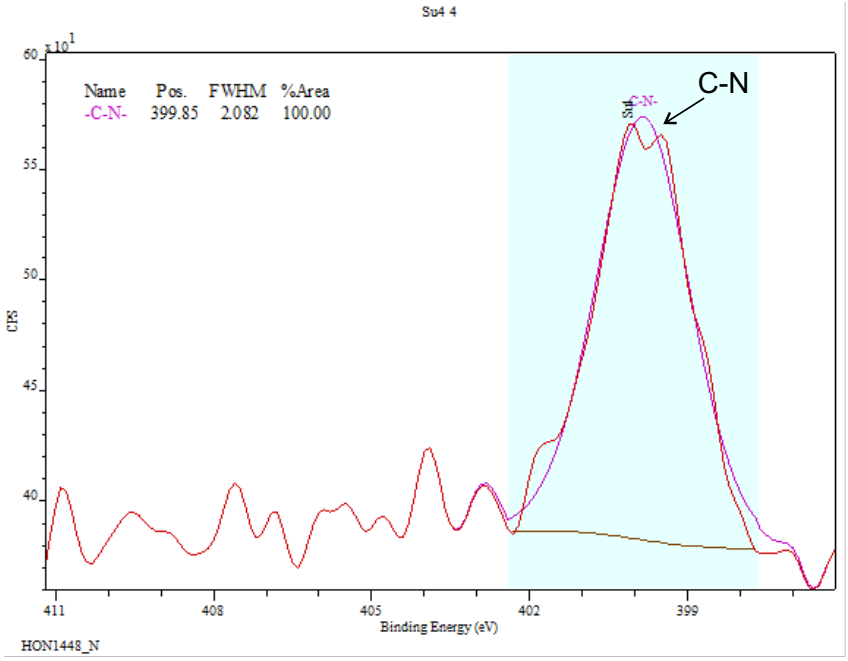

Figure 4.25: Missing azide peak at 407.63 eV refers to reduction of azide groups to amino groups

Contact angle measurement

Table 4.15: Measured contact angles for different functionalized NCD layer

Number of sample or type of treatment	**Contact angle - single drops (°)**	**Mean value of contact angle (°)**
Hydrogenated NCD layer		
1	60.7 ± 0.34 60.3 ± 0.16 59.7 ± 0.36	60.2 ± 0.53
2	60.2 ± 0.35 60.4 ± 0.22 61.3 ± 0.24	60.2 ± 0.35
Aminated NCD layer		
1	93.3 ± 0.32 97.1 ± 0.25 97.2 ± 0.25	95.8 ± 2.24
2	95.7 ± 0.11 103.8 ± 0.13 97.9 ± 0.22	99.1 ± 4.16
Oxidized NCD layer		
H_2SO_4 + KNO_3	42	-
H_2SO_4 + H_2O_2	68	-
Pure oxygen plasma	3.4 ± 0.25	-
Ozone treatment	100.3 ± 2.6	-

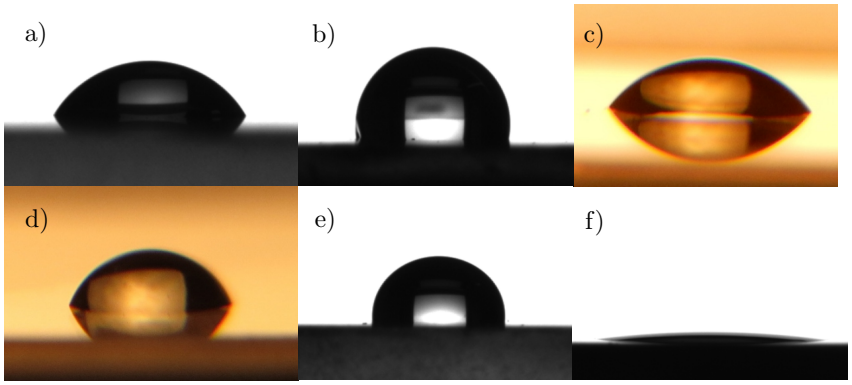

Figure 4.26: Droplet of water on NCD layers functionalized by: a) hydrogenation, b) amination, c) oxidization - H_2SO_4 + KNO_3, d) oxidization - H_2SO_4 + H_2O_2, e) oxidization - ozone treatment and f) oxidization - pure oxygen plasma treatment

Image of water droplet on hydrogenated surface is shown in figure 4.26 and measured contact angles are reported in table 4.15. Hydrogenated surface is considered to be hydrophobic, which corresponds to a contact angle greater than 90 °. Contact angle of water droplet on hydrogenated surface is approximately 60 °. Contact angles for three droplets on different places on one NCD layer are very close, which refers to the good homogeneity of hydrogenation of diamond layer. Oxidized NCD layer are reported to be hydrophilic, to which corresponds angle smaller then 90 °. This conditions is not fulfill by sample after ozone treatment, that had a contact angle 100.3 °. The best results were obtained after oxygen plasma treatment. Wettability of aminated ultra-nanocrystalline diamond (UNCD) layer is reported as hydrophilic. In this work, we aminated NCD layer and measured contact angles around 95 - 99 ° refer to hydrophobicity of the surface. Measured contact angle of three droplets on one NCD layer can also shows an inhomogeneity of surface functinalization. This different result from literature [55] can be caused by different size of diamond crystals (UNCD vs NCD layers) and different density of amino groups on the diamond surface.

4.2.2 Attachment of bacteriophages to the diamond surface

In this work, bacteriophages T7 were purchased from Leibniz Institute DSMZ-German Collection of Microorganisms and Cell Cultures, all of the other chemicals and materials were obtain from Microbiological institute CAS, v.v.i. At first, sensible strain of *Escherichia coli* had to be found and several strains were tested using Plaque assay method. Then, optimal conditions for multiplication and purification of bacteriophages had to be found. For bacteriophage attachment, experimental set of samples was fabricated using glass substrates coated with boron doped NCD layer. Conductive boron doped NCD layer was chosen to be compatible with SEM characterization.

Plaque assay method

Used bacteria strain:	*Escherichia coli LB21 DE3-*
Used bacteriophages:	Bacteriophage T7
Used buffers:	
PBS buffer	8 g of NaCl
	0.2 g of KCl
	1.44 g of Na_2HPO_4
	0.25 g of KH_2PO_4
	pH = 7.4, adjust with HCl
Used culture media:	
LB (Luria Bertani)	10 g of tryptone
	5 g of yeast extract
	10 g of NaCl,pH = 7 - 7.5
	1 l of distilled water and 1.5 % of agar
LB soft	10 g of tryptone
	5 g of yeast extract
	10 g of NaCl, pH = 7 - 7.5
	1 l of distilled water and 0.5 % of agar
LB liquid	the same composition without agar

Cultivation media was sterilized by autoclaving.
Bacteria cell culture was cultivated in liquid LB medium on the orbital shaker at 37 °C overnight. 10 ml of medium with 1.5 % of agar was poured on several Petri dishes and left until it become hard. 10 ml of soft medium was held in the tubes that were in water at 48 °C. 100 μl of bacteria cell culture was added into each tube with soft medium. Then 100 μl of bacteriophage's suspension in PBS buffer was added into tubes as well. In each tube the suspension had different concentration (10^{-1} – 10^{-8} pfu/ml). It was poured on the Petri dishes with solid medium. Petri dishes were left at 37 °C for 24 hours. Then the number of plaques was determined.

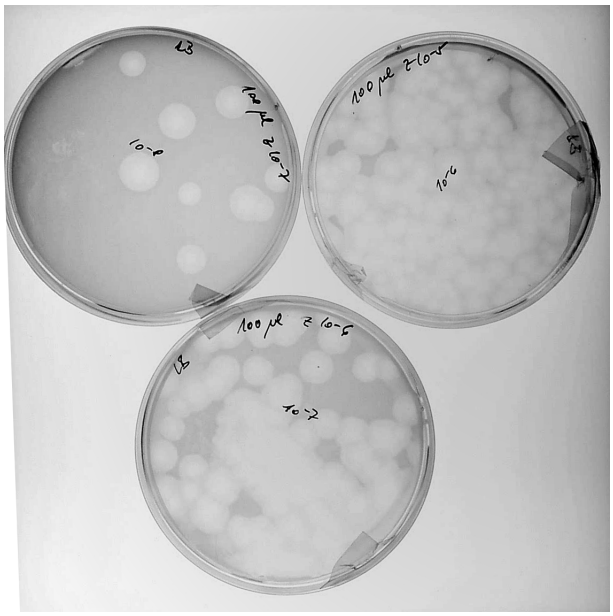

Figure 4.27: Results of plaque assay method, each plaque belongs to one bacteriophage particle

Multiplication of phages

Used bacteria strain:	*Escherichia coli LB21 DE3-*
Used bacteriophages:	Bacteriophage T7
Used culture media:	
2xTY + kanamycin	16 g of tryptone
	10 g of yeast extract
	5 g of NaCl, pH = 7 - 7.5
	+ kanamycin

Used buffers:	
Buffer for phages	5 g of NaCl
	17.6 g of $Na_2HPO_4 \cdot 12\ H_2O$
	3 g of KH_2PO_4
	pH = 7.4, adjust with HCl
Add before use:	1 ml of 1M $MgSO_4$
	0.1 ml of 1M $CaCl_2$
	1 ml of 1% gelatin
	too 1000 ml of distilled H_2O

At first, bacteria cell culture was cultivated in 100 ml of 2xTy culture medium with kanamycin at 37 °C on orbital shaker. When the culture was in exponential phase, 100 μm of bacteriophage solution was added and it was incubated at 37 °C on orbital shaker. The optical density was measured during cultivation and when it decrease, the lysis of bacterial cells occured. The solution was then centrifuged at 5000 rpm for 10 min in order to pellet bacteria and supernatant was removed into new flask.

This process of bacteriophages purification was insufficient, so ultracentrifugation of supernatant at 45 000 rpm for 1‘hour was done as another purification step. Then the supernatant was removed and pellet containing bacteriphages was dissolved in PBS buffer.

Attachment of bacteriophages

The procedure described in the study of A. Singh *et al.*‘ [13] was followed for attachment of bacteriophages to the diamond surface. Different types of functionalization of NCD layer were studied for this attachment - hydrogenation, oxidation, amination and activation of aminated NCD layer by gluteraldehyde. These functionalization steps were carried out according to procedures described in chapter 4.2.1.

At first, the phage titre of multiplicated phages was calculated using plaque assay method and all of the immobilization work was performed in an SM buffer (pH = 7.5). Activation of aminated NCD surface with gluteraldehyde was performed by immersing the sample in a 2% solution (v/v) of gluteraldehyde in PBS buffer for 1 hour at room temperature shaking on an orbital shaker at 500 rpm and finally washed twice in distilled water. Other samples were washed by 96% ethanol and distilled water for 5 min each on orbital shaker at 500 rpm. Then, all of the samples were immersed in 750 μm of phage solution with titre 10^{10} pfu/ml for 20 h at room temperature or 40 °C. Then, the substrates were washed in 0.05% (v/v) Tween-20 solution in SM buffer for 5 min, twice in SM buffer for 5 min each and twice in distilled water for 5 min each at orbital shaker at 200 rpm. Samples surfaces were then inspected by scanning electron microscopy at the Microbiological Institute CAS, v.v.i.

Figure 4.28 shows SEM micrographs of different functionalized NCD surfaces after process of bacteriophage attachment at 40 °C. There can be seen very clearly the crystalline struc-

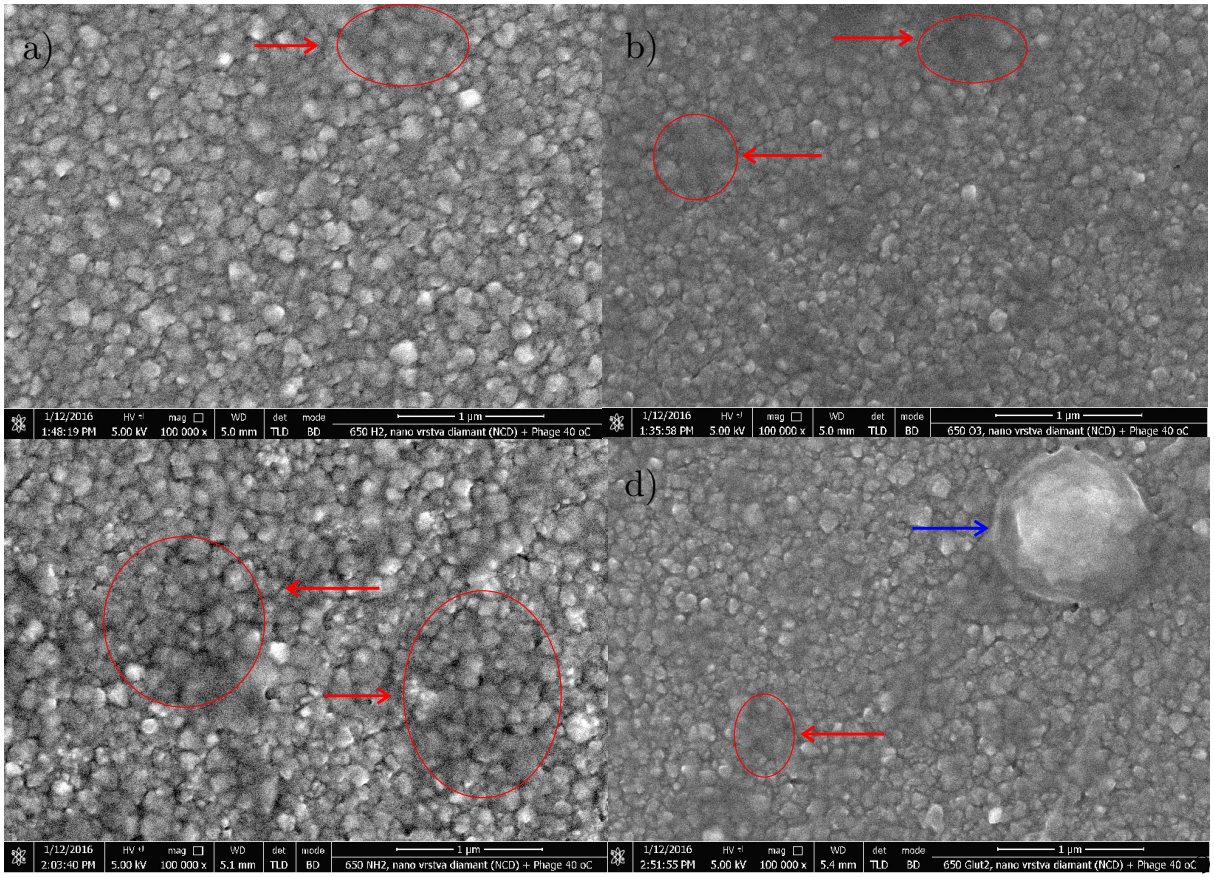

Figure 4.28: SEM micrographs of functionalized NCD layers: a) Hydrogenated NCD layer, b) Oxygenated NCD layer, c) Aminated NCD layer, d) NCD layer with activated amino groups with gluteraldehyde

ture of the NCD layer. In the red circles are highlighted places with attached proteins. It can be seen, that on the hydrogenated surface (4.28a) there is a lower density of attached proteins. This can be caused by hydrophobicity of the NCD surface. In contrary, on oxidized (4.28b) or aminated (4.28c) the surface has a high density of attached proteins. Oxidized surface is hydrophilic and amino groups easy bond to the biomolecules. On the aminated surface activated by gluteraldehyde (4.28d) can also be observed attachment of outer membrane of bacterium (blue arrow). This surface was the only one on which we observed attachments of outer membranes of bacteria. This result may suggest, that this surface functionalization is the most promising one for bacteriophage attachment. Attachment of proteins all over the surface is caused by insufficient purification of bacteriophages. From this SEM measurement we cannot confirm the presence of bacteriophages on the diamond surface. The reason could be, that T7 bacteriophage's head size is about 50 nm, which is comparable to the diamond crystals. 50 nm is also at the detection limit for nonconductive samples, because incident electrons causes charging of the sample

and it is not possible to focus properly at high magnification. Another reason is, that attached proteins covers almost the whole surface and it can make impossible to observe bacteriophages.

Because of these reasons, we decide to optimize bacteriophage's purification process and then observe bacteriophages on conductive surface. After the purification we did TEM measurement to check purity of solution. On the TEM image prepared by negative staining it is possible to observe the presence of proteins in the solutions and also distinguish bacteriophage particles with nucleic acid inside their head and particles without nucleic acid, called "ghosts".

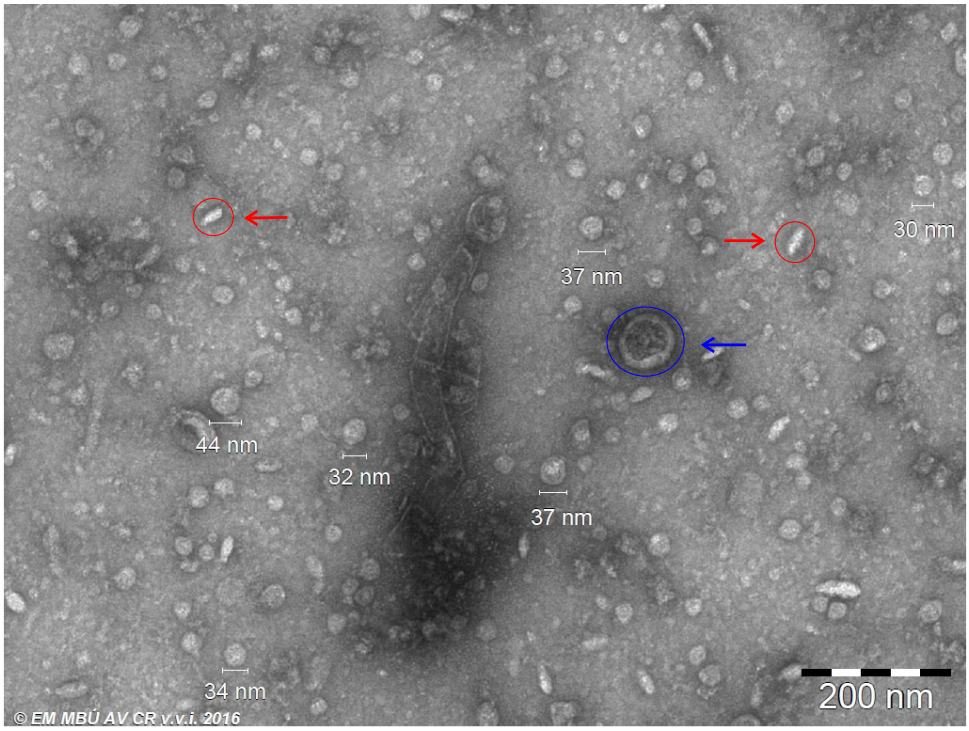

Figure 4.29: TEM image of bacteriophages solutions after negative staining

Figure 4.29 shows TEM image of bacteriophages solutions after negative staining. In the red circles can be observed bacteriophages particles without nucleic acid, these particles have deformed heads. In the blue circle highlighted is the outer membrane of bacterium. There can be also observed a huge amount of properly maturated bacteriophages particles, several of them have a white ruler close to them. This solution was then used for SEM observation of bacteriophages on silicone substrates. 100 μl of bacteriophage suspension was allowed to sediment overnight onto poly-L-lysine-treated Si-chip at 4°C. Si-chip was

then washed with cacodylate buffer and dehydrated through an alcohol series followed by absolute acetone and critical point dried from liquid CO_2 in a K850 Critical Point Dryer unit (Quorum Technologies Ltd., Ringmer, United Kingdom). The dried sample was sputter coated with 3 nm of platinum in a high resolution sputter coater Q150T ES (Quorum Technologies Ltd., Ringmer, United Kingdom). Finally, the sample was examined in FEI Nova NanoSEM 450 scanning electron microscope using ETD, TLD and CBS detectors in standard, immersion, and beam-deceleration (5kV $\rightarrow$ 2kV) modes. As it can be seen at figure 4.30, bacteriophages can be clearly observed and it is also possible to see icosahedral structure of bacteriophage's head.

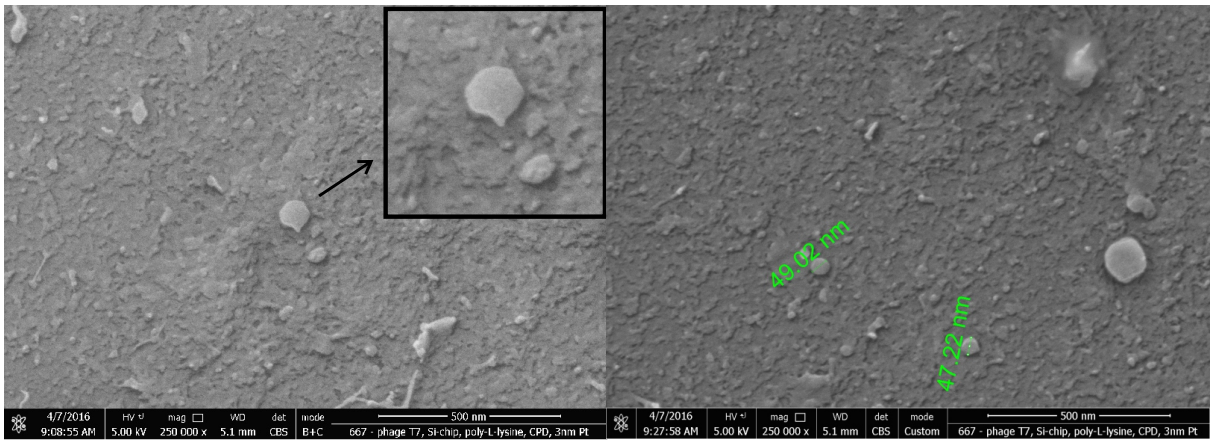

Figure 4.30: SEM image of silicon substrate with attached bacteriophage covered by 3 nm of platinum layer

This bacteriophage solution was then used for their attachment to the epitaxial grown boron doped diamond layer on SCD substrate. This layer was chosen because of its flat surface, so it should be easier to distinguish between bacteriophage particles and the diamond surface. For attachment the same procedure described above was used. Immobilization was performed on hydrogenated and oxidized diamond surfaces at 40 °C. For better SEM observation, dried samples were sputter coated with 3 nm of platinum in a high resolution sputter coater. Samples were then inspected in FEI Nova NanoSEM 450 scanning electron microscope at the Microbiological Institute CAS, v.v.i.

Figure 4.31 shows SEM micrographs of different functionalized diamond layers on SCD substrate with attached bacteriophages. In figure 4.31a) and 4.31b) is an oxidized diamond surface. It can be seen, that the surface of the diamond layer is not flat, but there is a very fine structure. This is caused by diamond etching during oxygen plasma treatment. In the figures 4.31a) and 4.31c) are highlighted in red circles attached bacteriphage parti-

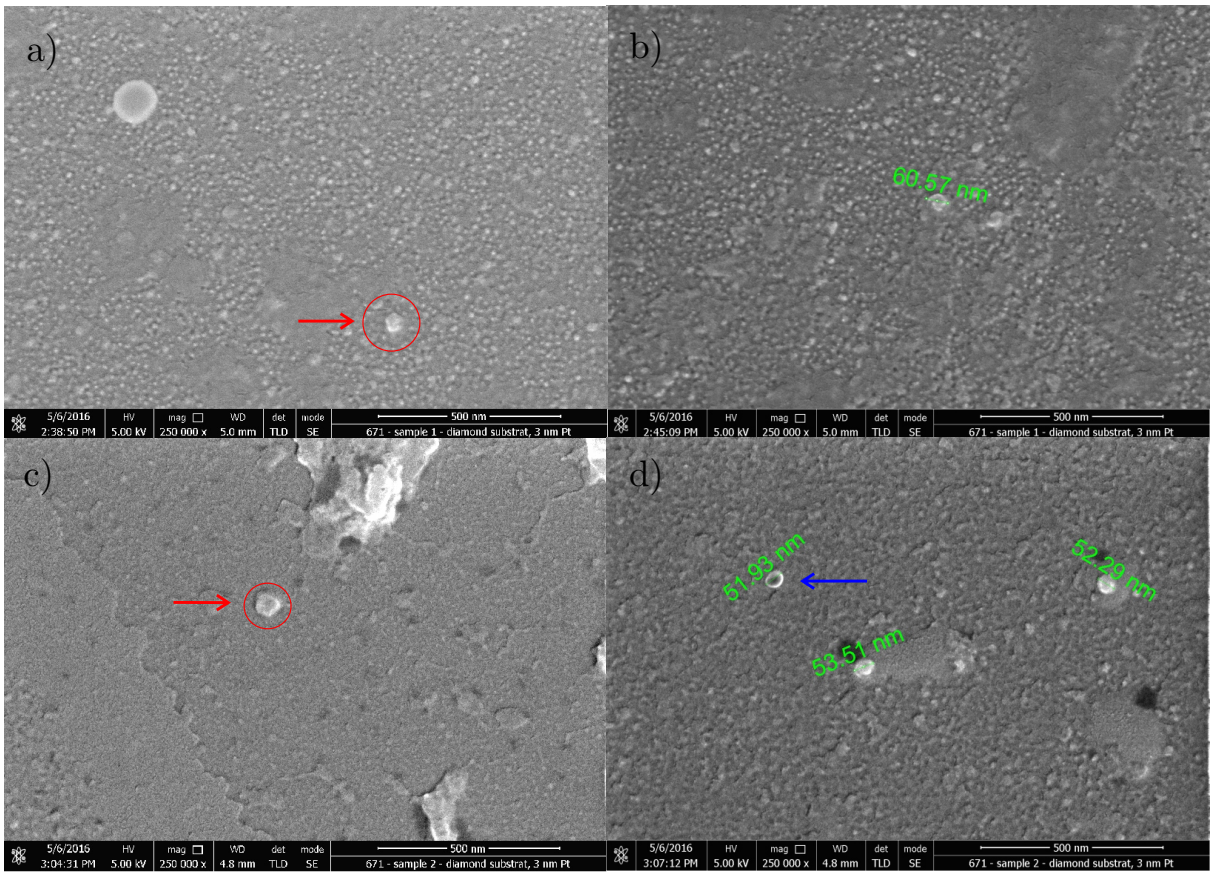

Figure 4.31: SEM image of SCD substrate with epitaxial diamond layer with attached bacteriophages covered by 3 nm of platinum layer, a) and b) oxidized surface, c) and d) hydrogenated surface

cles. In the figures 4.31b) and 4.31d) are measured bacteriophage particles and their size corresponds to the size of T7 bacteriophage head. In the figure 4.31d) are measured three particles, particle highlighted by blue arrow and its size 51.93 nm is probably bacteriophage's ghost, because it does not give any signal in backscattered electron imaging. This image is not presented here because of little contrast. It can be also observed, that there is attached a huge amount of organic proteins and biomolecules on the surface. This is caused by insufficient purification of bacteriophage particles. This caused problems during surface observation, because the organic layer is burned by incident electrons and it contaminate platinum layer and it cause deterioration of conductivity of platinum layer.

4.2.3 Attachment of bacteriophage's fiber tails to the diamond surface

For the attachment of bacteriophage's fibre tails to diamond surface we used following method: 1/ coating of diamond with a methacrylate-terminated thin silica layer, 2/ coating of diamond layer with polymers with antifouling properties, 3/ attachment of ligands by click reaction and 4/ attachment of His-tag linkers for fiber tails attachment, as is shown in figure 4.32.

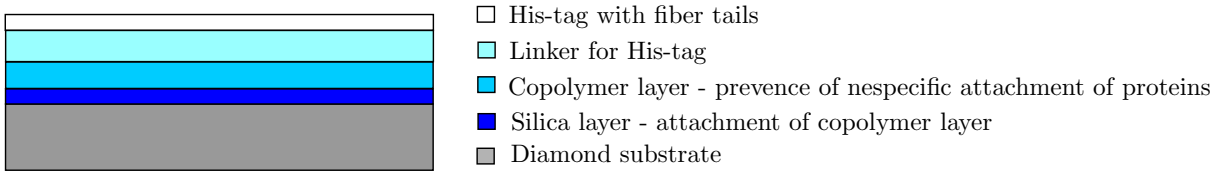

Figure 4.32: Scheme of attachment of bacteriophage's fiber tails to the diamond surface

A set of NCD samples was specifically fabricated by MW-LA-PECVD on glass substrates coated with 100 nm thick titanium layer deposited by RF sputtering. Deposited diamond layers were oxidized using optimal conditions for oxygen plasma. Purpose of titanium layer is to use it as reflective layer for PM-IRRAS measurement. In the following text, chemical protocol is described step by step.

Coating of diamond with a silica layer

Polyvinylpyrrolidone (PVP, M = 10 000, 2.28 mg, 0.228 μmol, purchased from Sigma-Aldrich) was added in distilled water (2.4 ml) in 20 ml vial and sonicated in ultrasonic bath until complete dissolution. Before to be added in the PVP mixture, the samples were washed in acetone, ethanol and distilled water and dried by compressed air. Vials with samples were left at gel-rocker overnight. Thin silica layer grows from a mixture of tetraethyl orthosilicate (TEOS) and 3-(trimethoxysilyl)propyl methacrylate. Samples were removed from mixture of PVP and added into new vials. Distilled TEOS (18 μl, purchased from Sigma-Aldrich) and 3-(trimethoxysilyl)propylmethacrylate (6 μl, purchased from Sigma-Aldrich) and ethanol (2.4 ml) were added in the vial with sample. Ammonia (25 %, 100 μl) was added after 20 s sonication in an ultrasonic bath. Vials were left at gel-rocker overnight. Samples were then washed 3 times with ethanol, putted into new vials and stored in methanol at -20 °C. Reaction equation to form silica layer is shown in

figure 4.33.

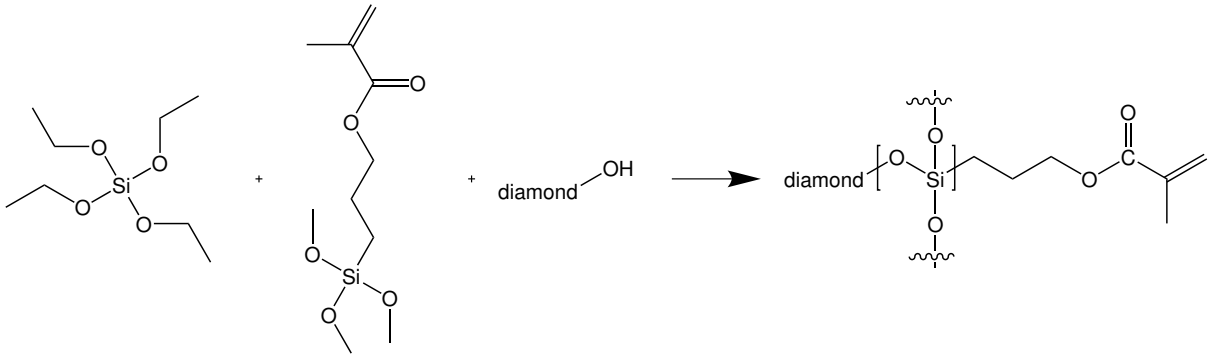

Figure 4.33: Reaction equation for grown of silica layer - Tetraethyl orthosilicate + 3-(trimethoxysilyl)propyl methacrylate + oxidized diamond layer forms silica coating of diamond

Presence of silica layer on the NCD layer was checked by PM-IRRAS method. Figure 4.34 clearly shows the formation of silica layer with a characteristic peak at 1200 cm^{-1} corresponds to the vibrations of the Si-O-Si bonds. Bands at 2900 cm^{-1} corresponds to the alkyl stretch vibration of the trimethylene chain of silylpropylmethacrylate and the corresponding vibration can be found at 1420 cm^{-1}. The peak around 1700 cm^{-1} corresponds also to the alkenyl C=C stretch vibration.

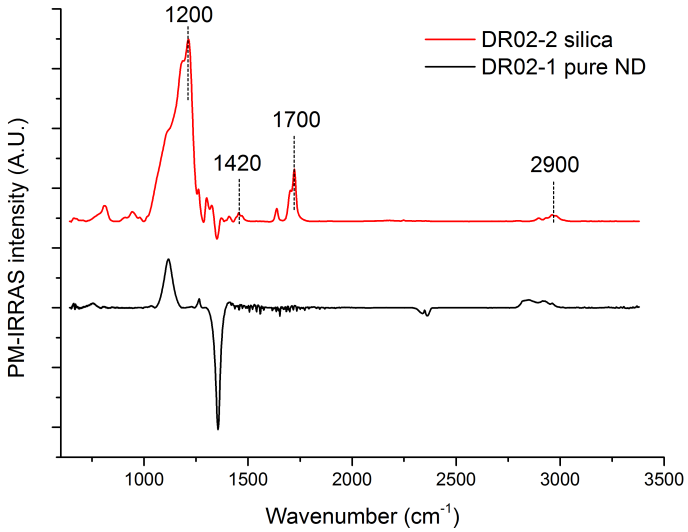

Figure 4.34: PM-IRRAS spectra of silica coated NCD layer and pure NCD layer.

Second experiment was done for the investigation of influence of PVP layer on the formation of silica layer. One sample was prepared reproducing the whole process described

above. For the preparation of second sample, the step with PVP modification was skip and process stared with grown of silica layer. Both samples were characterized by PM-IRRAS measurement. They show same characteristic peaks as in figure 4.34 of NCD coated with SiO_2 layer.

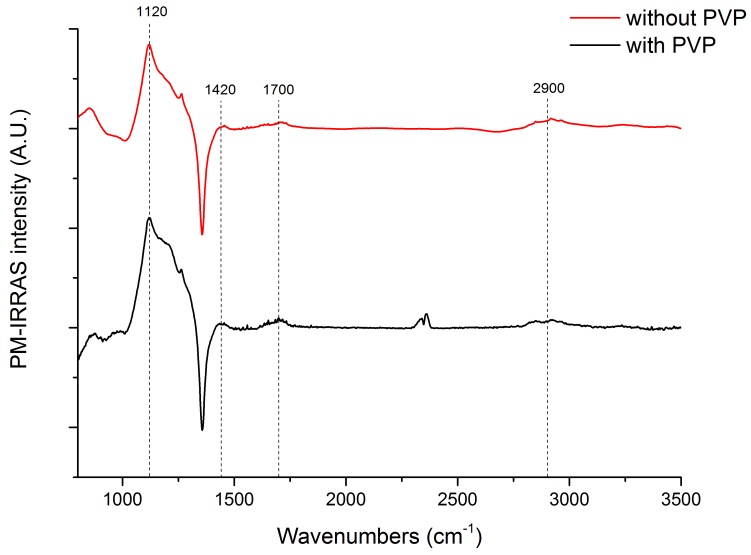

Figure 4.35: PM-IRRAS spectra of silica coated NCD layer with or without use of PVP.

Polymer layer coating

The deposited methacrylated silica layer was used to grown a dense layer of copolymers, which mainly consists of poly[N-(2-hydroxypropyl)methacrylamide] (poly(HPMA)). A fraction of HPMA in reaction mixture was replaced by 3-(azidopropyl)methacrylamide (AzMA) to introduce azide groups to the polymer, that were required for copper-catalyzed click reaction. This copolymer layer was grown using radical polymerization and azobis(isobutyronitrile) (AIBN) is used as an initiator.

In the reaction mixture, 5% or 30% of HPMA polymer was replaced by AzMA. HPMA [332.5 mg, 2.29 mmol (resp. 245 mg, 1.69 mmol) purified by flash chromatography] and AzMA [17.5 mg (resp. 105 mg)] were dissolved in DMSO (1 ml, filtered using a 0.2 μm polytetrafluorethylene microfilter) in the vial. AIBN (100 mg, 0.61 mmol, freshly recrystallized from ethanol solution on a rotary evaporator, maximum temperature 30 °C) was added. Mixture was dissolved using vortex. Methacrylate-terminated samples were dried using compressed air and added in the mixture. Vials were secured with argon

three times and left for 3 days under argon at 55 °C. Then, samples were washed once at DMSO, twice at EtOH and three times at milliQ water and stored at -20 °.

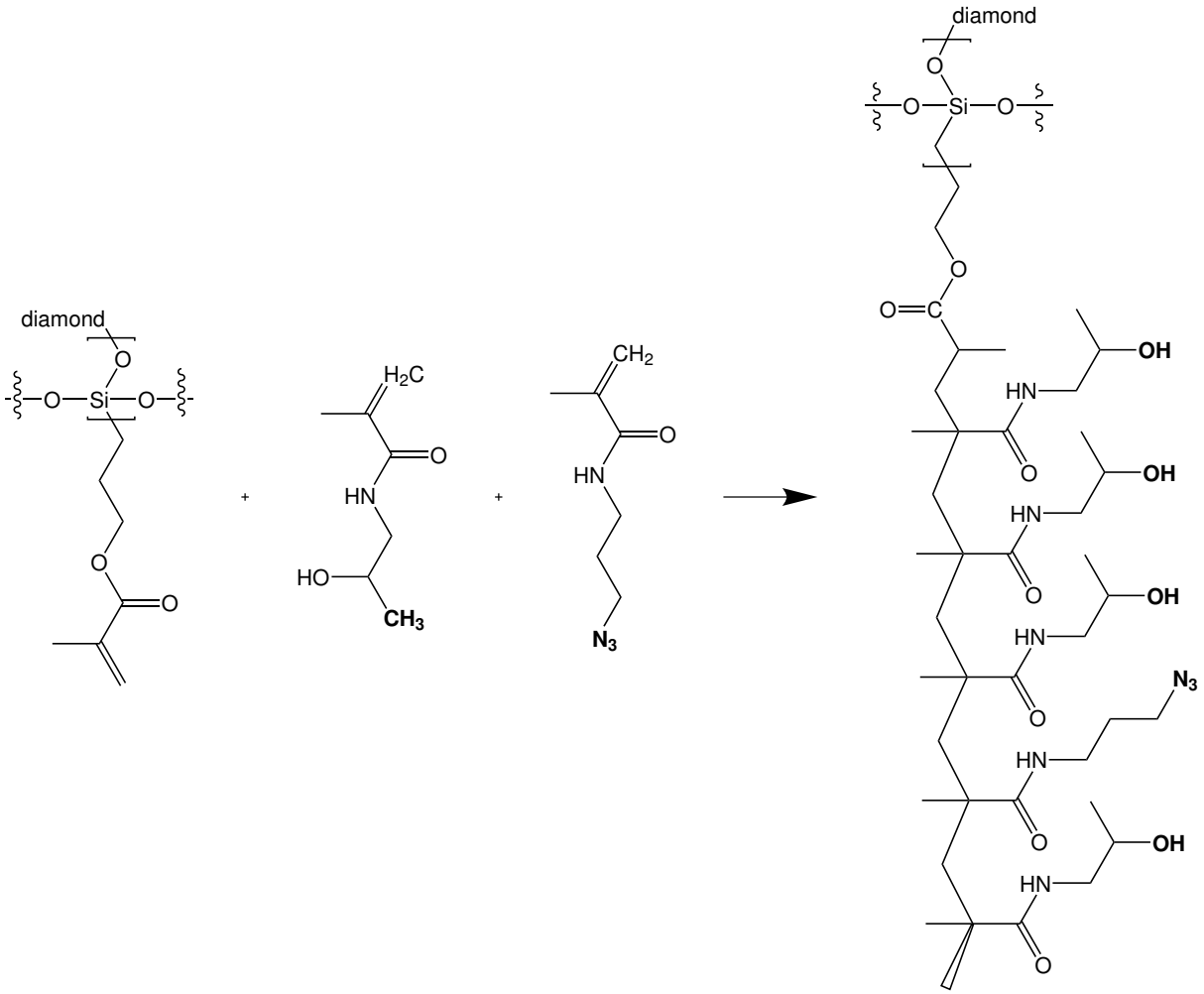

Figure 4.36: Reaction equation for polymer layer coating - silica layer + HMPA + AzMA forms copolymer layer with presence of azide groups

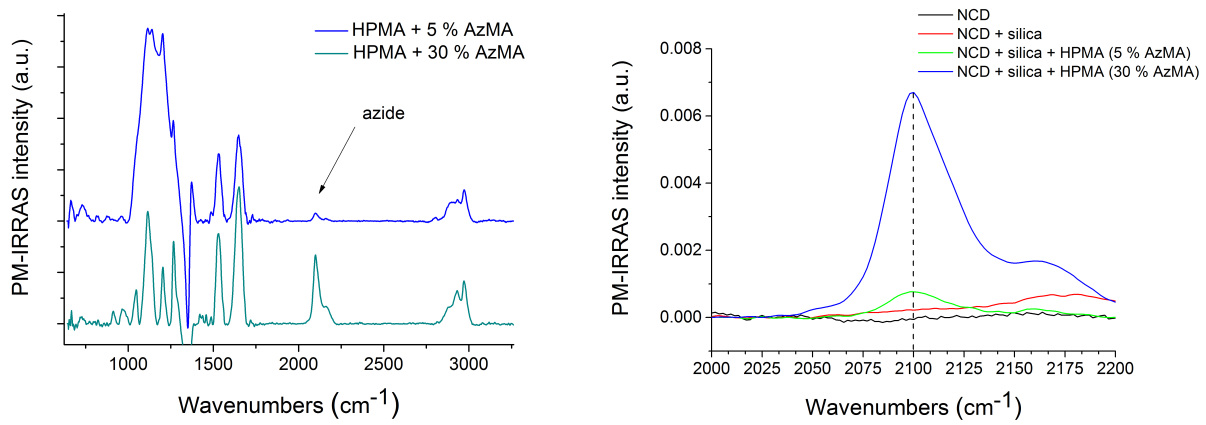

Figure 4.37: PM-IRRAS spectra of polymer coated NCD layer with significant peak at 2100 cm^{-1} related to azide groups

It was not possible to continue with further functionalization steps because of problem with synhtesis of ligand. This ligand is necessary for click reaction and further attachment of His-tag linkers with bacteriophage's fiber tails.

5 | Conclusions

This work was carried out to develop a diamond based LW-SAW sensor for bacteria detection and the following aims were achieved.

Fabrication and characterization of SAW sensors

Development of microfabrication processes

Optimal conditions were developed for microfabrication processes such as photolithography, wet etching, dry etching and metal deposition. For photolithography techniques we found optimal writing conditions with the MicroWriter ML for both positive and negative photoresist on different types of substrates. Wet etching and dry etching were developed on various materials: silicon, aluminum and diamond, which are relevant for future use in fabrication of different types of sensors: microcantilever sensor. For successful fabrication of diamond coated LW-SAW sensor optimal conditions for deposition of NCD layer were determined.

LW-SAW fabrication and characterization

LW-SAW sensors were fabricated at IEMN, France. LW-SAW sensors were fabricated on AT-cut or ST-cut quartz crystal with IDTs with different spatial periods and 1.3 μm thick SiO_2 guiding layer and thin NCD layer on top. The influence of different SiO_2 normalized thicknesses was studied. For a constant thickness of guiding layer 1.3 μm, the optimal frequency response is provide by SAW with 16 or 32 μm IDTs, which corresponds to a SiO_2 normalized thickness of 0.08 or 0.04. SAW devices with these two values of spatial periods were used to study dependence of metal used for fabrication of electrodes. Two metals were investigated - aluminum and chromium. SAWs with aluminum electrodes

have lower insertion loss. Study of dependence of diamond layer was carried out as well. We observed that with deposition of increasing NCD layer thickness resonant frequency of sensor increase, that is caused by an increase in phase velocity of acoustic waves due to an increase in rigidity of the surface. Results showed a decrease of resonant frequency until the NCD was closed. A decrease in resonant frequency is caused by mass loading of the sensor. Sensitivity of LW-SAW sensor were studied using diamond coated and uncoated sensor with deposited different number of LOR layers. These results showed better sensitivity for sensors with 0.08 SiO_2 normalized thickness. All of these results are consistent with theoretical studies of LW-SAW sensor.

Attachment of bioreceptors to the diamond surface

Diamond surface functinalization

Various functionalization was carried out for attachment of bioreceptors to the diamond surface. Three different types of termination of NCD layer were investigated. Optimal conditions for hydrogenation and oxidization of NCD layers were developed. Chemical functionalization of NCD layer was performed to introduce NH_2 groups onto the diamond surface. The wettability of prepared NCD layers was investigated using contact angle measurement.

Microbiological methods

Microbiological methods such as cultivation of bacteria, multiplication and purification of phages and plaque assay methods was carried out. Sensitive *E. coli* strains was found for bacteriophages T7 using plaque assay method. Efficiency of multiplication and purification of bacteriophages was investigated using negative staining and TEM measurement. We found that purification of bacteriophages was insufficient and better methods have to be developed to obtain clear bacteriphages suspension.

Attachment of bacteriophages T7 to diamond surface

For attachment of bacteriophages T7, procedure developed by Singh *et al.* [13] was followed. For this attachment, different diamond treatments were investigated - hydrogena-

tion, oxidization, amination and activation of amino groups by gluteraldehyde. It was not possible to observe attached bacteriophages to NCD layer, because the size of bacteriophage's head is approximately 50 nm and this size is comparable with the size of NCD grains. Observation was also impossible because of bad conductivity of the substrate and a huge amount of attached proteins to the diamond surface. Epitaxial grown diamond layers on SCD substrate were used also. The surface of this layer is flat without grains. Two types of termination were used - hydrogenated and oxidized surface. After the attachment process, samples were coated with 3 nm of platinum to obtain a conductive surface. The presence of bacteriophages T7 on this type of diamond surface was confirmed.

Bacteriophage's fiber tails attachment study

For attachment of bacteriophage's fiber tails several steps was carried out. Silica coating as well as introduction of a biocompatible copolymer with azide groups was confirmed and optimised by PM-IRRAS technique. Further functionalization of surface for attachment of fiber tails was unfortunately delayed due to synthesis complications. As soon as the ligand for attachment will be prepared, a study of attachment of fiber tails will proceed.

Future work

Conclusion of this study will lead to future work. Attachment study of bacteriophages to the aminated epitaxial diamond layers as well as the attachment of fiber tails as well as further optimization of SAW design shall be continued. After the introduction of a bioreceptor to the diamond surface, their capture ability and bacterial sensitivity shall be studied as sensitivity of LW-SAW sensor to bacteria capture. Other types of sensors such as microcantilevers or membrane acoustic sensors can be developed, studied and compared with LW-SAW sensor. Biofunctionalization results can also be used for fabrication of electrochemical sensors.

Bibliography

[1] N. Moll, E. Pascal, D.H. Dinh, J.-L. Lachaud, L. Vellutini, J.-P. Pillot, D. Rebière, D. Moynet, J. Pistré, D. Mossalayi, Y. Mas, B. Bennetau, and C. Déjous. Multipurpose Love acoustic wave immunosensor for bacteria, virus or proteins detection. *IRBM*, 29(2-3):155–161, April 2008.

[2] World Health Organization. Burden of disease and cost-effectiveness estimates. http://www.who.int.

[3] E. Berkenpas, P. Millard, and M. Pereira da Cunha. Detection of Escherichia coli O157:H7 with langasite pure shear horizontal surface acoustic wave sensors. *Biosensors and Bioelectronics*, 21(12):2255–2262, June 2006.

[4] Thomas M.A. Gronewold. Surface acoustic wave sensors in the bioanalytical field: Recent trends and challenges. *Analytica Chimica Acta*, 603(2):119–128, November 2007.

[5] Stanislav Rosypal. *Nový přehled biologie.* Scientia, Praha, 2003.

[6] Michael S Donnenberg. *Escherichia coli pathotypes and principles of pathogenesis.* Elsevier/Academic Press, Amsterdam, 2013.

[7] George M Malacinski. *Essentials of molecular biology.* Jones and Bartlett, Boston, 2003.

[8] Richard Calendar, editor. *The Bacteriophages.* The Viruses. Plenum Press, New York, 1988.

[9] Arghavan Shabani, Christophe A. Marquette, Rosemonde Mandeville, and Marcus F. Lawrence. Modern Probe-Assisted Methods for the Specific Detection of Bacteria. *Journal of Biomedical Science and Engineering*, 08(02):104–121, 2015.

[10] Kiev S Gracias and John L McKillip. A review of conventional detection and enumeration methods for pathogenic bacteria in food. *Canadian Journal of Microbiology*, 50(11):883–890, November 2004.

[11] ALBERTS , Bruce. *Základy buněčné biologie: úvod do molekulární biologie buňky.* Espero Publishing, Ústí nad Labem, 2. edition, 2004.

[12] Nicolas Moll, Emilie Pascal, Duy Haï Dinh, Jean-Paul Pillot, Bernard Bennetau, Dominique Rebière, Daniel Moynet, Yan Mas, Djavad Mossalayi, Jacques Pistré, and Corinne Déjous. A Love wave immunosensor for whole E. coli bacteria detection using an innovative two-step immobilisation approach. *Biosensors and Bioelectronics*, 22(9-10):2145–2150, April 2007.

[13] A. Singh, N. Glass, M. Tolba, L. Brovko, M. Griffiths, and S. Evoy. Immobilization of bacteriophages on gold surfaces for the specific capture of pathogens. *Biosensors and Bioelectronics*, 24(12):3645–3651, August 2009.

[14] Anil K Deisingh and Michael Thompson. Biosensors for the detection of bacteria. *Canadian Journal of Microbiology*, 50(2):69–77, February 2004.

[15] Jr Ballantine, D. S, Robert M White, S. J Martin, Antonio J Ricco, E. T Zellers, G. C Frye, H Wohltjen, Moises Levy, and Richard Stern. *Acoustic Wave Sensors Theory, Design, & Physico-Chemical Applications.* Elsevier Science, San Diego, 2014.

[16] Dmitri Ivnitski, Ihab Abdel-Hamid, Plamen Atanasov, Ebtisam Wilkins, and Stephen Stricker. Application of Electrochemical Biosensors for Detection of Food Pathogenic Bacteria. *Electroanalysis*, 12(5):317–325, March 2000.

[17] Sarang Dutt. Immobilization of P22 Bacteriophage Tailspike Protein on Si Surface for Optimized Salmonella Capture. *Journal of Analytical & Bioanalytical Techniques*, S7, 2013.

[18] Amit Singh, Sunil K. Arya, Nick Glass, Pejman Hanifi-Moghaddam, Ravendra Naidoo, Christine M. Szymanski, Jamshid Tanha, and Stephane Evoy. Bacteriophage tailspike proteins as molecular probes for sensitive and selective bacterial detection. *Biosensors and Bioelectronics*, 26(1):131–138, September 2010.

[19] L. Gervais, M. Gel, B. Allain, M. Tolba, L. Brovko, M. Zourob, R. Mandeville, M. Griffiths, and S. Evoy. Immobilization of biotinylated bacteriophages on biosensor surfaces. *Sensors and Actuators B: Chemical*, 125(2):615–621, August 2007.

[20] M. Tolba, O. Minikh, L. Y. Brovko, S. Evoy, and M. W. Griffiths. Oriented Immobilization of Bacteriophages for Biosensor Applications. *Applied and Environmental Microbiology*, 76(2):528–535, January 2010.

[21] P. M. Fratamico, T. P. Strobaugh, M. B. Medina, and A. G. Gehring. Detection of Escherichia coli O157:H7 using a surface plasmon resonance biosensor. *Biotechnology techniques*, 12(7):571–576, July 1998.

[22] Nancy Tawil, Edward Sacher, Rosemonde Mandeville, and Michel Meunier. Surface plasmon resonance detection of E. coli and methicillin-resistant S. aureus using bacteriophages. *Biosensors and Bioelectronics*, 37(1):24–29, August 2012.

[23] Seung Min Yoo, Do-Kyun Kim, and Sang Yup Lee. Aptamer-functionalized localized surface plasmon resonance sensor for the multiplexed detection of different bacterial species. *Talanta*, 132:112–117, January 2015.

[24] H. Baccar, M.B. Mejri, I. Hafaiedh, T. Ktari, M. Aouni, and A. Abdelghani. Surface plasmon resonance immunosensor for bacteria detection. *Talanta*, 82(2):810–814, July 2010.

[25] Aloka B. Bandara, Ziwei Zuo, Siddharth Ramachandran, Alfred Ritter, James R. Heflin, and Thomas J. Inzana. Detection of methicillin-resistant staphylococci by biosensor assay consisting of nanoscale films on optical fiber long-period gratings. *Biosensors and Bioelectronics*, 70:433–440, August 2015.

[26] Anna Mazhorova, Andrey Markov, Andy Ng, Raja Chinnappan, Olga Skorobogata, Mohammed Zourob, and Maksim Skorobogatiy. Label-free bacteria detection using evanescent mode of a suspended core terahertz fiber. *Optics Express*, 20(5):5344, February 2012.

[27] Abdolkarim Abbaspour, Fatemeh Norouz-Sarvestani, Abolhassan Noori, and Noushin Soltani. Aptamer-conjugated silver nanoparticles for electrochemical dual-aptamer-based sandwich detection of staphylococcus aureus. *Biosensors and Bioelectronics*, 68:149–155, June 2015.

[28] Ankan Dutta Chowdhury, Amitabha De, Chirosree Roy Chaudhuri, Krishnan Bandyopadhyay, and Pintu Sen. Label free polyaniline based impedimetric biosensor for detection of E. coli O157:H7 Bacteria. *Sensors and Actuators B: Chemical*, 171-172:916–923, August 2012.

[29] Helga Szalontai, Nóra Adányi, and A. Kiss. Development of Piezoelectric Immunosensor for the Detection of Probiotic Bacteria. *Analytical Letters*, 45(10):1214–1229, July 2012.

[30] Veli C. Ozalp, Gulay Bayramoglu, Zehra Erdem, and M. Yakup Arica. Pathogen detection in complex samples by quartz crystal microbalance sensor coupled to aptamer functionalized core–shell type magnetic separation. *Analytica Chimica Acta*, 853:533–540, January 2015.

[31] Hiromi Yatsuda, Takashi Kogai, Mikihiro Goto, and Naoyuki Yoshimura. Shear-horizontal surface acoustic wave biosensors for POCT. pages 1–4. IEEE, May 2014.

[32] Yi-Huang Chang, Hung-Der Jang, Chuan-Liang Hsu, and Ku-Shang Chang. Quantitative Determination of *Escherichia Coli* in Water Sources in the Environment Using a Surface Acoustic Wave Impedance System Modified with a Syringe Filter. *Analytical Letters*, 45(11):1485–1494, July 2012.

[33] Trang Hoang. Design and realization of SAW pressure sensor using Aluminum Nitride, 2009.

[34] Florinel-Gabriel Banica. *Chemical sensors and biosensors fundamentals and applications.* John Wiley & Sons Inc., Chichester, West Sussex, U.K., 2012.

[35] Yafei Zhang and Da Chen. *Multilayer Integrated Film Bulk Acoustic Resonators.* Springer, Heidelberg, 2013.

[36] Erika Kress-Rogers, editor. *Handbook of biosensors and electronic noses: medicine, food, and the environment.* CRC Press, Boca Raton, 1997.

[37] Kourosh Kalantar-Zadeh, Wojtek Wlodarski, Yuen Y. Chen, Benjamin N. Fry, and Kosmas Galatsis. Novel Love mode surface acoustic wave based immunosensors. *Sensors and Actuators B: Chemical*, 91(1-3):143–147, June 2003.

[38] Sergey V Biryukov, IU. V Guliaev, V. V Krylov, and Victor P Plessky. *Surface Acoustic Waves in Inhomogeneous Media.* Springer Berlin Heidelberg : Imprint : Springer, Berlin, Heidelberg, 1995.

[39] Z. Su and L. Ye. *Identification of damage using Lamb waves: from fundamentals to applications.* Number v. 48 in Lecture notes in applied and computational mechanics. Springer-Verlag, Berlin, 2009.

[40] Josef Krautkrämer and Herbert Krautkrämer. *Ultrasonic Testing of Materials.* Springer Berlin Heidelberg, Berlin, Heidelberg, 1990.

[41] Sebastiano Foti, editor. *Surface wave methods for near-surface site characterization.* CRC Press/Spon Press, Boca Raton, Fla., 2014.

[42] Ei-ichi Yasuda, editor. *Carbon alloys: novel concepts to develop carbon science and technology.* Elsevier, Amsterdam : London, 2003.

[43] Rani Elhajjar, editor. *Smart composites: mechanics and design.* Composite materials : design and analysis. CRC Press/Taylor & Francis Group, Boca Raton, FL, 2013.

[44] John C. Kotz, Paul Treichel, and John Raymond Townsend. *Chemistry & chemical reactivity.* Brooks/Cole, Cengage Learning, Belmont, CA, 8th ed edition, 2012.

[45] Sylvia Wenmackers. Morphology, functionality and molecular conformation study of CVD diamond surfaces functionalised with organic linkers and DNA, 2008.

[46] Philippe Serp, José Luís Figueiredo, and Wiley InterScience (Online service). *Carbon materials for catalysis.* John Wiley & Sons, Hoboken, N.J., 2009.

[47] Richard Daley. *Organic Chemistry, Part 1 of 3.* Daley Press, December 2013.

[48] Waqar Ahmed. *Chemical vapour deposition of diamond for dental tools and burs.* 2014.

[49] Anke Krueger and Daniel Lang. Functionality is Key: Recent Progress in the Surface Modification of Nanodiamond. *Advanced Functional Materials*, 22(5):890–906, March 2012.

[50] Vadym N. Mochalin, Olga Shenderova, Dean Ho, and Yury Gogotsi. The properties and applications of nanodiamonds. *Nature Nanotechnology*, 7(1):11–23, December 2011.

[51] Adarsh D. Radadia, Courtney J. Stavis, Rogan Carr, Hongjun Zeng, William P. King, John A. Carlisle, Aleksei Aksimentiev, Robert J. Hamers, and Rashid Bashir. Control of Nanoscale Environment to Improve Stability of Immobilized Proteins on Diamond Surfaces. *Advanced Functional Materials*, 21(6):1040–1050, March 2011.

[52] Yury Gogocij and Volker Presser, editors. *Carbon nanomaterials.* Advanced materials and technologies series. CRC, Taylor & Francis, Boca Raton, Fla., 2. ed edition, 2014.

[53] Sabine Szunerits, Christoph E. Nebel, and Robert J. Hamers. Surface functionalization and biological applications of CVD diamond. *MRS Bulletin*, 39(06):517–524, June 2014.

[54] Sabine Szunerits and Rabah Boukherroub. Different strategies for functionalization of diamond surfaces. *Journal of Solid State Electrochemistry*, 12(10):1205–1218, October 2008.

[55] J. Miksovsky, A. Voss, R. Kozarova, T. Kocourek, P. Pisarik, G. Ceccone, W. Kulisch, M. Jelinek, M.D. Apostolova, J.P. Reithmaier, and C. Popov. Cell adhesion and growth on ultrananocrystalline diamond and diamond-like carbon films after different surface modifications. *Applied Surface Science*, 297:95–102, April 2014.

[56] Guo-Jun Zhang, Kwang-Soup Song, Yusuke Nakamura, Taro Ueno, Takashi Funatsu, Iwao Ohdomari, and Hiroshi Kawarada. DNA Micropatterning on Polycrystalline Diamond via One-Step Direct Amination. *Langmuir*, 22(8):3728–3734, April 2006.

[57] Hugh O Pierson. *Handbook of chemical vapor deposition (CVD) principles, technology, and applications.* Noyes Publications, Park Ridge, N.J., U.S.A., 1992.

[58] Hari Singh Nalwa, editor. *Handbook of thin film materials.* Academic Press, San Diego, 2002.

[59] R.F. Pease and S.Y. Chou. Lithography and Other Patterning Techniques for Future Electronics. *Proceedings of the IEEE*, 96(2):248–270, February 2008.

[60] Lucie Drbohlavova, J. Bulir, M. Jakl Krecmarova, A. Taylor, A. Talbi, A. Soltani, and V. Mortet. Fabrication methods of diamond coated Love wave SAW biosensors for bacterial detection applications. In *Instruments and methods for biology and medicine 2015*, pages 11 – 14, Faculty of Biomedical Engineering of Czech Technical University in Prague, 2015.

[61] Guillaume Thomain. *Setup of a Reactive Ion-etching System.* ProQuest, 2008.

[62] Robert W. Kelsall, Ian W. Hamley, and Mark Geoghegan, editors. *Nanoscale science and technology.* John Wiley, Chichester, England ; Hoboken, NJ, 2005.

[63] Greg Haugstad. *Atomic force microscopy: understanding basic modes and advanced applications.* John Wiley & Sons, Hoboken, N.J, 2012.

[64] Pier Carlo Braga and Davide Ricci. *Atomic force microscopy: biomedical methods and applications.* Humana Press, Totowa, N.J., 2004.

[65] Bernhard Schrader, D Bougeard, and Wiley InterScience (Online service). *Infrared and Raman spectroscopy methods and applications.* VCH, Weinheim; New York, 1995.

[66] S. Prawer and R. J. Nemanich. Raman spectroscopy of diamond and doped diamond. *Philosophical Transactions of the Royal Society A: Mathematical, Physical and Engineering Sciences*, 362(1824):2537–2565, November 2004.

[67] Steven L. Suib, editor. *New and future developments in catalysis. Catalysis by nanoparticles.* Elsevier, Amsterdam ; Boston, 2013.

[68] John F. Watts and John Wolstenholme. *An introduction to surface analysis by XPS and AES.* J. Wiley, Chichester, West Sussex, England ; New York, 2003.

[69] Mittal K. L. *Advances in contact angle, wettability and adhesion.* John Wiley, [Place of publication not identified], 2015.

[70] Colin Campbell. *Surface acoustic wave devices and their signal processing applications*. Academic Press, Boston, 1989.

[71] J. R Norris and Douglas W Ribbons. *Methods in microbiology Vol 7A Vol 7A*. Academic Press, London, 1972.

[72] Keith Wilson and John M. Walker, editors. *Principles and techniques of biochemistry and molecular biology*. Cambridge University Press, Cambridge, UK : New York, 7th ed edition, 2009.

[73] A. Jayakumaran Nair. *Principles of biotechnology and genetic engineering*. Laxmi Publisher, New Delhi, 2 edition, 2010.

[74] Keith Wilson, editor. *Principles and techniques of practical biochemistry: [essential reading for all bioscience undergraduate students and pre-clinical medical students for whom practical biochemistry, molecular biology and immunology form part of the syllabus]*. Cambridge Univ. Press, Cambridge, 5. ed., repr edition, 2001.

[75] A. Talbi, A. Soltani, A. Rumeau, A. Taylor, L. Drbohlavová, L Klimša, J. Kopeček, L. Fekete, M. Krečmarová, and V. Mortet. Simulations, fabrication, and characterization of diamond-coated Love wave-type surface acoustic wave sensors: Characterization of diamond-coated Love wave-type surface acoustic wave sensors. *physica status solidi (a)*, 212(11):2606–2610, November 2015.

Appendix A

List of publication published during the traineeship

Talbi A., Soltani A., Rumeau A., Taylor A., Drbohlavova L., Klimsa L., Kopecek J., Fekete L., Krecmarova L., Mortet V.: Simulations, fabrication, and characterization of diamond-coated Love wave-type surface acoustic wave sensors. Physica status solidi (a) 2015, 212(11), 2606-2610

Drbohlavova L., Bulir J., Vales V., Krecmarova M., Taylor A., Talbi A., Soltani A., Mortet V.: Fabrication methods of diamond coated Love wave SAW biosensors for bacterial detection applications. In Instruments and Methods for Biology and Medicine 2015. Kladno: Czech Technical University in Prague, 2015, p. 18-23. ISBN 978-80-01-05851-0

Participation to international conferences

Oral presentation

"Fabrication methods of diamond coated Love wave SAW biosensors for bacterial detection applications" at Instruments & Methods for Biology and Medicine 2015 (IMBM 2015) student conference, Faculty of Biomedical Engineering, Czech Technical University in Prague, Sitna Sq. 3105, Kladno Czech Republic May 28th, 2015

Poster presentation

"Simulations, fabrication and characterisations of diamond coated Love wave surface acoustic wave sensors" at Hasselt Diamond workshop 2015 - SBDD XX, Cultureel centrum Hasselt, Hasselt, Belgium, February 25th-27th, 2015